The University of Texas-Pan American
College of Science & Engineering
Department of Mechanical Engineering

MECE 4362
Senior Design Project
Fall 2011 & Spring 2012
Laboratory Section A (1:10-6:30)

Bio-energy Harvesting of Human Mechanical Movements

Technical Advisors: Drs. Miguel A. Gonzalez & Dumitru Caruntu
Northrop Grumman Advisor: Mr. Gregory West & Allen Kelly
Course Advisors: Drs. Kamal Sarkar& Robert A. Freeman

By:

Steve Zambrano
Amador Sotelo
Jason Perez
Israel Morado

Due date: May 9, 2012

Date received: _____

Table of Contents

List of Figures

List of Tables

Abstract

Ambient bio-energy harvesting generators are attractive as supplemental energy sources for batteries in low-power electronic devices. This paper addresses the development of a biomechanical energy harvester that generates electricity by harnessing the bimodal, lower extremity motion produced at the knee-joint section. An orthotic knee brace was implemented to act as the mechanical connection to the host; therefore, angular displacement could later be transferred to a three-stage transmission for higher electrical flux development through use of an electromagnetic generator. Test subjects with one device on one leg produced an average of 0.075 to 0.5 watts with a testing range of 3 to 7 MPH.

1.0 Background

The following provides information on the company/client and project to provide the reader with a holistic view of the project.

1.1 Project Title

Bio-energy Harvesting of Lower Extremity Human Mechanical Movements (aka: Pedometer Energy Harvester)

1.2 Company/Client Information

Northrop Grumman Corporation is an American global aerospace and defense technology company formed by the 1994 purchase of Grumman by Northrop. As of 2010 the company was the fourth-largest defense contractor in the world and the largest builder of naval vessels. The company currently employs over 120,000 people worldwide, was ranked number 72 on the 2011 Fortune 500 list of America's largest corporations, and ranks in the top ten of military friendly employers. (Northrop Grumman, 1994)

1.3 Project Information

Phones and electrical accessories are a common part of our early 21st century lives. As they consume energy by producing virtual transport of data to and from sources of information and commerce, individual power requirements increase. Sometimes users cannot be near a vehicle or an AC power adapter to recharge one of these accessories. However, more frequently the standard USB output configuration is applied to many and the 12 DC volt car lighter configurations. This type of configuration has expanded as a consumer accepted power charging sources. Another source of portable power could be useful. Although it cannot be seen, the body produces energy when in motion. Harvested body power coming from pedometer type energy sources presents possibilities especially for the active, young and or physically mobile market.

2.0 Overall Design Methodology

The proceeding section will provide a framework for the process which the design team will employ to complete the biomechanical energy harvester. (Continuous Improvement Center, 2008)The overall design methodology will consist of:

- Market Search/User Need
- Problem Formulation
- Conceptual Designs
- Detail Design
- Manufacture

As with all engineering design projects a detail timeline for project goals must be formulated, below is a proposed timeline of project deadlines throughout the course of the project period.

Table 1: Design Gantt Chart

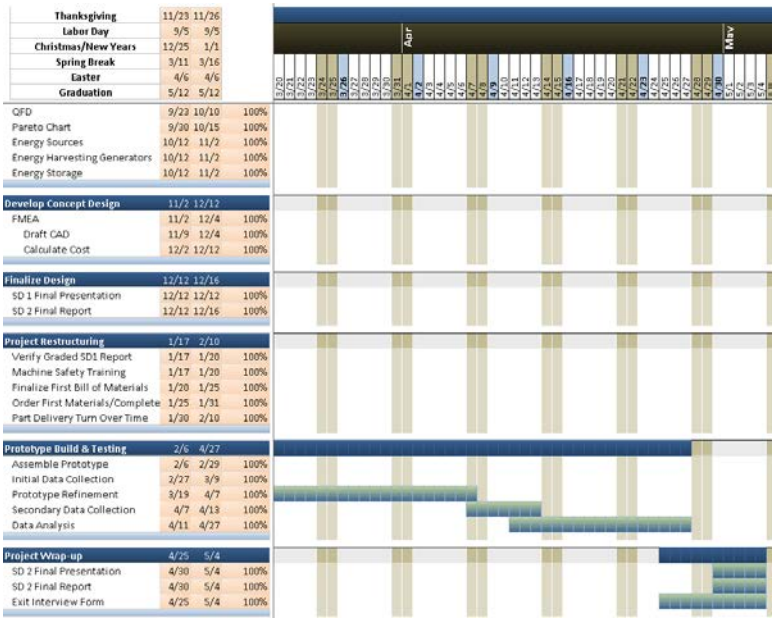

*The preceding item is an electronic document link to the proposed project timeline of the biomechanical energy harvester project. *Note: In order to the Excel document double click on the above table.*

3.0 Market Search

The proceeding section will identify several direct competitors to the proposed research topic.

3.1 Sanyo Pedometer Charger

SANYO Electric Co., a major distributer of energy, is researching the viability of creating a device which self generates power while you use it. The company has created a pedometer that

captures the kinetic energy of an individual while running or walking. Currently, SANYO claims there device can generate 40 microwatts of power; enough to power the step counter of the pedometer. (Heimbuch, 2008)

3.2 Step Energy Generator: Ugly Sneakers

What if you could power your iPod with every step that you take, that is the claim that the Japanese company NTT DoCoMo claims they can do. Their design utilizes water filled shoe soles that are attached to a small turbine. With every step the water is displaced and pumped through the turbine which in turn powers the electric generator. According to Hideomi Tenma, a spokesman for NTT their system can generate 1.2 watts of power which could very well power an iPod. (Alter, 2008)

3.3 Knee Brace Generator

Researchers from Simon Fraser University, University of Pittsburgh, and University of Michigan have been working to create a knee brace prototype to harness biomechanical energy. This prototype seeks to find a medium between generating a viable amount of energy while at the same time remaining light and taking into account human ergonomics.

Arthur Kuo, an engineer who worked on the device, said it works similar to the way that regenerative brakes charge a battery. The knee device collects energy lost when a person breaks the knee after swinging the leg forward during the normal gait cycle. Preliminary testing has been performed where a device was placed on the each leg of volunteers. At walking speed of 2.2 mph nominal generation was about five watts. (J. M. Donelan, 2008)

3.4 PowerWalk™ M-Series Brace

Bionic Power Inc. is a Simon Fraser University spinoff company in which Dr. Max Donelan serves as the chief science officer. The company focus is to provide cost-effective and reliable energy to individuals whom depend on portable power. Their principle product, PowerWalk™

Figure 1: PowerWalk™ M-Series

The PowerWalk™ M-Series is the flagship model of Bionic Power Inc.; this system was originally pioneered as a joint project by Simon Fraser University, University of Pittsburgh, and University of Michigan.

The M-Series was developed in collaboration with the Canadian Special Forces and resembles a knee brace. The system weighs approximately 1.7 pound and with a device on each leg Bionic Power Inc. claims to produce an average of twelve watts of electricity. (Bionic Power Inc.)

3.5 sOccket 1.0 & 2.0 Soccer Ball

For undergraduate students at Harvard University decided the world's most popular sport of soccer might just be a viable source to harvest kinetic energy. The electromechanical concept behind there generator is straightforward: it operates off the principle that as a magnetic component displaces position between an inductive coil this interaction creates an electro differential. (Hanna, 2011)

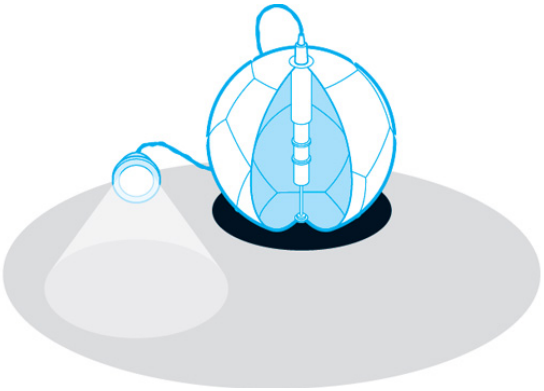

Figure 2: sOccket 1.0 Soccer Ball

*The above figure is a simple diagram of the sOccket 1.0 soccer ball and the internal mechanism this harnesses and stores the potential energy in a classical system C-element-an electrical capacitor. *Pictorial source: Electricity from a Soccer Ball - Breakthrough Award Innovator - Popular Mechanics*

According to www.socket.com the original design, sOccket 1.0, will be redesigned and may not utilize the same type of inductive coil mechanism to generate power. sOccket 2.0 is expected to launch September 2011.

3.6 Philips Knee Mounted Power Generator

The Philips knee mounted power generator is a concept design currently not available for purchase. No data for energy generation has been released pertaining to the Philips generator, however, according to the concept design captions kinetic motion at the knee is transferred through a set of gears then passed to a flywheel magnet. The "flywheel magnet freely rotates in one direction, in a process of induction; the magnetism is then picked up by a coil of wire and becomes electricity." This electricity is then stored by on-board capacitors ready to charge any device. (Kumar, 2008)

Figure 3: Philips Generator Conceptual CAD Model

*The preceding figure is a computer aided design model of the Philips knee mounted power generator alongside a depiction of human device placement. *Pictorial source: [Ecofriend RSS Feed (Instablogs Community)]*

3.7 Lighting Packs, LLC: Suspended-load Backpack

Lightning Packs is a company whose goal is to develop innovative backpacks that recover electricity from normal walking and that provide wearers with ergonomic benefits such as reduced joint stress. Their design is based on the patented technology developed by Dr. Lawrence C. Rome. (Rome, 2006)

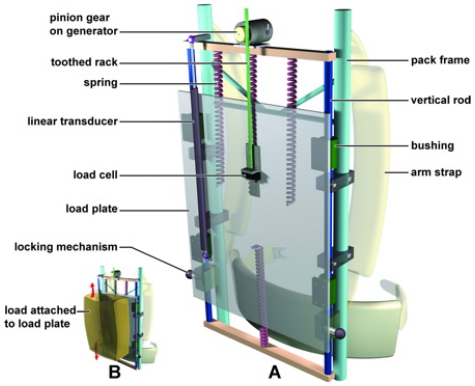

Figure 4: Lighting Packs CAD Design Model

*Above is a computer aided design model of the suspended-load backpack design from Lighting Packs, LLC. *Pictorial source: [http://lightningpacks.com/favicon.ico]*

3.8 Louisiana Tech. University Piezoelectric Shoe

Dr. Ville Kaajakari, an assistant professor at Louisiana Tech. University developed a prototype shoe power generator which utilizes polymeric piezoelectric material embedded within the sole of the shoe to generate an electric charge when mechanically compressed. The shoe generator works off the principle that when a piezoelectric transducer is coupled together with two rectifying diodes this is sufficient to produce a DC output voltage.

However, due to the high voltages (>50 volts) and low current outputs piezoeletrical materials are optimal for generating a conversion circuit was developed at Louisiana Tech. to a convert the high voltage to a regulated three volts at a conversion efficiency of 70%. (Kaajakari, 2010)

4.0 Battery Burdens for the Military

In this section the burden that batteries place on the military will be analyzed. The burdens will be discussed on a section-by-section scenario, where the is how the sections have been sub-divided: demand, acquisition costs, purchase price, transaction costs, transportation costs, storage costs, dissipation/loss of battery capacity, and disposal costs.

4.1 Demand

The demand burden refers specifically to a particular number of variables that determine the number or the amount of batteries required by the war fighter. These variables are dependent on the situation of the user or soldier and can be analyzed by using a spreadsheet tool developed by CECOM (U.S Army Communications-Electronics Command) which is called POWER (Power Optimizer for the War fighter's Energy Requirements). Variables include temperature, equipment that is being powered, and how frequently it is being used. Below is a flow chart of how POWER works. (T. O. Kiper, 2010)

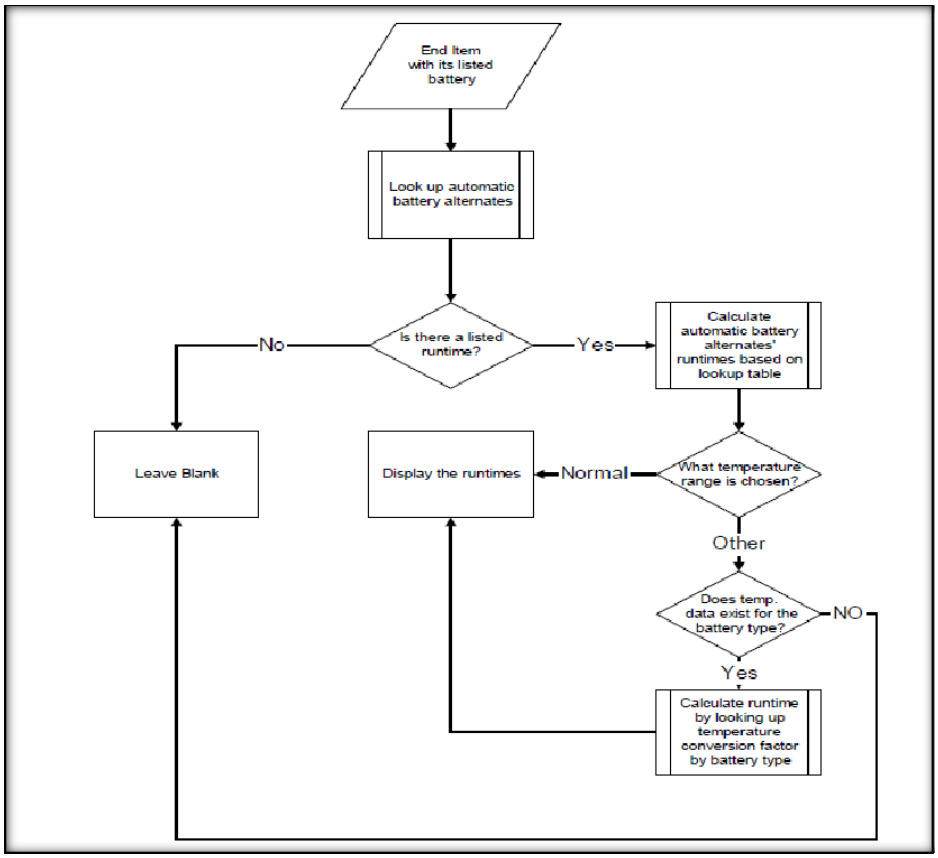

Figure 5: Power Flow Chart

The flow chart is a description of the steps that the program POWER takes in order to determine the runtime of the batteries in use according to the individual situation of the user. With this information it is possible to determine the amount of batteries which will be required.

4.2 Acquisition Costs

The acquisition costs were derived by analyzing several purchasing data made during the years of 2000 and 2009 which includes the time period of the war on terror. This means more military activity and operations. The purpose of this analysis was to determine the price difference between the military purchase and the manufacture's regular charges. The results show how the DLA's (Defense Logistics Agency) unit price was much higher than the normal manufacture price. In this case, the researchers used the manufactures contract price instead of the AMDF (Army Master Data File) to analyze the price difference. To further analyze these costs they were divided into sub elements which included purchase price, transaction costs, and proprietary costs factors.

4.3 Purchase Price

Table 2: Contracts of Purchases Made to SAFT for the BA-5590 Battery

Contract	Period (FY)	Quantity*	Unit Price* (FY$2000)
1	2000-2002	350,000	$60
2	2003-2007	2,000,000	$55
3	2008-present	37,000	$50

The preceding table shows the three primary contracts to purchase the BA-5590 Battery from SAFT. (T. O. Kiper, 2010)

Not all contracts were made by the same branch. Contract 1 was administered by the U.S Army Communications and Electronics Command (CECOM). In 2005 the DOD transferred all of CECOM contract activity to the DLA making them mostly responsible for contract 2. Contract 3 is to this day currently administered by the DLA as well.

Table 3: Battery Price Comparison between AMDF & SAFT

FY	AMDF unit price (FY00$)	Saft unit price* (FY00$)	% difference (AMDF/Saft*)
FY00	N/A	$60	
FY01	N/A	$60	
FY02	N/A	$60	
FY03	$79.80	$55	145%
FY04	N/1A	$55	
FY05	$72.29	$55	131%
FY06	N/A	$55	
FY07	N/A	$55	
FY08	$80.83	$50	162%
FY09	$83.24	$50	166%
FY10	$58.91	$50	118%
AVG	*$75.01*	*$54.73***	*145%*

*The preceding table represents the price difference in what the DLA charges to the service compared to what the DLA initially purchased from SAFT. *Note: Figures are rounded estimates; actual data is preserved by the authors and unable to be released because it is proprietary. **Note Average unit price calculated using actual proprietary data.*

It is clearly seen that the DLA charges the service considerably more than the original price paid to SAFT.

4.4 Transaction Costs

The transactions costs were analyzed by taking the average hourly salary for an 1102 Contract specialist and multiplying it by 9 hours or 200 hours depending on what type of contract they had (citation). In the following table the transaction costs of the purchases made by the DOD to Saft are shown. The average transaction cost per battery was set at $0.12 for practicality purposes. (T. O. Kiper, 2010)

Table 4: Transaction Cost for Several Contracts

Contract	Base Cost	Delivery Orders	Delivery Order Cost	Total Cost	Battery qty*	Cost per battery
1	$10,000	2	$900	$10,900	350,000	≈$0.03
2	$10,000	11	$4,950	$14,950	2,000,000	≈$0.01
3	$10,000	5	$2,250	$12,250	37,000	≈$0.32

*The table clearly shows the comparison of the cost per battery and the total cost paid by the DOD. We can see that delivering a $0.32 cent battery can become much more expensive due to all the transaction costs and fees. *Note: All figures are rounded estimates*

4.5 Transportation Costs

The costs for the military to deliver batteries to the soldier are divided into two sections. The first section is the cost that it takes to get batteries from the manufacturer to the location of where acceptances occur or the DOD supply depots. This first section is called First Destination Costs (FDC) by the 1998 Marine Corp Cost Estimating Handbook for estimating transportation costs. (T. O. Kiper, 2010) The second section is the cost it takes to deliver the batteries from the acceptance location to the deployment location; this is called Second Destination Costs (SDC). In order to be more specific in the cost calculation the Marine Corp cost estimating procedure involves taking into consideration weight, mileage, and dollar/ton/mile rate. According to the DOD Transportation Command the price per pound for over 100 batteries is $0.70.

4.6 Storage Costs

The Defense Logistics Agency (DLA) charges the service for the storage based on the amount of space it occupies and based on the storing conditions. Storing conditions offered by the DLA are open, covered, and special. Special conditions are design for hazardous material or for high value. The BA-5590 battery falls under such special conditions in which case would have to be stored in a more expensive environment. The following is a list of storage conditions along with their designated prices for the year 2010. (T. O. Kiper, 2010)

- Open $4.03 per cubic foot
- Closed $0.39 per cubic foot
- Special $5.59 per cubic foot

4.7 Dissipation/Loss of Battery Capacity

Although batteries may be re-chargeable, as time passes they tend to lose the ability to fully re-charge to their maximum capacity. This can be another financial burden to the service as they will have to spend more on batteries as time passes by, even for those they already have in their possession. The BA-XX90 battery was used as an example to determine the financial loss due to battery degeneration over time. The BA-XX90 has a cost of about $100 and a max capacity of about 1000 Watt/hrs. The battery cost in watt-hours is about $.010 Watt-Hours. Data collected for these batteries show that they lose 30% of capacity in 5 years. This means that at the end of 5 years this battery will only have the capacity of about 700Watt/hr, losing 60 W-h a year or 5 W-h a month. In the conditions that this battery would be used, the military, this battery could be in storage for up to 15 months, meaning that the battery would cost $7.50 more. (T. O. Kiper, 2010)

4.8 Disposal Costs

The disposal cost for batteries becomes more complicated simply because batteries being disposed of many times still have charge remaining. In which case this would be hazardous material and the method of disposal would have to be different with different expenses. In the paper Batteries on the Battlefield both methods, hazardous and non-hazardous, of disposal were analyzed. According to the document, batteries with hazardous material are disposed at $9.30 per battery. For those batteries with non-hazardous material the charge is $1.63 per battery. The only problem with these two methods is determining how much hazardous material remains in each battery which leads to more time and money loss. The Toxco Corporation manages disposal of Lithium Sulfur Oxide batteries for commercial use and have conducted disposal for the DOD as well. According the Batteries on the Battlefield article, Toxco's own testimony was that the price to dispose of battery per pound was on average between $2.50 and $3.50 regardless of the

hazardous condition. The difference in pricing can be due to the type of battery or the distance between the battery pick up and the disposal site. (T. O. Kiper, 2010)

4.9 Environmental Costs/Overall Burden Scenarios

Some batteries can be harmful to the environment if not properly disposed of and even when they are disposed of properly they can have some minor effects that over time can develop into more serious situations. The main worry is that in the heat of combat or for other convenient reasons soldiers may inappropriately dispose of batteries unwillingly causing harm to the surrounding environment. A study done by Ross and Hull from April 1997-April 1998 on the usage of the BA-5590 by the military in simulated combat missions at Joint Readiness Training Center, shows that 29% of batteries that units turned in still had about 70% of charge left. (T. O. Kiper, 2010) This gives an insight of the amount of damage that can be caused to the environment along with monetary costs. According to the study done be Ross and Hull, the starting environmental cost for a single BA-5590 would be about $9.00.

In the document Batteries on the Battlefield (BOB) two scenarios were developed in order to simulate overall costs and burdens of batteries for the military.

4.9.1 Scenario 1: Time of Peace/No Immediate War

In this scenario the document BOB states a time of peace in which soldiers are not deployed but training operations are ongoing. For this research they used a U.S Light Infantry Company at Fort Stewart, Georgia which was conducting peace time operations over a seven day period. The following figure demonstrates the cost of implementing the BA-5590 battery in this specific scenario.

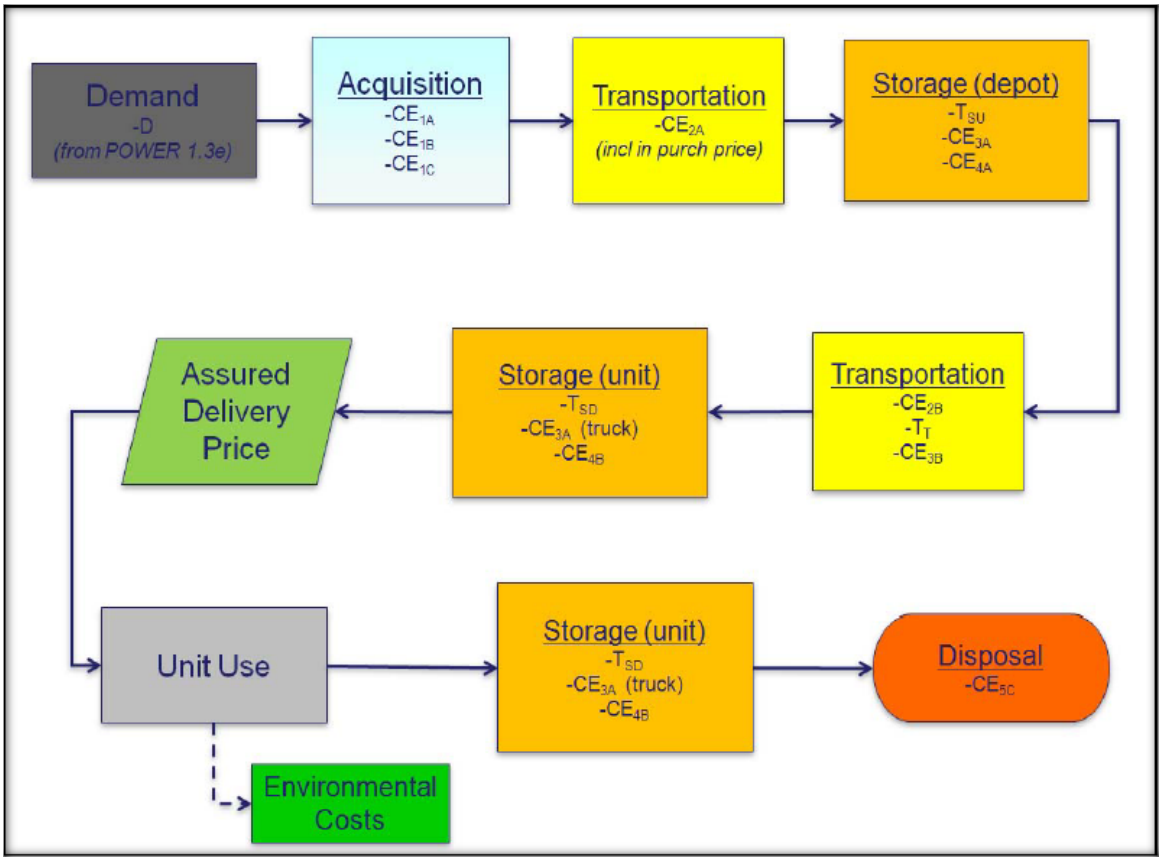

Figure 6: Flow Analysis of BA-5590 Battery on Peace time Scenario

Flow analysis of typical costs allocated during life of BA-5590 battery with respect to a typical peace time scenario.

Using the program previously mentioned, POWER, the authors of BOB, Troy O.Kiper et al., were able to determine the amount of batteries that the soldiers from this scenario would need for various day's missions and the amount of weight that it would total to. They analyzed specifically the batteries required to power the AN/PRC-117F radio for this training missions.

Table 5: Total Weight, Orders, and Batteries Respective to Scenario One

Battery: BA-5590B/U (4 per pkg) **Device: AN/PRC-117F radio (21 per mission)**	# Batteries Required	# Packages to order	Battery Weight (lbs)
Minimum for 1 day mission (chg every 12 hrs)	84	21	189
Minimum for 1 day mission (chg every 18 hrs)	84	21	189
Minimum for 7 day mission (chg every 12 hrs)	588	147	1323
Minimum for 7 day mission (chg every 18 hrs)	420	105	945
Minimum for 30 day mission (chg every 12 hrs)	2520	630	5670
Minimum for 30 day mission (chg every 18 hrs)	1680	420	3780

The preceding table outlines the batteries required and battery weight carried during a peacetime scenario in order to operate AN/PRC-117F radios during several scenario missions.

4.9.2 Scenario 2: Operational Time/War

In this scenario the time period of war is simulated. For this, the authors of BOB utilized a Marine Energy Assessment Team (MEAT) visit to Afghanistan. The team performed and energy for USMC forces operating in Helmand Province Afghanistan in September 2009. The following is a figure demonstrating the burden of the BA-5590 battery in this specific scenario. (T. O. Kiper, 2010)

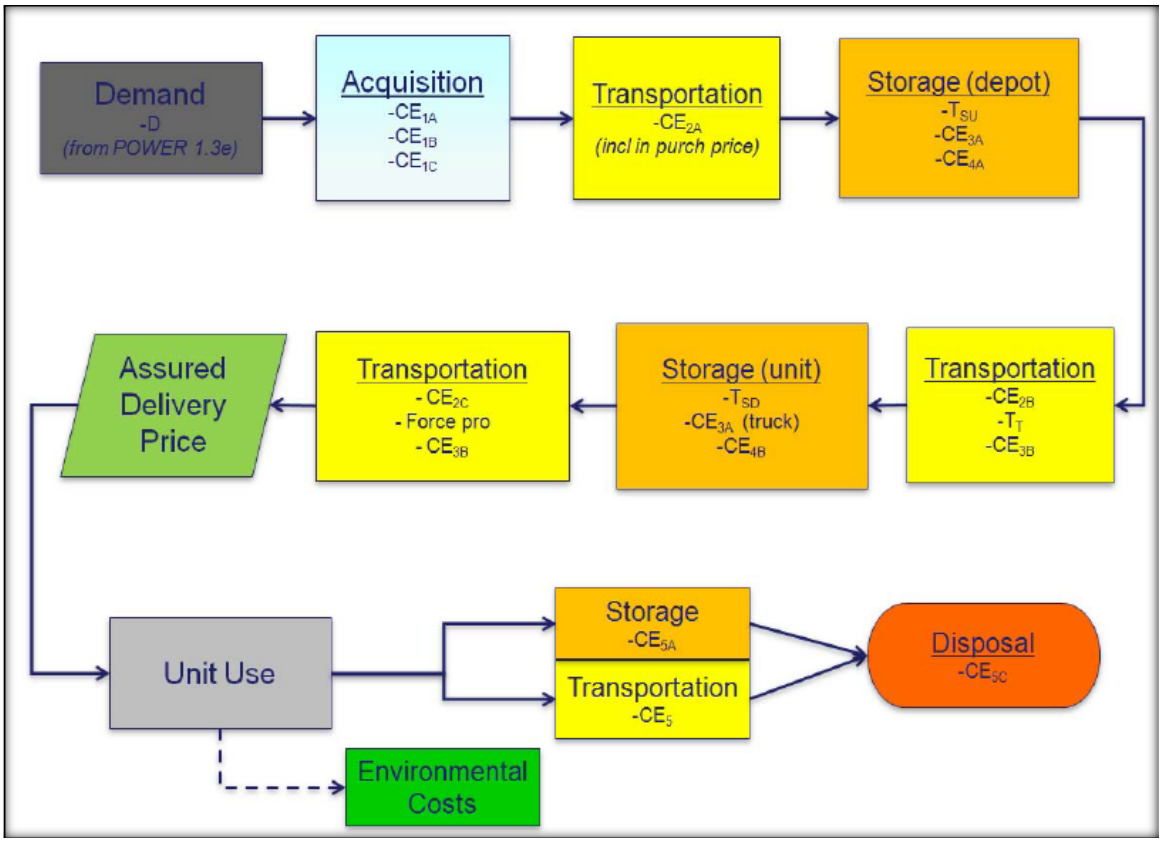

Figure 7: Burden of BA-5590 Battery on Operational Scenario

Flow analysis of typical costs allocated during life of BA-5590 battery with respect to a typical war time scenario.

Again the authors of BOB used POWER in order to determine the amount of batteries used for the AN/PRC-117F radio along with the weights in various missions with different duration periods.

Table 6: Total Weight, Orders, and Batteries Respective to Scenario Two

Battery: BA-5590B/U (4 per pkg) **Device: AN/PRC-117F radio (46 per mission)**	# Batteries Required	# Packages to order	Battery Weight (lbs)
Minimum for 1 day mission (chg every 12 hrs)	184	46	414
Minimum for 1 day mission (chg every 18 hrs)	276	69	621
Minimum for 7 day mission (chg every 12 hrs)	1288	322	2898
Minimum for 7 day mission (chg every 18 hrs)	1932	483	4347
Minimum for 30 day mission (chg every 12 hrs)	5520	1380	12,420
Minimum for 30 day mission (chg every 18 hrs)	8280	2070	18,630

The preceding table outlines the batteries required and battery weight carried during a wartime scenario in order to operate AN/PRC-117F radios during several scenario missions.

5.0 Problem Formulation

The problem formulation methodology for this project will be as follows:

- Define *Need Statement*
- Problem Definition
  - Quality Function Deployment (QFD)
  - Objectives& Constraints
  - Key Topics

5.1 Need Statement

The *Need Statement* is a document which outlines the true user need, for this instance our need statement is as follows:

> *Design and develop a biomechanical energy harvester which adheres to the product specifications outlined by Northrop Grumman: with the intent of supplanting a fraction of soldier dependence on batteries.*

5.2 Customer Survey

In order to determine the wants/needs data from the consumer a customer survey was developed; a sample of the survey may be seen below and in the appendices.

The customer survey was presented to a group of ten people based on a careful analysis of those things needed to be answered in order to meet desired design criteria. The audience was given several questions in various topics like specifications of the device, environment in which it would be used, and type of output port. It was necessary to know the level of importance given to each of the given options presented under these categories in order to save time, money, and focus our energy with the more critical issues of the design.

CUSTOMER SURVEY

Name:	Age:	Gender:
Objective: To produce a wearable mechanism which converts biomechanical motion into storable electrical energy.		

For each question below, circle the number to the right that best fits your opinion on the importance of the issue. Use the scale to match your opinion.

Question	Scale of Importance				
	Not at all	Not very	No Opinion	Some-what	Extremely
Physical look of the mechanism	1	2	3	4	5
Device's weight	1	2	3	4	5
Durability and impact resistance	1	2	3	4	5
Flexibility and freedom of movement	1	2	3	4	5
Ergonomics of device	1	2	3	4	5
Ease of attachment	1	2	3	4	5
Power level indicator feature	1	2	3	4	5
Charge rate	1	2	3	4	5
Price	1	2	3	4	5
Inconspicuousness of the device	1	2	3	4	5
Compliance with general safety regulations	1	2	3	4	5

Rate the following according to amount of expected use

Question	Scale of Importance				
	Never	Rarely	Casually	Often	Very often
Environment					
Athletic training	1	2	3	4	5
Water sports	1	2	3	4	5
Daily Commuting	1	2	3	4	5
Continuous wear	1	2	3	4	5
Charge port type					
Micro/mini-usb	1	2	3	4	5
Standard usb	1	2	3	4	5
Car cigarette lighter	1	2	3	4	5
U.S. standard outlet	1	2	3	4	5

Figure 8: Customer Survey

*An example of the customer survey distributed to several project associated individuals.*Note: Please see a full-size version in the appendices*

The results of this survey were used to create a Pareto chart which will help us graphically visualize the weighted importance of the design preferences; therefore, aiding us in the concept design process.

5.3 Quality Function Deployment (QFD)

Quality Function Deployment (QFD) was a technique originally developed by the Japanese Automobile industry as a tool to compile several sources of data. It is not easy to gather and interpret the wishes of a consumer, but the task of designing a product for a general success is even more difficult since the consumer is only the end point in the product pipeline. Between the product's conception and consumer usage lays a long path that includes design issues and problems, manufacturability issues, marketing, and competitive issues.

The design group was able to gather the data for our QFD chart from the results of our customer survey; the proceeding figure is a representation of the resulting QFD; however, a full-size version may be seen in the appendices.

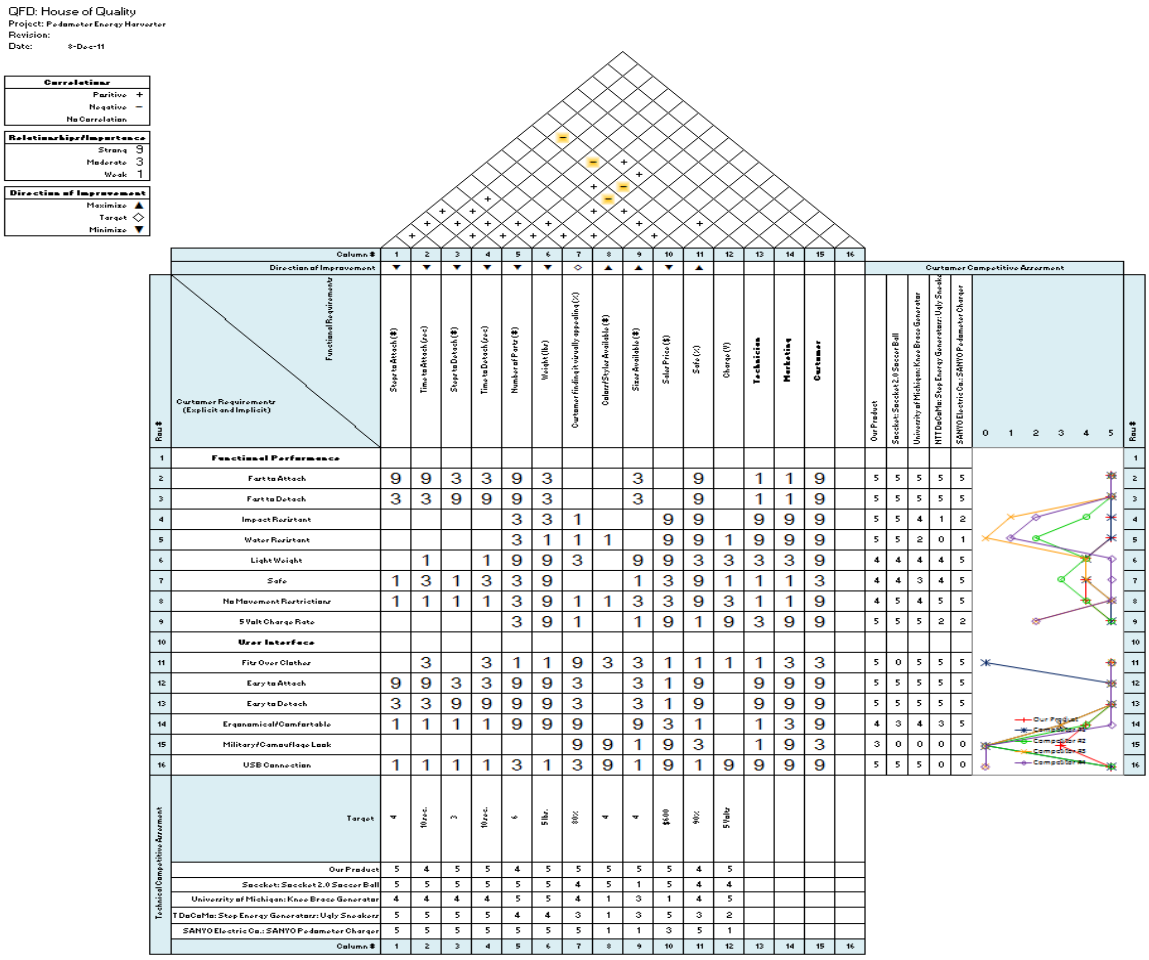

Figure 9: Quality Function Deployment Chart

*The House of Quality, otherwise known as the: Quality Function Deployment chart, was utilized to identify the strength of correlation between the design project's customer and functional requirements.*Note: Please see a full-size version in the appendices*

The top portion of our QFD chart shows the correlation between each of the function requirements. These correlations are labeled with a plus sign, meaning a positive correlation, or with a minus sign, meaning a negative correlation. If the section between two functions is left blank, there is no correlation. The middle section shows the relationship between our customer requirements and our functional requirements. These relationships are identified with a 1, being a weak relationship, 3, being a moderate relationship, and 9, being a strong relationship. From these relationships we were able to prioritize our customer requirements. For Example, based on the data we know that we must focus on integrating a USB port into our device. The bottom portion of our QFD chart includes our target goals. A scale of 1-5, 1 being the least and 5 being the greatest, was used to show how close our competitors' products and our ideal concept is to the goals we have set. The data shows that we have more than 1 competitor that is close to our

set goals. Although, some of these products don't fall in the same design category of our product but do contain the same concept of our project.

5.4 Pareto Analysis

In the proceeding section the design group will describe and present the Pareto analysis with the data collected from our customer survey.

The Pareto analysis helped the design group to visualize the level and order of importance of each customer requirement by utilizing a chart that integrates both a bar graph and a line graph. The bar graph was created in a descending order by placing higher importance requirements on the left of the chart and the least important on the right. This graph utilizes the frequency and category axes.

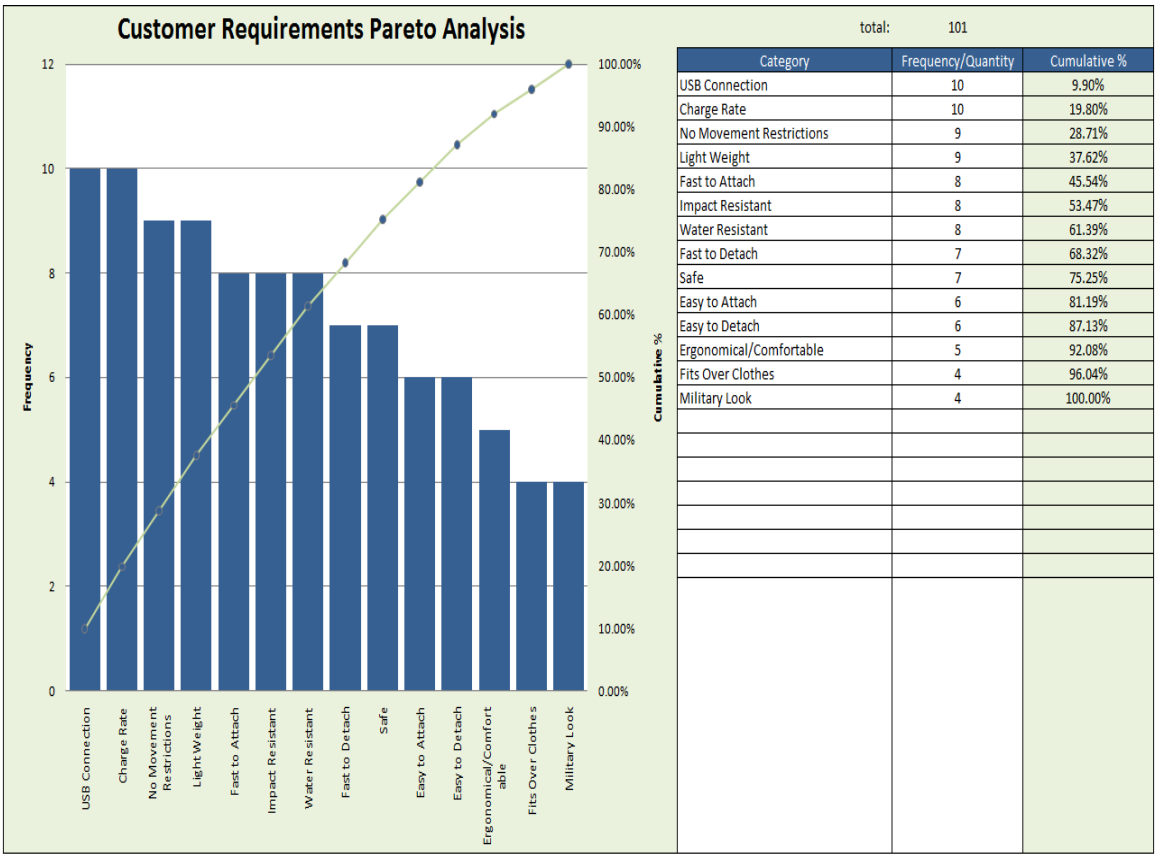

total: 101

Category	Frequency/Quantity	Cumulative %
USB Connection	10	9.90%
Charge Rate	10	19.80%
No Movement Restrictions	9	28.71%
Light Weight	9	37.62%
Fast to Attach	8	45.54%
Impact Resistant	8	53.47%
Water Resistant	8	61.39%
Fast to Detach	7	68.32%
Safe	7	75.25%
Easy to Attach	6	81.19%
Easy to Detach	6	87.13%
Ergonomical/Comfortable	5	92.08%
Fits Over Clothes	4	96.04%
Military Look	4	100.00%

Figure 10: Pareto Analysis of Customer Analysis

*Pareto analysis of customer requirements garnered from distribution of customer survey. The Pareto analysis's primary purpose is to assign a quantitative level of importance to customer requirements.*Note: Please see a full-size version in the appendices*

For this design case, the customer's main requirement for our product is for it to have a USB interface/connection and is least concerned with the requirement for the product to have a military look. The line graph was created using a cumulative percentage obtained from the frequency percentage of each requirement and the category axis. This graph allows us to see what category will lead us into the most problems by focusing more on it. In our case, by focusing more on integrating a USB connection into our product we will have more success than if we were to focus on giving it a military look. This graph also serves the purpose for a tie braking situation. Since some of our requirements were of equal importance the line helped us visualize which category we would have more trouble working with. The Pareto analysis extended to our decision making process and helped us clarify our main focus points for our product.

5.5 Objectives & Constraints

The objective is to produce a prototype pedometer accessory that produces and locally stores a useable amount of power and demonstrate its capability. Desired outputs include 5 volts USB type power and or 12 Volt DC cigarette outlet type power. Goals would be for a substantial proposal or better yet a styled and ergonomically cohesive model which installs easily to the knee, ankle, or shoe.

The proceeding list is a set of design requirements as set forth by Northrop Grumman:

- Detect & convert human motion into useable energy
- Generate 5 volts DC and 50 milliamps of voltage and current, respectively
- Operating temperatures: 10 to 25º C
- Deliver nominal power to a USB port charged device

The preceding list, in essence, is what the design group deems to be the product design specifications (PDS).

5.6 Key Topics

The following is a set of key topics which must be explored in order for adequate completion of this project:

- Mechanical and Packaging
- Electrical/Power Conversion/Batteries
- Simulation (CAD, Mathematical, etc.)
- Materials Selection
- Safety/Human-Component Interaction
- Industrial Design
- Human and Ergonomic Engineering
- Embedded Software/ PC Interface Software

6.0 Technical Research

6.1 Electrical Energy Storage

Broadly speaking there are two ways to store electrical energy, chemically and statically, these two storage methods are examples of the following electrical components: batteries and capacitors, respectively. The way each method stores its energy is distinct from one another and whichever component is chosen is based upon system design requirements, limitations and ultimately the end purpose of the system.

6.1.1 Batteries

We will begin our discussion of electrical energy storage mediums with an overview of the batteries.

Electrons that are a part of the molecules of the chemicals or substances in a battery are coaxed to leave those chemicals or substances and become a part of the electrical current that we use. In virtually all batteries the process is reversible to some extent. If electrons are returned to the chemicals or substances in a battery, the electrons can again be used as electrical current. In disposable batteries the process cannot be reversed very well, and in most cases, it is either impractical or unsafe to do so. In reusable or rechargeable batteries, the process can be more readily reversed with a battery charger. Battery chargers return electrons to the chemicals or substances in batteries. In the case of most batteries sold as rechargeable, the process can be reversed very well, but not perfectly. Even with the best of care, after a number of years rechargeable batteries become unusable.

Common types of rechargeable batteries:

- Lead Acid
- Lithium Ion
- Lithium Ion Polymer
- Nickel Cadmium
- Nickel Metal Hydride
- Reusable Alkaline

Lead Acid-The acid in some lead acid batteries is a liquid, as is the case with automobile batteries; however, in other lead acid batteries the acid is in the form of a gel.

Lithium Ion Polymer-Lithium ion polymer batteries have similar energy for their mass as Lithium ion batteries, but at potentially lower cost. The technology of Lithium polymer batteries is very new and still evolving.

Nickel-Metal Hydride (NiMH)-NiMH batteries store somewhat more energy than NiCad, but for a shorter period of time. Low Self Discharge (LSD) batteries are a new type of NiMH battery. LSDs are different than other rechargeable batteries because they lose significantly less charge when not in use. Data shows that LSD batteries discharge at a rate of 15 percent per year, compared to 4 percent per day for ordinary NiMH.

Lithium Ion-Lithium ion batteries can store much more energy for their mass than most other types of batteries. Lithium is the lightest of all metals and is the third lightest element after Hydrogen and Helium. Lithium ion batteries are more expensive than other types.

Nickel Cadmium (NiCad)-NiCad technology is mature and well understood, however NiCad batteries store relatively less energy than Lithium ion and Lithium ion polymer batteries. NiCad batteries are used where long life, high discharge rate, and low price are important. See Rechargeable Batteries and Changers for more details.

Reusable Alkaline-Reusable alkaline batteries provide fewer charge/discharge cycles than any other rechargeable battery. However, they hold their charge longer than some types. (CalRecycle, 2011)

6.1.2Capacitors

Before there were batteries there were was the method of storing electrical charge statically. Experimenters learned that an electrical charge could be stored between two sheets of metal that were positioned close to each other. Although, this type of device has had multiple names throughout history we now associate the name term “capacitor” with technology of this sort.

Capacitors store electrical energy in an electrostatic field and consist of two electrodes of opposite polarity separated by a dielectric or electrolyte. A capacitor is charged by applying a voltage across the terminals which cause positive and negative charges to migrate to the surface of the electrode of opposite polarity. The capacitance of the charge stored between the electrodes can be determined by the following equation:

$$C = \varepsilon_o \varepsilon_r \frac{A}{d}$$

In the preceding equation the following variables are defined as:
C-capacitance (Farads)
A-area of the electrodes (m2)
ε_o-permittivity of free space (8.854 × 10-12 F/m)
ε_r-dieletric constant or relative permittivity of the material between the plates
d-distance between the plates (m)

The energy stored is related to the charge at each interface, q (Coulombs), and potential difference, V (Volts), between the electrodes. (Electropedia, 2005) The energy, E (Joules), stored in a capacitor with capacitance C (Farads) is given by the following formula:

$$E = \frac{1}{2} qV \; or \; \frac{1}{2} CV^2$$

6.1.3 Battery to Capacitor Comparison

Capacitors have some significant advantages over batteries, for example, the energy in a capacitor can be transmitted more quickly, the storage capacity doesn't degrade as much with use, and the materials are generally not toxic. However, some major issues capacitors need to overcome and which may or may not prove insurmountable have to do with the amount of energy a capacitor can store-even the best currently store less than batteries. Due to the fact capacitors store charge only on the surface of the electrode they, relatively speaking, have lower energy storage capability and lower energy densities when compared to batteries. A comparison between batteries and capacitors are shown below:

Table 7: Capacitor/Battery Comparison

Device	Energy Density (Wh/L)	Power Density (W/L)	Life Cycle (cycles)	Discharge Time (sec.)
Batteries	50-250	150	$1\text{-}10^3$	>1000
Capacitors	.05-5	$10^5\text{-}10^8$	$10^5\text{-}10^6$	<1

The preceding table is a comparison of typical energy and power density, life cycle, and discharge time figures of batteries and capacitors.

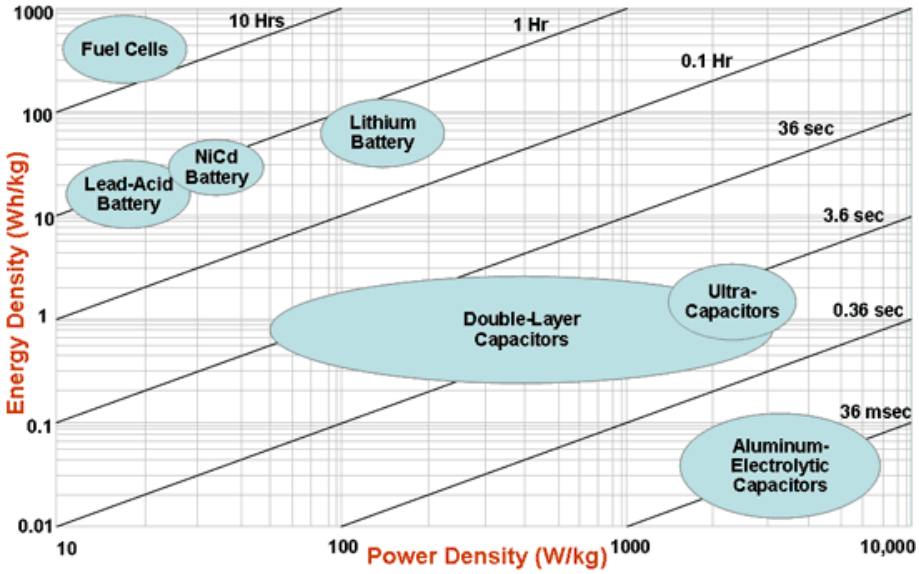

Figure 11: Ragone Plot of Electrochemical Devices

The Ragone plot above compares power density, energy density, and relative charge/discharge times for a range of electrochemical devices. The sloping lines on the Ragone plots indicate the relative time to charge/discharge the device.

6.2 Biomechanical to Electrical Energy Generators

Energy harvesting generators are attractive in the sense of being used to replace batteries in low-power electronic devices. Ambient motion can produce more than enough energy to power these

devices. Below are different methods and devices that can help transform this energy into usable electricity in order to power our portable electronic devices.

Energy harvesting generators are attractive in the sense of being used to replace batteries in low-power electronic devices. Ambient motion can produce more than enough energy to power these devices. Below are different methods and devices that can help transform this energy into usable electricity in order to power our portable electronic devices.

6.2.1 Direct Force Generators

A driving force $f_{dr}(t)$ acts on a proof mass, m, supported on a suspension with spring constant, k, with a damping element present to provide a force $f(\dot{z})$ opposing the motion. If the damper is implemented using a suitable transduction mechanism, then in opposing the motion, energy is converted from mechanical to electrical form. There are limits of (+ or -) Z_l on the displacement of the mass, imposed by device size. Direct force generators must make mechanical contact with two structures that move relative to each other, and can thus apply a force on the damper. The system dynamic model can be seen below. (P. D. Mitcheson, 2008)

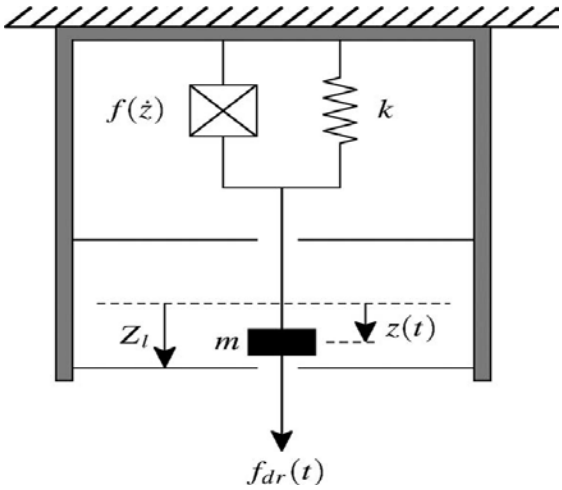

Figure 12: System Dynamic Model of Direct-Force Generator

The preceding figure is simplified model of how various I, C and R-elements, respond in relation to the effort source input $f_{dr}(t)$ when considering the system model of direct-force generators.

6.2.2 Inertial Generators

A proof mass is supported on a suspension and its inertia results in a relative displacement z(t) when the frame, with absolute displacement y(t), experiences acceleration. The range of z(t) is again (+ or -) Z_l. Energy is converted when work is done against the damping force $f(\dot{z})$, which opposes the relative motion. Inertial generators require only one point of attachment to a moving structure, which gives much more flexibility in mounting than direct-force devices and allows a

greater degree of miniaturization. The proceeding figure shows the system dynamic model for an inertial generator. (P. D. Mitcheson, 2008)

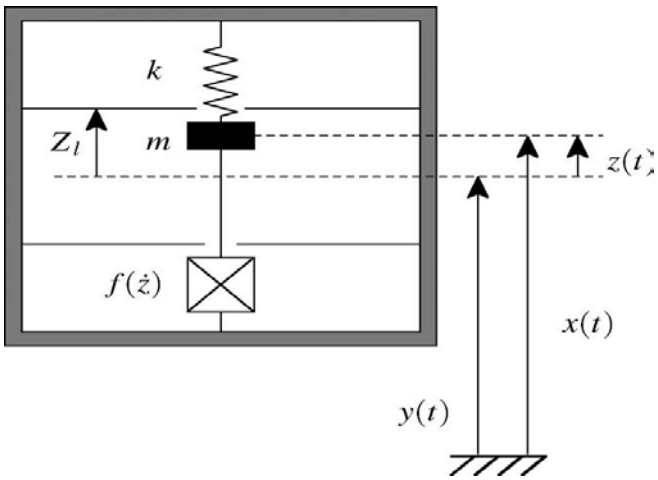

Figure 13: System Dynamic Model of an Inertial Generator

The preceding figure is simplified system dynamic model of the inertial storing element, mass, and how this element responds in relation to C and R-elements: spring and damper, respectively.

6.2.3 Transducer Type

In order to generate power, the damper must be implemented by a suitable electromechanical transducer. These can be done using one of the following methods described below.

- **Electromagnetic (IG):** An example of this type of mechanism is an asymmetric proof mass, freely rotating about a point some distance from the center of mass, attached to a permanent magnet electrical generator, through high gear ratios (Ex: Seiko Kinetic watch). A more generic patent on inertial generators, from Tiemann in 1996, proposes the use of relative movement between magnets and coils in a mass-spring system to generate electrical energy from linear vibrational motion. (P. D. Mitcheson, 2008)

- **Electrostatic (IG):** Mechanical forces are imposed to do work against the attraction of oppositely charged parts. Such devices are mechanically variable capacitors whose plates are separated by the movement of the source. They have two fundamental modes of operation: switched and continuous. A practical restriction of electrostatic transducers is that they require a pre-charge voltage in order to operate. An electric, or a permanent charge buried in a dielectric layer, can help solve this problem. (P. D. Mitcheson, 2008)

- **Piezoelectric (DFG & IG):** A phenomenon whereby a strain in a material produces an electric field in that material, and conversely an applied electric field produces a mechanical strain. When an external force is applied, some of the mechanical work done is stored as elastic strain energy, and some in the electric field associated with the

induced polarization of the material. If an external conduction path through a load is provided, a current that neutralizes the net charge results. Piezoelectric materials with high electromechanical coupling coefficients are generally ceramics, with lead zirconate titanate being the most common. Such materials do not tolerate high strain levels, so some form of lever is required to combine them with devices of significant relative displacement. The most common geometry is to apply the piezoelectric as a thin layer on a cantilever beam from which the proof mass is suspended. (P. D. Mitcheson, 2008)

6.2.4 Comparison of Transducer Systems

The proceeding tables show the several key factors such as: effectiveness, power generation, generator volume, etc. of pre-existing transducer systems composed by a myriad of researchers.

Table 8: Comparison of Effectiveness of Published Electromagnetic Motion Harvesters

Author	Reference	Generator Volume [cm^3]	Proof Mass [g]	Input Amplitude [μm]	Input Frequency [Hz]	Z_l [μm]	Power (unprocessed) [μW]	Power (processed) [μW]	Power Density [$\mu W/cm^3$]	Harvester Effectiveness [%]	Volume Figure of Merit [%]
Li	[91]	1.00	0.22	200	60	5000		100	100	1.70	0.08
Li	[91]	1.00	0.22	200	120	1000		100	100	1.07	0.01
Ching	[130]	1.00		210	107		1.50		1.50		0.2×10^{-3}
Ching	[130]	1.00		190	104		5.00		5.00		0.8×10^{-3}
Li	[131]	1.24	210	100	64			10	8.06		0.01
Williams	[89]	0.02	2.4×10^{-3}	0.50	4400	63	0.33		22	0.04	7×10^{-5}
El-hami	[132]	0.24	0.50	25	322	940	530		2208.3	1.09	0.14
Ching	[133]	1.00		200	60			680	680		0.52
Ching	[133]	1.00		200	110			680	680		0.08
Ching	[92]	1.00		200	60			830	830		0.64
Ching	[92]	1.00		200	110			830	830		0.1
Mizuno	[108]	2.10	0.54	0.64	700	6.5	0.4×10^{-3}		0.2×10^{-3}	0.42×10^{-3}	2.26×10^{-6}
Lee	[134]	7.30	0.14	150	85	7500	830		114	6.92	0.02
Glynne-Jones	[135]	0.84		13	322	360	37		44.0		0.003
Beeby	[136]	0.10	0.03	5.4×10^{-3}	9500	500	0.02		0.21	2.6×10^{-3}	3.27×10^{-5}
Beeby	[137]	0.06	0.44	0.62	350	217	2.85		47.5	0.90	0.15
Beeby	[137]	0.07	0.03	0.98×10^{-3}	9500	240	0.12		1.79	0.02	0.174×10^{-3}
Serre	[138]	0.68	1.56	3.40	360		0.05		0.07		1.6×10^{-5}
Saha	[96]		43	115	13.1	1250	2000				
Saha	[96]		25	28	84	1500	3200				
Huang	[139]	0.04	0.03	50	100	5200	1.44		40	0.14	0.08
Perpetuum	[140]	131		0.633	99			800	6.1		0.065
Perpetuum	[140]	131		2.54	99			3500	27		0.07
Perpetuum	[140]	131		25.4	99			40000	306		0.08
Ferro Solutions	[141]	133		1.73	60		800		6.0		0.1
Ferro Solutions	[141]	133		3.45	60		3100		23		0.2
Ferro Solutions	[141]	133		6.9	60		10800		81		0.35

Tables 2, originally published by Mitcheson, et al. (2008) in the article titled Energy Harvesting from Human and Machine Motion, compares several effectiveness parameters of electromagnetic energy harvesters.

Table 9: Comparison of Effectiveness of Published Electromagnetic Motion Harvesters

Author	Reference	Generator Volume [cm^3]	Proof Mass [g]	Input Amplitude [μm]	Input Frequency [Hz]	Z_l [μm]	Power (unprocessed) [μW]	Power (processed) [μW]	Power Density [$\mu W/cm^3$]	Harvester Effectiveness [%]	Volume Figure of Merit [%]
Tashiro	[104]		640	380	4.76	19000		58		0.09	
Tashiro	[142]	15	780	9000	6		36		2.42		0.02
Mizuno	[108]	0.6	0.7	0.64	743	4.9	7.4×10^{-6}		1.23×10^{-3}	6.6×10^{-6}	1.86×10^{-9}
Miyazaki	[143]		5	1	45	30		0.21		12.4	
Arakawa	[144]	0.4	0.65	1000	10	1000	6		15	7.42	0.68
Despesse	[145]	18	104	90	50	90	1760	1000	56	7.66	0.06
Yen	[146]				1500			1.8			
Tsutsumino	[147]			600	20	600	278				
Tsutsumino	[148]			1000	20	1000	6.4				
Mitcheson	[109]	0.6	0.12	1130	20	100	2.4		4	17.9	0.02

Table 3, originally published by Mitcheson, et al. (2008), compares several effectiveness parameters of electrostatic motion energy harvesters.

Table 10: Comparison of Effectiveness of Published Piezoelectric Motion Harvesters

Author	Reference	Generator Volume [cm^3]	Proof Mass [g]	Input Amplitude [μm]	Input Frequency [Hz]	Z_l [μm]	Power (unprocessed) [μW]	Power (processed) [μW]	Power Density [$\mu W/cm^3$]	Harvester Effectiveness [%]	Volume Figure of Merit [%]
Glynne-Jones	[149]	0.53			80.1	800	1.5		2.83		
Roundy	[2]	1	8.5	4	120	150	80		80	7.3	0.39
Roundy	[2]	1	7.5	7.9	85	143	207	90	90	14	0.62
Roundy	[2]	1	8.2	16	60	150	365	180	180	34	1.74
Wright	[2], [123]	4.8	52.2	36	40		1700	700	145		1.25
Lefeuvre	[150]	113	228		56	2000		10000	88		
Lefeuvre	[150]	113	228		56	2000		300000	2650		
Lefeuvre	[151]				Random				15000		
Tanaka	[152]	9		10	50		180		20		0.26
Fang	[153]	0.0006	0.0015	4.4	609		2.16		3510		1.39
Elvin	[154]	0.101	1.2	earth quake spectrum	0.5	2000	0.25		2.47		
Duggirala	[155]				38		0.17				
Duggirala	[155]				38		1.13				
Jeon	[156]			32.5	13900	2.56	1				
Ng	[157]	0.20	0.96	184	100		35.5	16.3	82		0.03
Ferrari	[158]		82	0.053	41			0.27			
Mide	[159]	40.5		99	50			8000	198		0.16
Mide	[159]	40.5		11	150			1800	45		0.012

Table 4, originally published by Mitcheson, et al. (2008) in the article titled Energy Harvesting from Human and Machine Motion, compares several effectiveness parameters to one another of piezoelectric systems.

6.3 Human Energy Sources

The following section aims to explain the theory and the logic underlying energy harvesting from humans by exploiting human mechanical motions.

The idea of harvesting energy from human motion is based upon the fact that the average energy expenditure a person or amount of energy used by the body is 1.07*107 joules per day. (McArdle W.D., 2001) This amount of energy is equal to an estimated 800 AA batteries rated at 2500 mAh, whose total weight is approximately 20 kg; however, instead of carrying the load of 20 kg in batteries the human body utilizes the highly energy dense source of 0.2 kg of body fat to produce this type of energy output. (Raziel Riemer, 2011)

The significant amount of energy released from the human motion and the energy dense source of body fat give substantial reasoning for attempting innovation of technologies which may harvest this energy for powering electrical devices. The body motions which will be analyzed are as follows: heel strike, center of mass motion, along with ankle, knee, and hip motions.

6.3.1 Heel Strike

The term heel strike refers to the part of the walking gait cycle in which the heel of forward leg extremity impact with the ground.

Based upon previous research done by Penglin Niu and et al, the maximum ground reaction force acting upon the heel is equal to approximately 1.2 times the body weight. (P. Niu, 2004) If a displacement of 4 mm from the shoe sole and body weight of 80 kg (176.37 lbs) of the human subject are assumed then by utilizing the following equation work done during the heel strike may be calculated:

$$W = \int_{s_0}^{s_f} F_s(s)ds$$

where $F_s(S)$ is the force function along the direction of movement, ds is the differential displacement, and s_o and s_f are the initial and final location. Utilizing the preceding information the done by the heel strike was calculated to be approximately 2 J/step. Due to the fact that the average walking speed has a frequency of 1 Hz (two steps per second), the maximum power generated per walking stride is approximately 2 watts. (Raziel Riemer, 2011)

6.3.2 Joint Movement

During the course of the normal walking gait torques at the ankle, knee, and hip are created. The work performed at different leg joints during a single step was calculated by Winter and et al; furthermore, they coalesced their work into categories and divided the net work done into several phases of motion.

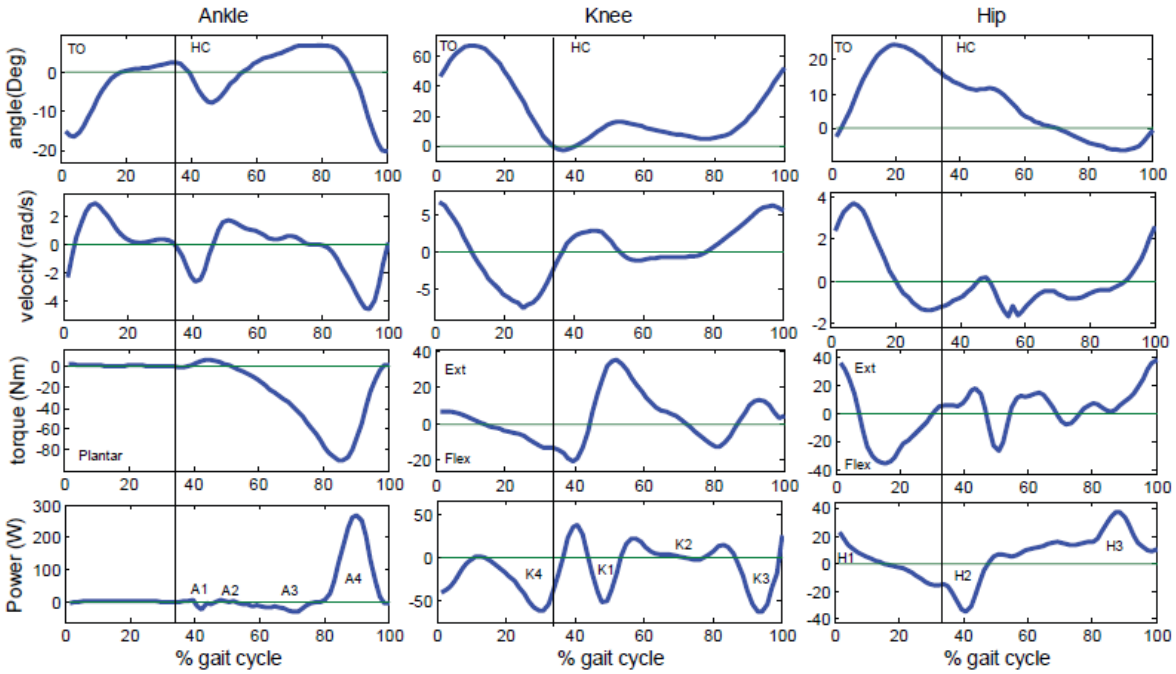

Figure 14: Typical Kinetics during a Walking Cycle

The preceding figure shows the typical kinematic and kinetic forces each joint experience during the walking gait. The subject parameters are were defined as an individual with a mass of 58 kg, walking at a speed of 1.3 meters per second, and a cycle frequency of 0.9 hertz. (Winter A. D., 2005)

From the preceding figure Riemer and Shapiro calculated the joint work for each step of an 80 kg subject utilizing the following equation:

$$\frac{Work}{Step} = Weight \times [|phase_1| + |phase_2| + \cdots + |phase_n|]$$

Table 11: Work at Leg Joints during Walking Step Normalized by the Subject's Mass

work during the phase (J/kg)	average (J/kg)	standard deviation (J/kg)
Ankle A-1	-0.0074	0.0072
Ankle A-2	0.0036	0.0046
Ankle A-3	-0.111	0.042
Ankle A-4	0.296	0.051
Knee K-1	-0.048	0.032
Knee K-2	0.0186	0.026
Knee K-3	-0.047	0.015
Knee K-4	-0.114	0.015
Hip H-1	0.103	0.047
Hip H-2	-0.044	0.029
Hip H-3	0.090	0.027

The preceding table outlines the work during several phases of human mechanical joint movements where phases A1-4, K1-4, and H1-3 are for the ankle, knee, and hip joints, respectively.

Table 12: Work by Human Mechanical Motion of the Body during Normal Walking Gait

joint	work [J]	power [W]	max torque [Nm]	negative work	
				%	J
Heel strike	1-5	2-20		50	1-10
Ankle	33.4	66.8	140	28.3	19
Knee	18.2	36.4	40	92	33.5
Hip	18.96	38	40-80	19	7.2
Center of mass	10**	20**		***	
Elbow	1.07	2.1	1-2	37	0.8
Shoulder	1.1	2.2	1-2	61	1.3

*With the exclusion center mass and heel strike, all calculations were performed for an 80 kg person at a walking frequency of 1 Hz per cycle. ** Energetic cost of transporting a 20 kg payload with a walking frequency of 1 HZ per cycle. *** Center of mass also includes muscle negative work, however the magnitude is not known.*

6.3.3 Center of Mass Motion (CMM)

The next type of motion which could be analyzed is the human center of mass motion. During the normal walking cycle the center of mass motion can be expressed in the x, y, and z coordinate planes, i.e. side-to-side, front-to-back, and up-down. This type of motion causes a unique problem because unlike the mostly single degree of freedom (DOF) movements expressed at the knee and heel strike areas the center of mass motion source would require a 3rd DOF energy harvesting design in order to optimally harness all degrees of motion.

However, due to the limitations of this design project the center of mass motion will be simplified as a single DOF movement, whereas, analysis will be performed taking into account the vertical motion movement, approximately 5cm. (Raziel Riemer, 2011)In order to estimate the upper bound limitation of energy required to generate relative motion between the external mass and subject motion Riemer et al. utilized the following equation:

$$E = 2m \times g \times h$$

Where E is defined as energy, m is the external mass figure, g is the gravitational acceleration, and h is the height. By idealizing the scenario to a zero degree of exchange between kinetic and potential energy, applying a CMM of 5 cm, external mass of 20 kg, and gravitational acceleration of 9.81 m/s^2 it is determined there is a potential for harvesting 20 watts of energy from this specific movement.

7.0 Concept Design

In this section the designers will generate solutions to meet the primary needs of the product design specifications. Within the conceptual design core there are two major components:

- Generation of solutions to meet the stated need.
- The evaluation of these solutions to select the one which is most suited to match the product design specifications.

Based upon an analysis of the two preceding points the design group decided to divide the conceptual design methodology into the following: concept generation and concept selection.

7.1 Concept Generation

In order to facilitate concept generation the design group sub-divided the processes as follows:

$$System\ Concept \xrightarrow{Divide} Structure\ Function \xrightarrow{Divide} SubFunctions$$

The following is a rendition of the functional decomposition which resulted from division of the system concept.

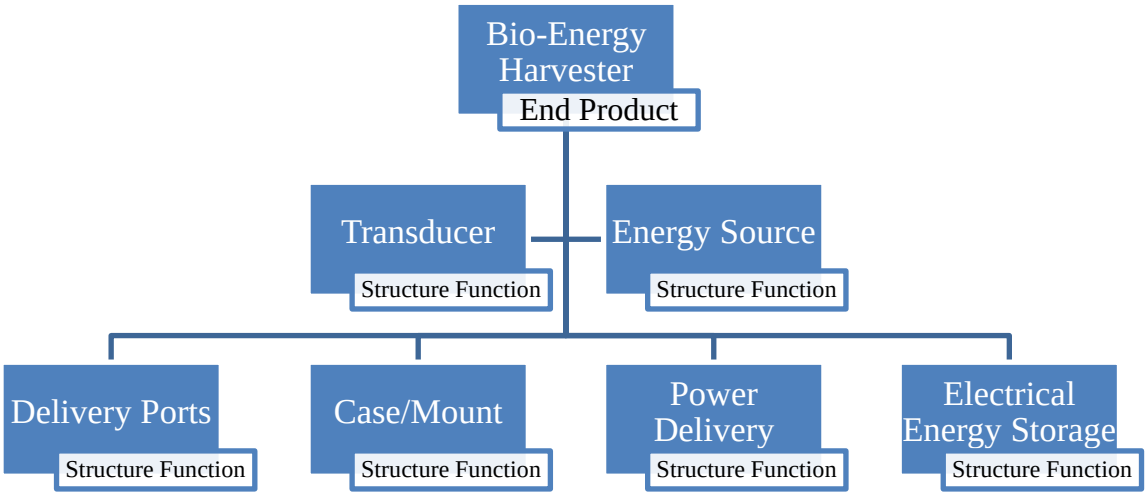

Figure 15: Hierarchal Deconstruction of End Product

The preceding figure is a functional decomposition of the bio-energy harvester system concept (end product) into several structure functions.

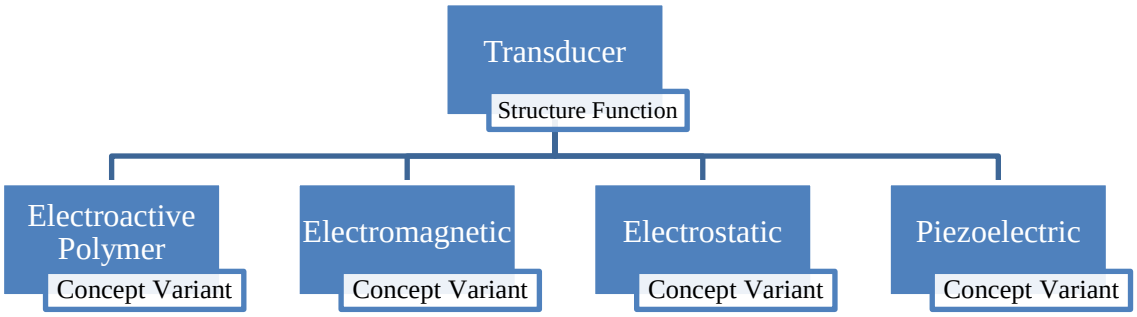

Figure 16: Transducer Sub-division to Concept Variants

The preceding figure divides the structure function of the transducer system into several possible concept variation solutions.

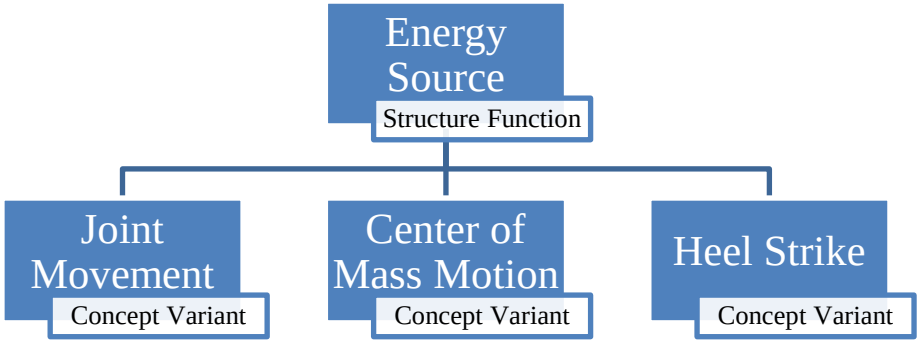

Figure 17: Energy Source Sub-division to Concept Variants

The preceding figure is a functional decomposition of energy source function along with three possible concept variations which may address the function.

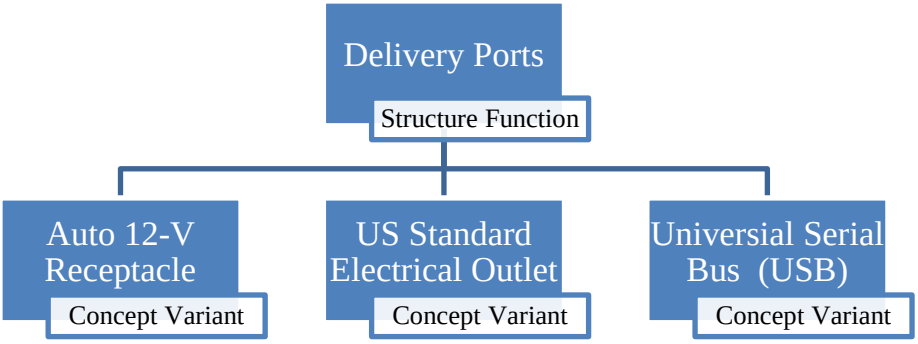

Figure 18: Delivery Port Sub-division to Concept Variants

The preceding figure is a functional decomposition delivery port structure function into several concept variation solutions.

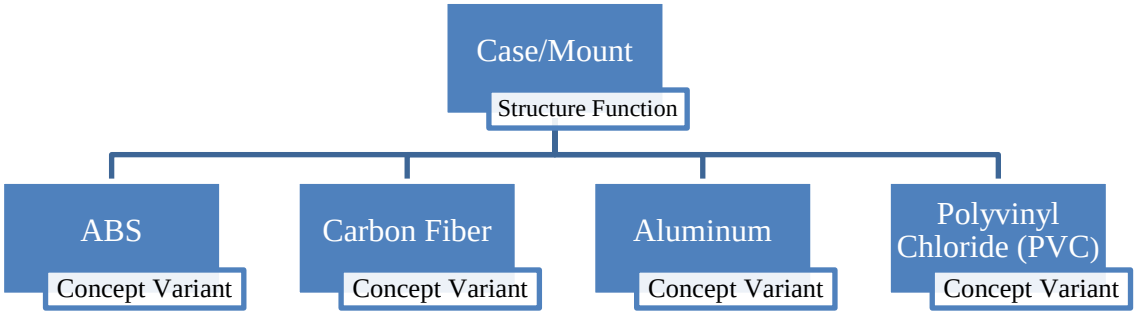

Figure 19: Case/Mount Sub-division to Concept Variants

The preceding figure is a functional decomposition of the case/mount structure function into several concept variants.

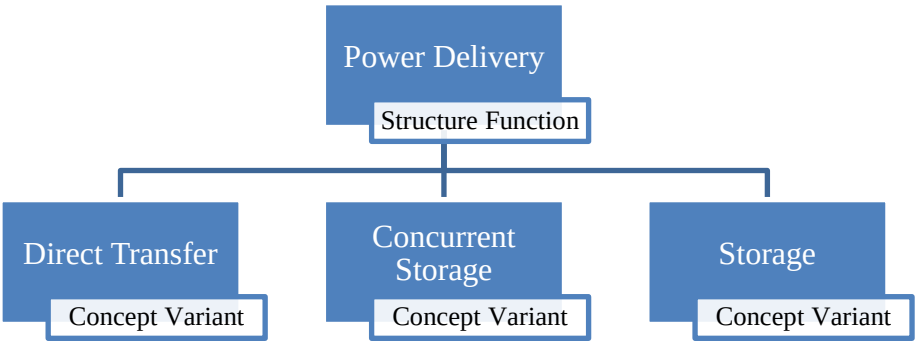

Figure 20: Power Delivery Sub-division to Concept Variants

The preceding figure is a functional decomposition of the power delivery structure function into several possible concept variants.

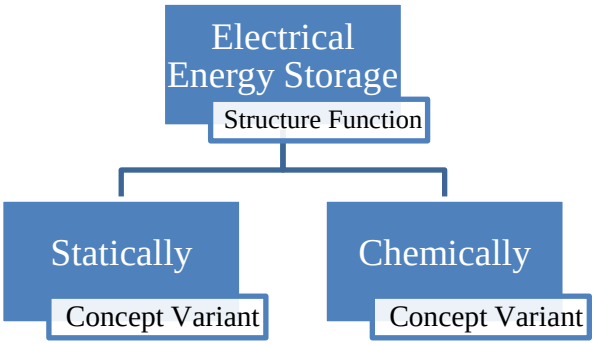

Figure 21: Electrical Energy Storage Sub-division to Concept Variants

The preceding figure is a functional decomposition of the electrical energy storage structure function into several possible concept variation solutions.

7.2 Senior Design Concepts

The proceeding report section will outline several possible design concepts generated to address the design objective and will describe their proposed ideas of operation.

7.2.1 Rotational Electromagnetic Knee Brace

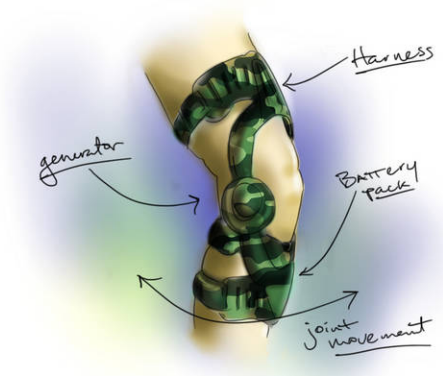

Figure 22: Concept Design of Electromagnetic Knee Brace Generator

Above is a concept drawing of what the production product may look like. The proposed transducer type for this concept is electromagnetic due to the inherit ability of electromagnetic transducer types to take advantage of rotational translation.

7.2.2 Piezoelectric Knee Mounted Generator

Piezoelectric materials have inherent material properties which make them ideal candidates for energy harvesting; when they are mechanically stressed an electric charge response occurs. The intent of this design is to utilize the flexion/extension motion that occurs between the tibiofemoral joint to strain the piezoelectric material.

The proposed idea of operation is to rigidly attach one end of a system of piezoelectric fibers, with a specialized clamp, to the femoral segment of the joint; the other end of the fibers will be attached to a spring system, which will serve to limit the forces on the piezoelectric system; and the other end of the spring system will be rigidly attached to a point on the tibia. As joint rotation occurs, during the walking gait, the piezoelectric fibers will be stressed; however, due to the implementation of the spring system the fibers will be limited to a maximum stress point below the fibers elastic limit.

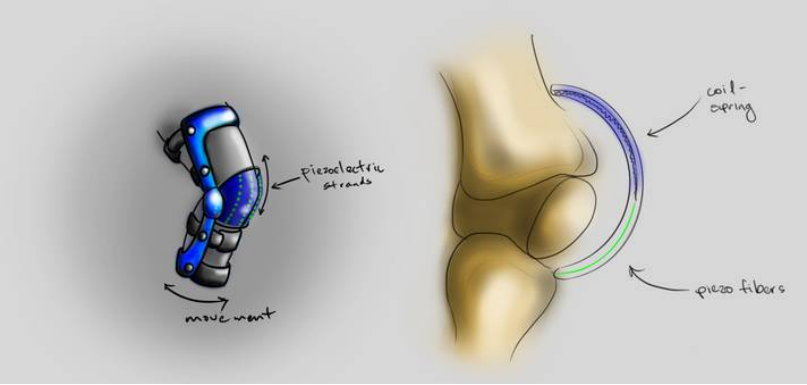

Figure 23: Concept Design of Piezoelectric Knee Mounted Generator

The preceding figure shows a conceptual drawing of a biomechanical generator which utilizes piezoelectric material fibers. As flexion/extension occurs between the tibiofemoral joint subsequent electrical power is generated by the piezoelectric material; due to its inherent material properties.

7.2.3 Electromagnetic Ankle Brace Generator

Due to the high power generation and torque values produced, 66.8 Watts and 140 Newton-meters, the ankle was identified as a prime candidate for implementation of a human mechanical generator. (Winter A. D., 2005)

A similar principle of operation to the one taken for the electromagnetic knee brace generator would be adopted for this design. As rotation occurs at the talocrural (ankle) joint, brace supports above the ankle and around the talus section of the foot would actuate a transmission system in the generator. This transmission system would utilize the relatively high output torque of the ankle to rotate the rotor with respect to the stator; however, since we know that electromagnetic transducers have higher efficiency rates at ranges above the rotational frequency of the ankle the transmission's job is to step up the output frequency.

Figure 24: Concept Design of Electromagnetic Ankle Brace Generator

The concept design of the ankle brace generator, for all intensive purposes, is identical to the electromagnetic knee brace generator with the exception that the energy harvesting site has been transposed to the ankle.

7.2.4 Linear Actuation Electromagnetic Boot

Another proposed design concept is the linear actuation electromagnetic boot. The proposed idea of operation is to implement a fluid filled container in the heel of the boot, when the heel makes contact with the ground the fluid will be displaced, this fluid displacement will actuate a permanent magnet through an armature assembly and cause a magnetic flux to be created.

Figure 25: Concept Design of Linear Actuator Electromagnetic Boot

Above is a proposed design of the linear actuation electromagnetic boot; it utilizes linear motion through an armature assembly to convert heel strike impact energy into electrical energy.

7.2.5 Electrostatic (ES) Heel Strike Generator

Another design conceptualized by the group is the electrostatic heel strike generator. In this design a contact member, which will interact with the ground during the heel strike process, will

drive the rack component of a rack and pinion system: effectively converting linear movement to rotational. This rotational motion will be multiplied through a series of gears and the output of transmission will rotate one side of a variable capacitor plate system. As the rotating capacitor plate is displaced with respect to a secondary static capacitor plate an electromagnetic flux will be generated, and subsequently harnessed.

Figure 26: Prior Art Design of ES Heel Strike Generator

*Above is a prior art design which was the inception of the proposed concept of the ES heel strike generator. Our design will not rest under the ball of the heel as the preceding figure suggests; however, our contact point will rest alongside the heel and be mounted in a similar fashion. *Pictorial source:* http://half-life.wikia.com/wiki/Advanced_Knee_Replacement

7.3 Concept Selection

Through systematic dismissal of concept variants utilizing the decision matrices, seen in the appendices, the concept of the electromagnetic knee brace was ultimately decided upon. Because of the high power generation of the knee, robustness and conversion efficiency of electromagnetic generators, and mostly one-dimensional motion of

It is at this point important to emphasize the necessity for a deeper engineering and numerical analysis of the selected design. Although enough information about the desired behavior and shape of the energy harvester exists, potential pitfalls cannot be identified simply by looking at the picture as is, and must be examined more carefully, using tools described in the subsequent chapters.

8.0 Military Devices

The proceeding section of material aims to list several common types of equipment which active military forces commonly utilize when deployed on field work missions.

8.1 PVS-7: Night Vision Goggle

The PVS-7 is the standard issue goggles for U.S. ground forces to conduct night operations. Using the latest 2nd/3rd generation image intensifier tubes the PVS-7 will perform in the darkest of nights. The system has a built-in IR Illuminator for no light operations and a high light cut off sensor for any sudden burst of bright light for protection. The PVS-7 is a completely MIL-SPEC system that has been ruggedized and waterproofed for harsh environments.

- Weight: 18 oz.
- Focus Range: 20 cm to Infinity
- Range: 150 m (Starlight), 300 m (Moonlight)
- Battery: (2) AA or (1) BA-5567/U
- Battery Life: 30 hours
- Magnification: 1X
- Field of View: 40°
- Interpupilary Adjustment: 55 to 71 mm
- PVS-7D and PVS-7B include head mount for hands free operation

8.2 AN/PEQ-1A SOFLAM

The PVS-13 is a companion, image intensified night sight for the SOFLAM. Using it assures that the designator is operating and pointing exactly at the target. It has 6X magnification, weighs 4.2 pounds, and operates for 40 hours on 2 "AA" batteries. (Rogers, 2001)

8.3 MPSIDS

The MPSIDS consists of a base station (a laptop, printer and assorted cables) and 3 outstations (Palmtop 586 computer, digital camera, lenses, cables etc.). It can be interfaced with most radio systems.

The team can shoot pictures of something of interest, send it back to the Reconnaissance Operations Center via tactical satellite radio or HF, and print out hard copies in near real time. Images can be annotated in the field, decreasing the chance of misinterpretation of conventional reporting.

8.4 Nightstar: Night Vision Binoculars

The new night vision binocular is the Nightstar from DRS Technologies. This 3.5 pound, 3X binocular has a Gen 3 filmless, gateless image intensifier with a laser rangefinder, laser pointer, electric flux gate compass, an electric inclinometer and RS 232 interface.
The laser ranging is from 20-2000 meters. The laser pointer is also viable out to 2000 meters. The RS 232 Interface can transfer data to GPS and SINGARS radio. Its target bank can hold up to 10 targets. It operates on six "AA" batteries that are good for 36 hours of continuous operation, including 200 measurements.

8.5 M2120 SOPHIE Long Range Thermal Imager

This is another new tool for the Company. The SOPHIE is a lightweight (5.3 pounds) advanced second generation thermal camera. The detector resolution and high definition liquid crystal display allow images to match day-time television. The detector is cooled to operating temperature in about 5 minutes. (Thales)

This is a very capable unit. We were able to acquire a large radio transmission tower at night at 7km, with enough clarity to sketch it.
Power supply
15 VDC 5 hours of battery life (rechargeable battery)

8.6 AN/PRC117F

The multi band 117 operates near simultaneously in VHF AM and FM, UHF AM, and UHF DAMA SATCOM. (Demand Assigned Multiple Access —this allows several hundred users to share one narrowband SATCOM channel based on need or demand). It is voice/ data and has embedded crypto, SATCOM and ECCM capabilities.

9.0 System Analysis & Design

9.1 Device System Flowchart

The device system flowchart serves to show the forward progress of the system flow. For example the transmission system is the third link of the design; without it the relatively high torque production from the knee joint may not be converted to subsequently higher angular velocities for proper electrical conversion in the next system stage, the electromagnetic generator.

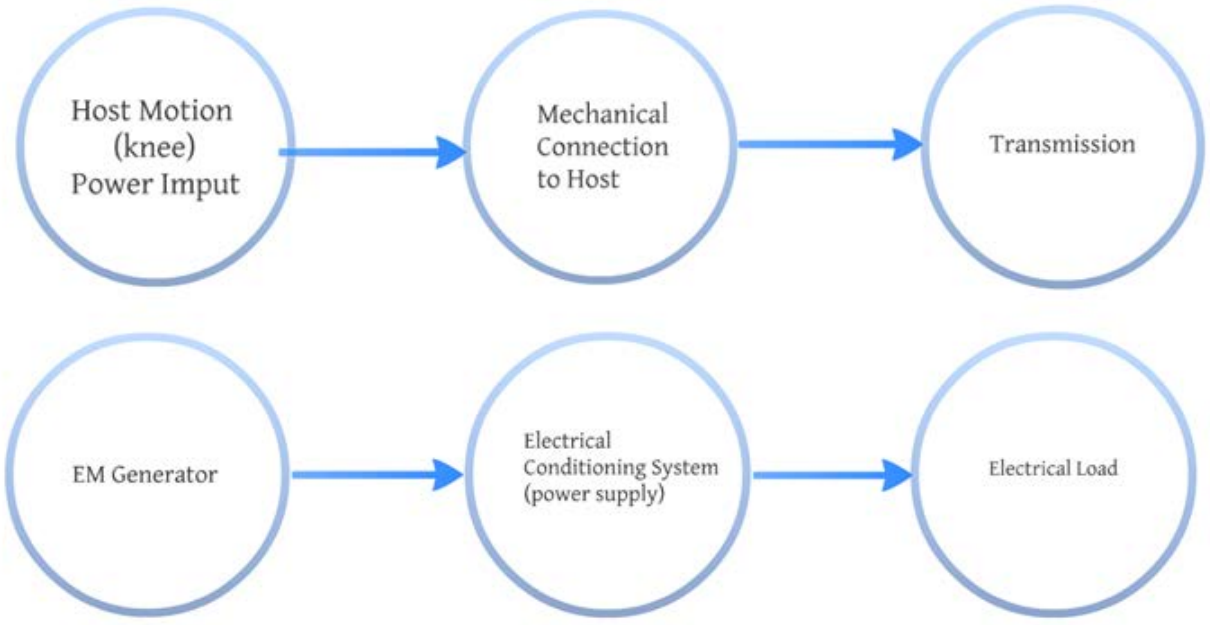

Figure 27: Biomechanical Energy Harvester Flowchart

Above is the system analysis flow chart which describes the expected mechanism flow of energy from the initial power input to the expected output.

9.2 Human Motion Analysis

The following section serves to describe the first integral part of the total device system; as the driver of all subsequent processes the human motion will be analyzed to develop an understanding of the initial power input supplied.

Human motion analysis is composed of several variants which are essential to understand the maximum output energy a regular walking gait can deliver. These variants include Energy output of the knee, cost of harvesting (COH) which deals with the metabolic power and the electrical power, and the analysis of gait cycle percentage vs. knee power.

9.2.1 Energy Calculation for the Knee

The gait cycle percentage is divided into 4 regions which involve negative work. Negative work happens when the motion of the leg is countered by opposing forces caused by certain muscle tensions. The graph below, Knee power vs. Gait%, depicts the different regions of the gait cycle including those which involve negative work.

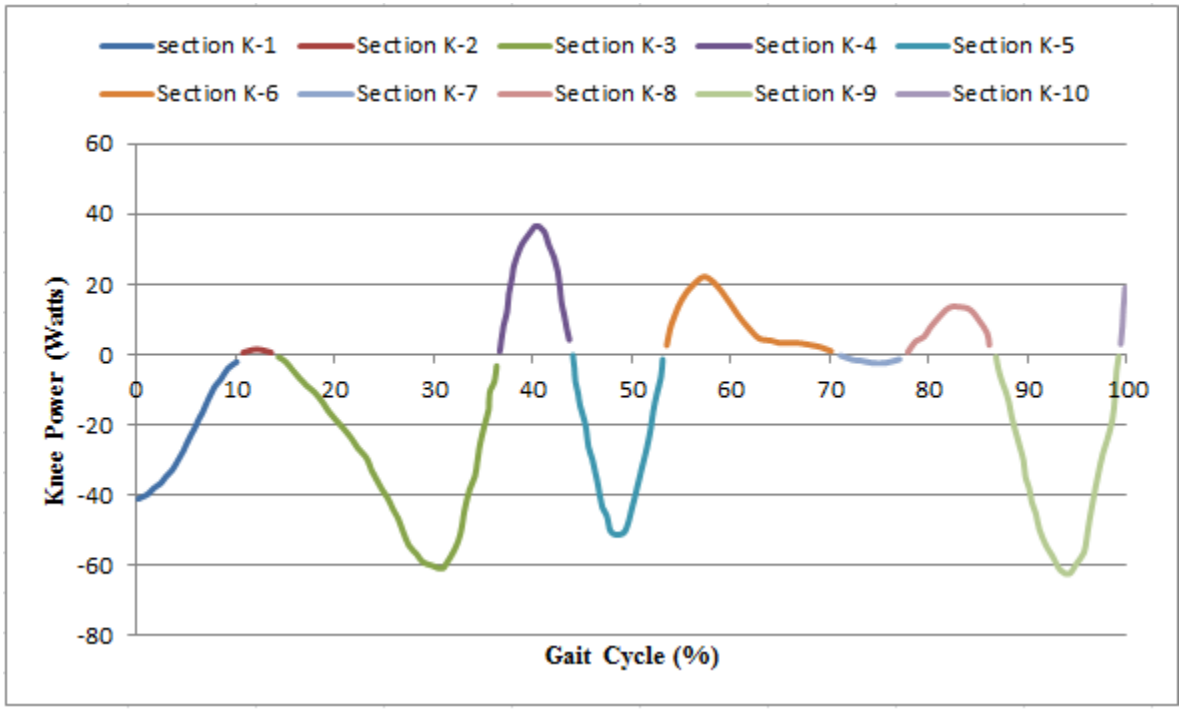

Figure 28: Power Production as a Function of Gait Cycle

Above is the Knee Power vs. Gait% chart divided into its respective regions including negative work.

The energy calculation for the knee comes from the addition of the negative work times the mass of the person. In the case of the preceding figure, the energy calculation is derived by the following formula:

$$E_{total=mass(|K5|+|k7|+|k9|+|k3|)}$$

Each individual (negative) work can be calculated by finding the area above the curve for K-3, K-5, K-7, and K-9. By finding the equation of each individual curve we can integrate and get accurate results regarding the work produced by each one. Below are the individual curves and their corresponding equations for their lines.

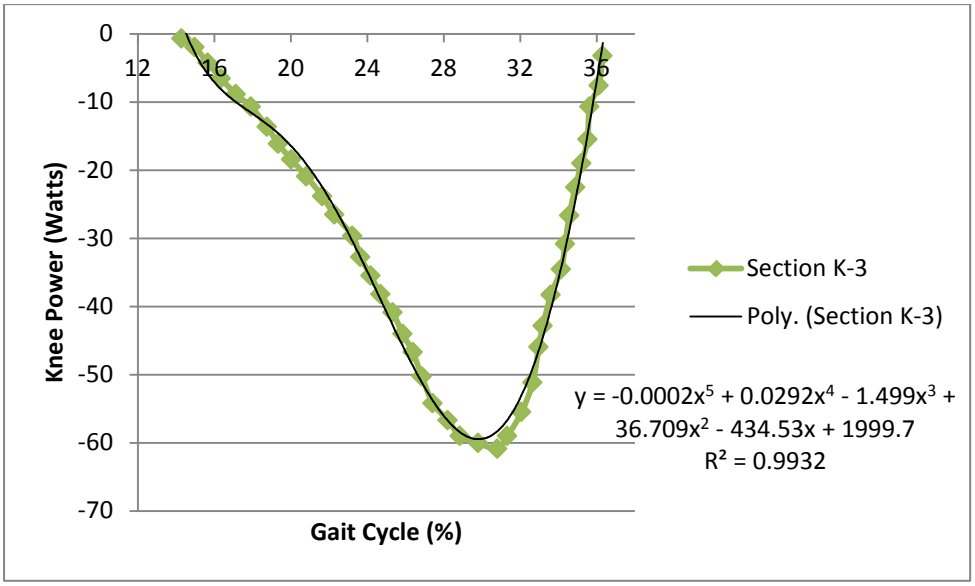

Figure 29: Power Generation during Section K-3

The preceding graph shows the power results for the K3 graph which falls under the 16-36% gait cycle. According to the article written by Dave Thompson, this percentage takes place during the mid-stance section.

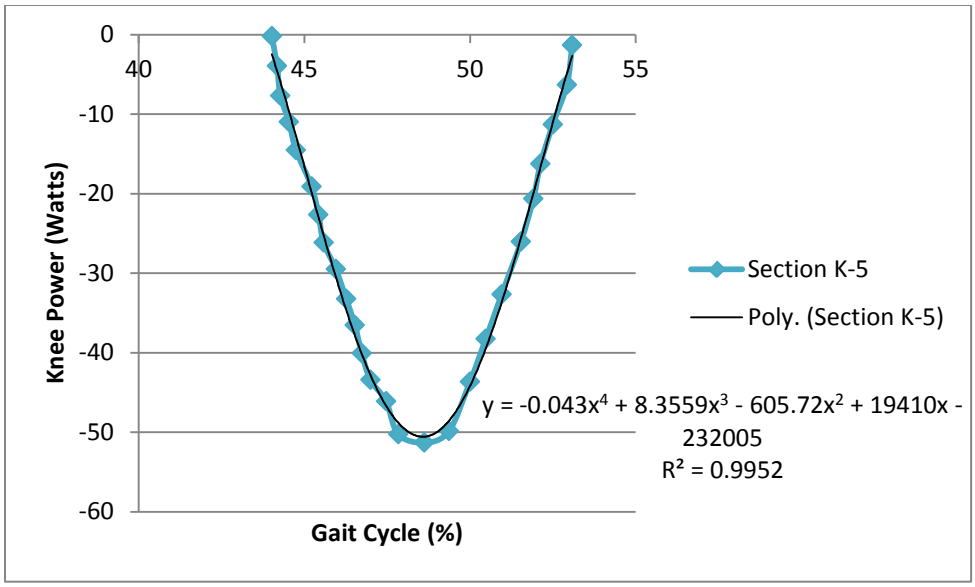

Figure 30: Power Generation during Section K-5

The graph shows the power results for the K5 graph which falls under the 43-53% gait cycle. According to the article written by Dave Thompson, this percentage takes place during the pre-swing section.

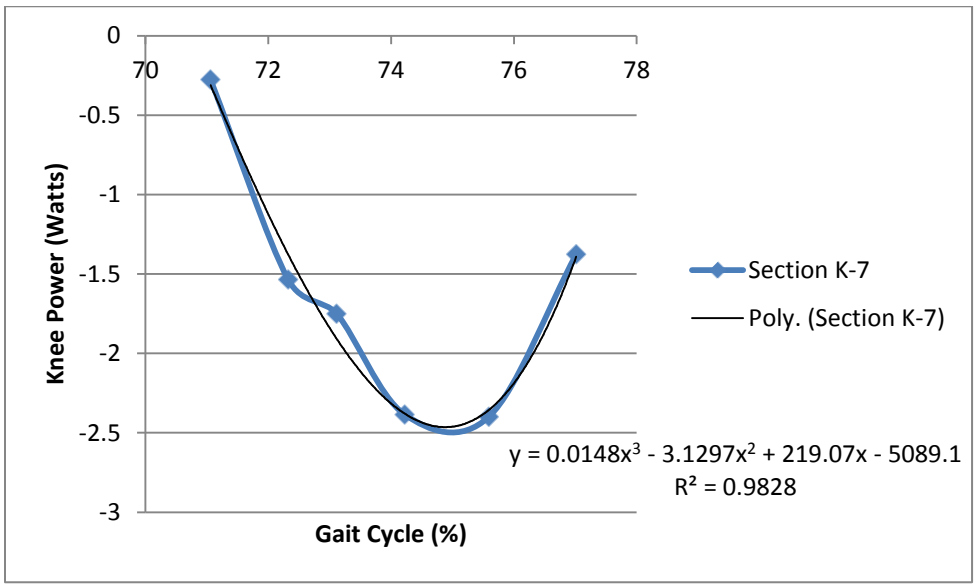

Figure 31: Power Generation during Section K-7

The graph shows the power results for the K5 graph which falls under the 71-77% gait cycle.

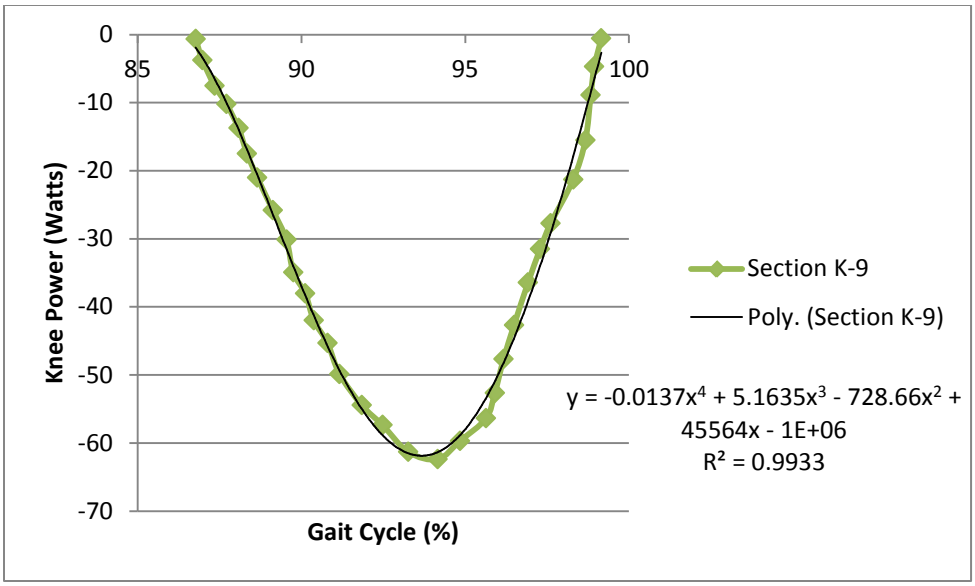

Figure 32: Power Generation during Section K-9

The graph shows the work results for the K9 graph which falls under the 87-99% gait cycle.

9.3 Host Mechanical Connection Analysis

The following section shall describe the method for connection of the host to further system components.

9.3.1 Factors for Knee Brace Selection

In order to adequately choose a knee brace several factors pertaining to the brace must be chosen; the design group has identified the following as criteria for choosing a brace system:

1. Brace Design
2. Breathability/Product Comfort
3. Unit Cost
4. Ergonomics
5. Range of Motion

Brace design must be taken into account when choosing a brace for two reasons. First, since the rotational motion of the knee must be transmitted to subsequent system stages rigid structure arms must be part of the existing brace design. Secondly, original intended brace use must be factored; for example, rehabilitative knee braces would not be ideal for our project since they limit motion of the knee. (Joint Pain Institute, 2010)

Prophylactic, functional, and other minimally invasive orthotic devices will be considered for use; rehabilitative, and unloader knee braces along with knee sleeves will not be considered.

Since prolonged periods of use are expected for the energy harvesting system special consideration of the harness material must be taken. Materials such as polystyrene and polychloroprene have been identified as suitable material for their flexibility. The ergonomics of each brace will also need to be taken into account for each of these systems.

Unit cost will be designated to be below $100.00 due to the fact that this project is meant as solely a proof of concept project.

9.3.2 Market Search for Knee Brace

Three products were identified for possible use as the host mechanical connection, they are as follows:

Figure 33: Don Joy Playmaker Wrap IROM

The IROM Playmakers is designed primarily for post-op care following meniscal repairs as well as ACL/PCL reconstruction. The IROM hinge allows independent range of motion control.

Figure 34: ProCare WeekENDER Recreational Brace

The ProCare WeekENDER Recreational Activity Knee Brace uses a Dual Axis Hinge that allows for convenient dial-in adjustment of flexion/extension stops.

Figure 35: Muller Hinged Knee Brace

The Mueller hinged knee brace is an orthopedic brace designed for medial-lateral support.

9.3.3 Selection of Knee Brace System

According to comparison of the systems described in the preceding section, *Market Search for Knee Brace*, the preferred method of connection between the host and the generator is using an adjustable hinged knee brace; to be more precise, a Mueller adjustable hinged knee brace.

The following will identify several brace properties which lead to the selection of utilizing the Mueller hinged knee brace.

Figure 36: Mueller Hinged Knee Brace

Pictured in the preceding figure are isometric and back views of the Mueller adjustable hinged knee brace. The brace contains an opening in the anterior and posterior locations of the knee which provide comfort for the knee cap and prevents bunching under flexion of the joint.

Figure 37: Texture Sample of Neoprene/Polystyrene Blended Material

Brace harness material is made from a Neoprene/Polystyrene blend and contains small perforations which increase breathability.

Figure 38: Cross Support Straps Feature

Criss-crossing support straps are also found above and below the knee. A hook and loop belt closure is used to secure the knee brace on the user.

Figure 39: Polycentric Hinge System

The knee brace contains both medial and lateral geared polycentric hinges. These hinges are made from a 6000 type metal alloyed with magnesium and silicon. The purpose of the hinges is to protect the knee from hyperextension.

Other features not depicted include the ability for nearly universal size alteration. Two side hinge pockets are used for size alteration; these sizes include small/medium, and large/extra-large which correlates to a knee size of about 13-17 in and 17-21 in, respectively.

Overall, this knee brace is ideal for active individuals during sports and other physical activities. It is a very cost effective knee brace compared to other orthopedic knee braces that contain the necessary components. This is what earned its spot at the top of the list.

9.3.4 Secondary Selection of Knee Brace System

During the prototype construction and impromptu trial testing the original selection of the Mueller Hinged Knee Brace proved ineffective at transferring the full range of motion of the knee joint due to the flexibility of the hinge pocket material.

For the preceding reason, use of analternative knee brace which featured a rigid frame structure was utilized.

Figure 40: Bledsoe Axiom Knee Brace

The preceding photo shows the Axiom knee brace which was original designed for increased support of knees following injury to or reconstruction of the anterior cruciate ligament, posterior cruciate ligament, or menisci. (Bledsoe Brace Systems, 2009)

Table 13: Bledsoe Functional Knee Brace Line Comparison

	Z-12	Axiom Mg	Axiom	Ultimate	Crossover
Custom	x	x	x	x	
Patient Ready/OTS	x	x	x	x	x
Length	13" & 15"	16"	16"	15"	13" & 15"
Frame	Mg	Mg	Al	Al	-----
Frame Shape	Square	Swooping Thigh	Swooping Thigh	Square	-----
Weight	14 oz	16 oz	24 oz	19 oz	22 oz
Special Features/Options					
OA Correction	x	x	x		
Dynamic			x	x	
Reinforced Frame			x	x	
Activity Level					
Extreme Sports			x	x	
High Contact Sports			x	x	
Low Contact Sports	x	x	x	x	x
Athletic	x	x	x	x	x
Weekend Warrior	x	x	x	x	x
Activities of Daily Living	x	x	x	x	x
Suggested HCFA Code					
Custom	L1846	L1846	L1846	L1846	
Patient Ready/OTS	L1845	L1845	L1845	L1845	

According to Bledsoe Brace Systems, the Axiom knee brace weight is 24 ounces and is manufacturer rated as one of their highest activity level bracing systems. (Bledsoe Brace Systems, 2009)

Table 14: Axiom Brace Sizing Information

Thigh Circumference	Calf Circumference STD	Calf Circumference Athletic			Aluminum Left	Aluminum Right	Magnesium Left	Magnesium Right
13.5" - 16.0" (34.3 cm - 40.6 cm)	12.5" - 14.0" (31.7 cm - 35.6 cm)	11.0" - 12.5" (27.9 cm - 31.7 cm)	XS	STD	PK114101	PK114201	MG114101	MG114201
				Athletic	PK119101	PK119201	MG119101	MG119201
16.0' - 18.75" (40.6 cm - 47.6 cm)	14.0" - 15.5" (35.6 cm - 39.4 cm)	12.5" - 14.0" (31.7 cm - 35.6 cm)	S	STD	PK114103	PK114203	MG114103	MG114203
				Athletic	PK119103	PK119203	MG119103	MG119203
18.75" - 21.5" (47.6 cm - 54.6 cm)	15.5" - 17.0" (39.4 cm - 43.2 cm)	14.0" - 15.5" (35.6 cm - 39.4 cm)	M	STD	PK114105	PK114205	MG114105	MG114205
				Athletic	PK119105	PK119205	MG119105	MG119205
21.5" - 24.25" (54.6 cm - 61.6 cm)	17.0" - 18.5" (43.2 cm - 47.0 cm)	15.5" - 17.0" (39.4 cm - 43.2 cm)	L	STD	PK114107	PK114207	MG114107	MG114207
				Athletic	PK119107	PK119207	MG119107	MG119207
24.25" - 27.0" (61.6 cm - 68.6 cm)	18.5" - 20.0" (47.0 cm - 20.0 cm)	17.0" - 18.5" (43.2 cm - 47.0 cm)	XL	STD	PK114109	PK114209	MG114109	MG114209
				Athletic	PK119109	PK119209	MG119109	MG119209
27.0" - 29.5" (68.6 cm - 74.9 cm)	20.0" - 21.375" (50.8 cm - 54.3 cm)	18.5" - 20.0" (47.0 cm - 20.0 cm)	2XL	STD	PK114111	PK114211	MG114111	MG114211
				Athletic	PK119111	PK119211	MG119111	MG119211
29.5" - 31" (74.9 cm - 78.7 cm)	21.375" - 22.75" (54.3 cm - 57.8 cm)	20.0" - 21.375" (50.8 cm - 54.3 cm)	3XL	STD	PK114113	PK114213	-----	-----
				Athletic	PK119113	PK119213	-----	-----

The model utilized for prototype development was a size small, athletic model, composed of a magnesium alloy and intended for left leg mounting. From the table, thigh and calf circumference for the brace was determined to be 13.5"-16.0" (40.6-47.6 cm) and 12.5"-14.0" (35.6-39.4cm), respectively. (Bledsoe Brace Systems, 2009)

Although not the original selection for a knee brace system, the Bledsoe Axiom knee brace met multiple factors for the knee brace selection. Since, the Axiom brace design was recommended for prophylactic use and rated for "extreme" and "high contact" sports this system is ideal for our design selection.

The product breathability received high marks due to the brace's open frame design and four-point harness system. Unfortunately, frame rigidity also decreased product comfort and the four-point harness system created points of concentrated loading; for the preceding reasons the *Bledsoe Axiom* brace was ranked lower in product comfort and ergonomics compared to the *Mueller Adjustable Hinged* brace.

A unit cost of the *Bledsoe Axiom*brace was retailed at $1007.38, which is higher compared to the $24.99 retail cost of the *Mueller Adjustable Hinged* knee brace.

Similar range of motion was identified in comparison for both brace designs.

9.4 Transmission System Analysis

The following section shall describe the method of power transmission from the host to the transducer.

9.4.1 Gear Nomenclature & General Calculations

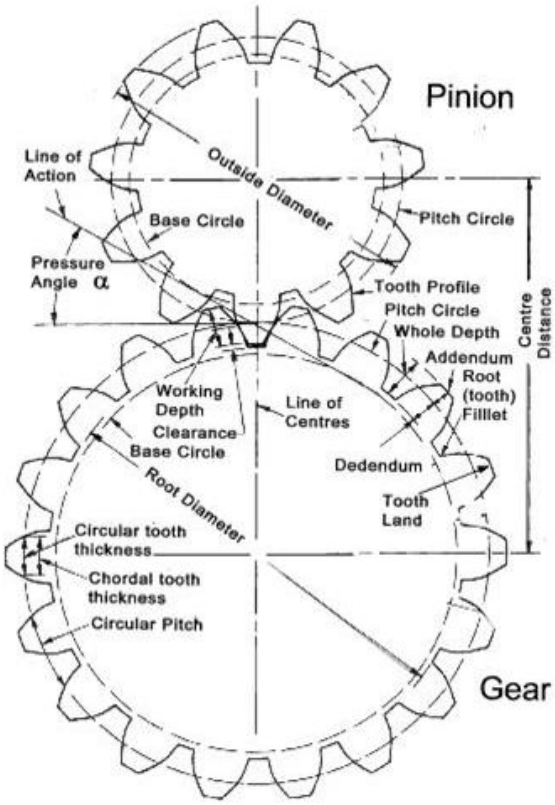

Figure 41: Gear & Pinion Nomenclature

The preceding figure outlines the nomenclature related to general gear and pinion spur gear systems.

Table 15: Gear Formulae

Calculate	When Defined	Formula
Diametral Pitch (P)	Pitch Diameter (D) and the Number of Teeth (N)	P = N / PD
Diametral Pitch (P)	Circular Pitch (p)	P = 3.1416/p
Diametral Pitch (P)	Outside Diameter (OD) and the Number of Teeth (N)	P = (N+2)/OD
Pitch Diameter (PD) .	Number of teeth (N) and the Diametral Pitch (P)	PD = N/DP
Outside Diameter (OD)	Number of teeth (N) and the Diametral Pitch (P)	OD = (N+2)/DP
Number of Teeth (N).	Pitch Diameter (D) and the Diametral Pitch (P)	N = PD * DP
Addendum (a) .	Diametral Pitch (P)	a = 1/DP
Dedendum (d)	Whole Depth and Addendum	d = hw - a
Tooth Thickness (t) at the Pitch Diameter	Diametral Pitch (P)	t = 1.5708/P
Working Depth (WD).	Addendum	WD = 2(a)
Center Distance (C)	Normal Diametral Pitch (P) and the Number of Teeth in Both Gears	C = (N1+N2)/2P
Center Distance (C)	Pitch Diameters of both gears	C = (PD1+PD2)/2
Circular Pitch (p)	Diametral Pitch (P)	p = 3.1416 / P
Whole Depth (hw) for 20 Pitch & finer .	Diametral Pitch (P)	hw = 2.2/P + .002
Whole Depth (hw) for Coarser than 20 Pitch .	Diametral Pitch (P)	hw = 2.157/P

The gear formula table serves to outline the interrelationship between gear features and geometry.

9.4.1 Analytical Calculation of Efficiencies

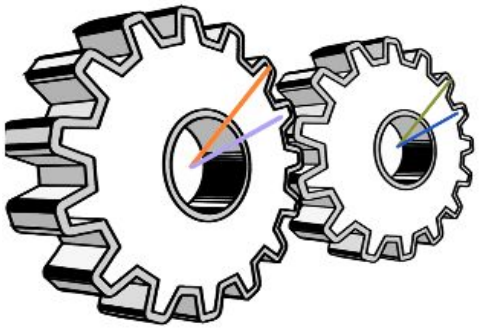

Figure 42: Gear Schematic for Assignment of Formula Nomenclature

Figure 42*shows color coding of gear and pinion components for assignment of variables in the subsequent equations for*

The following equations were utilized by the design group to calculate the approximate potential power transmitted, P%, through the gear mesh. (Beardmore, 2012)

$$Efficency\ (\%) = 100 - P$$

$$P = \frac{50\mu}{F}\left[\frac{(H_s^2 + H_t^2)}{(H_s + H_t)}\right]$$

$$H_s = (R_g + 1)\left[\sqrt{(\frac{R_o}{R_p})^2 - cos^2\alpha} - sin\alpha\right]$$

$$H_t = \left(\frac{R_g + 1}{R_g}\right)\left[\sqrt{(\frac{r_o}{r_p})^2 - cos^2\alpha} - sin\alpha\right]$$

$$F = cos\alpha$$

9.4.2 Factors for Transmission Selection

In order to choose an adequate transmission system several requirements have to be met. The criterion listed below corresponds to these requirements:

1. High efficiency power transmission
2. Reliable gear material
3. Output angular velocity
4. Compact design

Since the torque and angular velocity produced by the host is not nearly sufficient to power a small electric device, a transmission system is necessary in our design. The system must be efficient enough to transmit and up step the small amount of power produced by the host. The generator used in our design is most efficient at an angular velocity of 1000 revolutions per minute or greater. The transmission system must contain a gear ratio that will output angular velocities around the range in which the generator is most efficient. Considering all these requirements the transmission system must be compact and should not interfere with the host's range of motion.

9.4.3 Market Search for Transmission

Four transmission systems were taken into consideration after research was done. These systems are as follows:

Figure 43: Tamiya High Speed Gear Box 11.6:1 and 18.0:1

The Tamiya high speed gear box contains gears made from a polyacetyle resin which permit efficient power transmission with less mechanical noise than metal gears. Two gear ratios can be selected by altering the gears. The ratios are 11.6:1 and 18.0:1

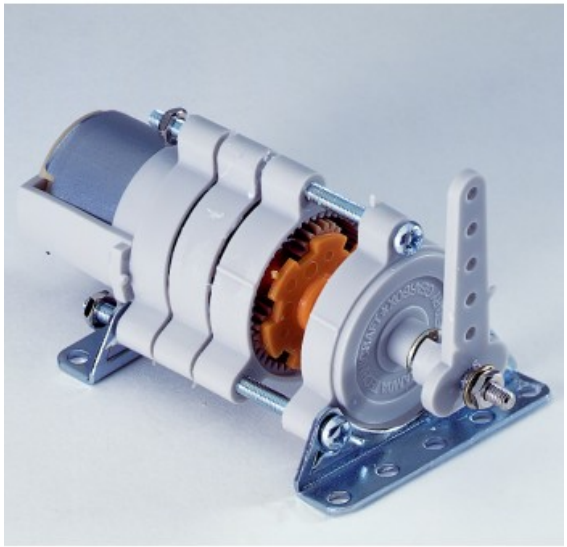

Figure 44: Tamiya Planetary Gear Box 16:1 to 400:1

The Tamiya planetary gear box system is a highly versatile system for reduction of high RPM electric motors for high torque low RPM applications. This type of gear system is often used in precision instruments because of its reliability and accuracy. Other aspects of the planetary gear box are its wide range of gear

ratios and its compactness. The following gear ratios can be achieved by altering the system: 4:1, 5:1, 16:1, 20:1, 25:1, 80:1, 100:1, and 400:1.

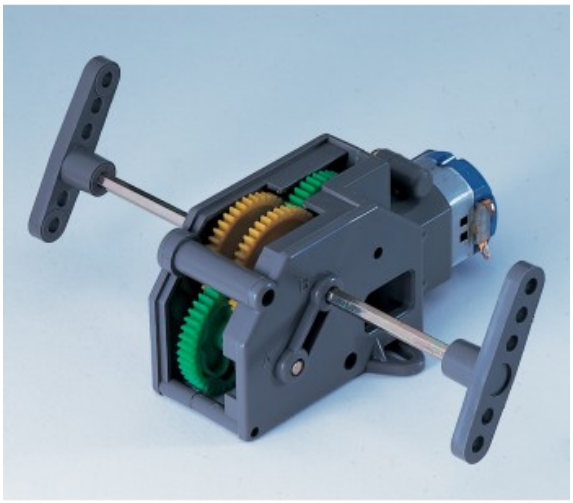

Figure 45: Tamiya 4-Speed Crank Axle Gear Box

The Tamiya 4-speed crank axle gear box produces low output speeds but is ideal when high torque is required. By altering the combination of four gears, four different gear ratios can be obtained. These ratios are as follows: 126:1, 441:1, 1543:1, and 5402:1.

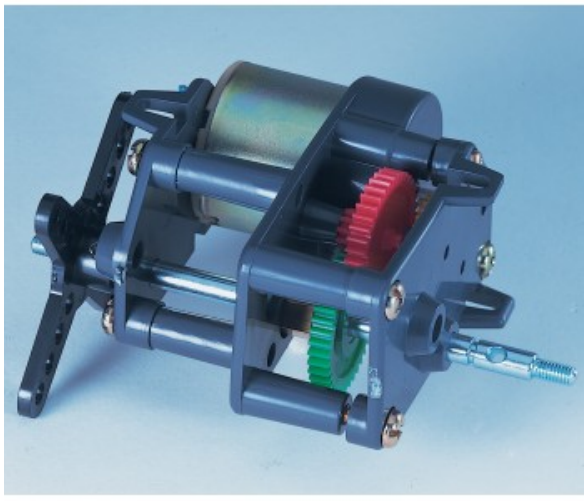

The Tamiya high power gear box's case is injection-molded ABS and the gears are made of polyacetal resin which reduces mechanical noise. This system is designed for high torque output. The gear box allows for two ratios which are

47.1:1 and 64.8:1. Once the gear box is assembled, it measures approximately 60mm x 80mm x 28mm.

9.4.4 Selection of Transmission System

9.5 Generator Analysis

In the proceeding section the group will analyze the options of generators for use in the system. The choice of generator system will ultimately rest as on several factors such as: size, mechanical-to-electrical conversion efficiency, and availability

9.5.1 Design of Experiment

The following is a description of the methods employed in order to determine the generator information pertinent to the design of the electrical conditioning system.

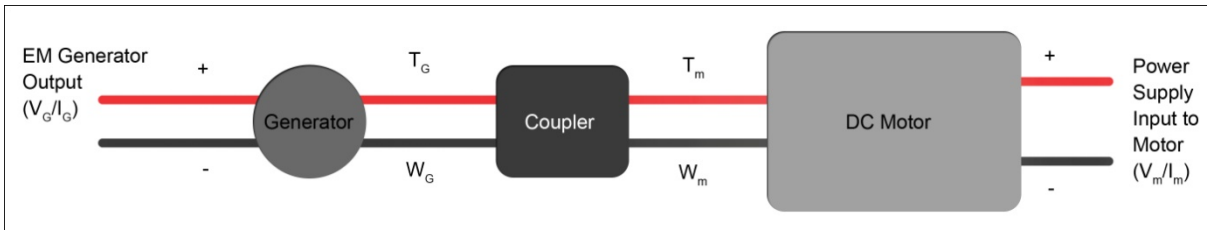

Figure 46: Schematic of Experimental Set-up for Generator Testing

The driver motor utilized was a product of Servo Systems Company (model number: RDM103), the flexible coupler was distributed by McMAster-Carr, and the generators purchased were obtained from multiple companies.

The above figure shows the experimental set-up utilized to test the efficiency values of the individual generators. The DC motor was supplied electrical voltage and current from an external power supply. The mechanical motions of the motor were subsequently directed to the generator by use of a flexible coupler to account for difference in shaft size and misalignment. Generator voltage and current were measured from the output leads of the generator and recorded for further calculations and analysis.

An equation to relate the driver and generator shaft dynamics was formulated as the following:

$$\tau_{Generator}(\omega_{Generator}) = (e)\tau_{Motor}(\omega_{Motor})$$

According to manufacturer specifications of the flexible coupler the efficiency factor,e, was >98.99%; therefore, the above equation was simplified to include an efficiency factor of one.

9.5.2 Adjustment of Driver Motor Constants

A tachometer was utilized in order to verify the voltage and torque constants provided by the manufacturer of the DC motor driving system; however, due to difference in loading conditions

accurate torque and angular values at the motor shaft were not obtained utilizing the original constants.

ELECTROCRAFT BRUSH TYPE DC SERVO MOTOR SPECIFICATIONS	
MOTOR RATINGS	
Continuous Stall Torque	55 oz-in.
Peak Torque	400 oz-in.
Max. Terminal Voltage	60VDC
Max. Operating Speed	6000 RPM
MECHANICAL DATA	
Rotor Inertia	0008 oz-in. /sec/sec
Damping Constant	0.25 oz-in./KRPM
Thermal Resistance	4 Deg. C/Watt
Max. Armature Temp	155 Deg. C
Max. Friction Torque	3 oz-in.
Max. Radial Load (1" from Bearing)	10 lbs.
Weight	3.5 lbs. (motor only)
ELECTRICAL DATA	
Torque Constant	13.7 oz-in./amp
Voltage Constant	10.2 V./KRPM
Terminal Resistance	1.6 Ohms
Electrical Time Constant	2.6 msec.
Mechanical Time Constant	8.9 msec.
Max. Continuous Current	4 Amps
Armature Inductance	4.1 mH.

Figure 47: Manufacturer Datasheet of DC Driver Motor

The driver motor torque and voltage constant were derived from the preceding datasheet and utilized for calculations of driver system mechanical output behavior as a function of electrical input.

In order to mediate this conflict of data we can calculate the "expected" motor torque/velocities utilizing the torque/voltage constants garnered from the data sheet. At voltage input increments of five volts, from five to thirty volts, the group will record the corresponding current input into the motor and resulting angular velocity utilizing the tachometer.

The following equations describe the method for calculating the "calculated" data trends:

$$\omega = \left(\frac{1}{V_{Constant}}\right) V_{Input}$$

$$\tau = (\tau_{Constant}) I_{Input}$$

We can formulate an equation utilizing common ratios to relate the "calculated"velocities/ torques to what we shall consider as the "actual" velocity/torque figures. Since the "actual" velocity trend line was experimentally measured the "actual" torque will be the only numerical data figure to be derived. The equation is as follows:

$$\frac{\omega_{Calculated}}{\tau_{Calculated}} = \frac{\omega_{Measured}}{\tau_{Adjusted}} \xrightarrow{alternatively} \tau_{Adjusted} = \left(\frac{\tau_{Calculated}}{\omega_{Calculated}}\right) \omega_{Measured}$$

Table 16: Data for determining Angular Velocity-Voltage Interrelationship

Voltage (Volts)	$\omega_{Measured}$ (RPM)	$\omega_{Calculated}$ (RPM)
5.000	583.5	490.2
9.997	1221.4	980.1
14.993	1886.9	1469.9
19.995	2539.1	1960.3
24.992	3186.4	2450.2
30.988	3917.6	3038.0

Voltage was set by the design team from the power supply as the voltage input to the driver system. Angular velocity was subsequently measured and recorded while a secondary "calculated" angular velocity was also determined.

Table 17: Data for determining Torque-Current Interrelationship

Current (Amps)	$\tau_{Adjusted}$ (Oz*in/Amp)	$\tau_{Calculated}$ (Oz*in/Amp)
0.276	3.177	3.781
0.34	3.738	4.658
0.356	3.799	4.877
0.397	4.199	5.439
0.425	4.477	5.823
0.476	5.057	6.521

The current, which was set as a function of voltage input and loading conditions, was recorded from the power supply. The "adjusted" torque was calculated utilizing the above equation of this section, while "calculated" torque was calculated utilizing the manufacturer torque constant.

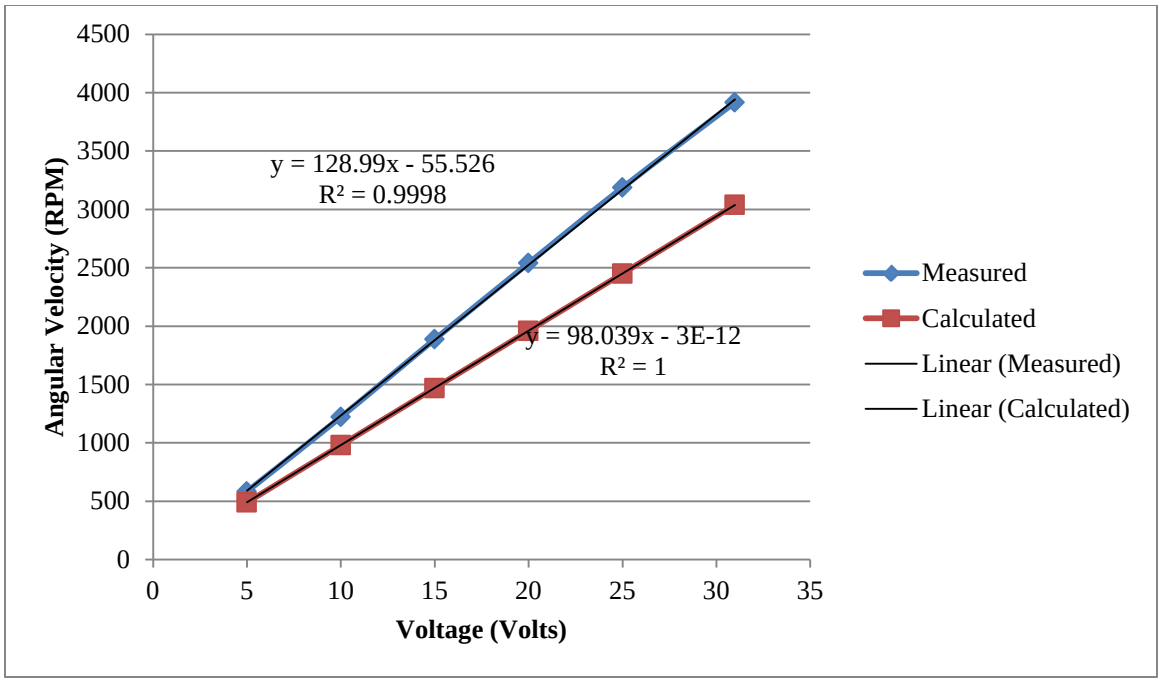

Figure 48: Driver Motor Angular Velocity Behavior

The preceding figure shows the behavior of the driver motor angular velocity as a function of input voltage. The "calculated" data line represents the behavior of shaft angular velocity had the provided manufacturer voltage constant worked, whereas the "measured" data line was experimentally obtained by use of a tachometer.

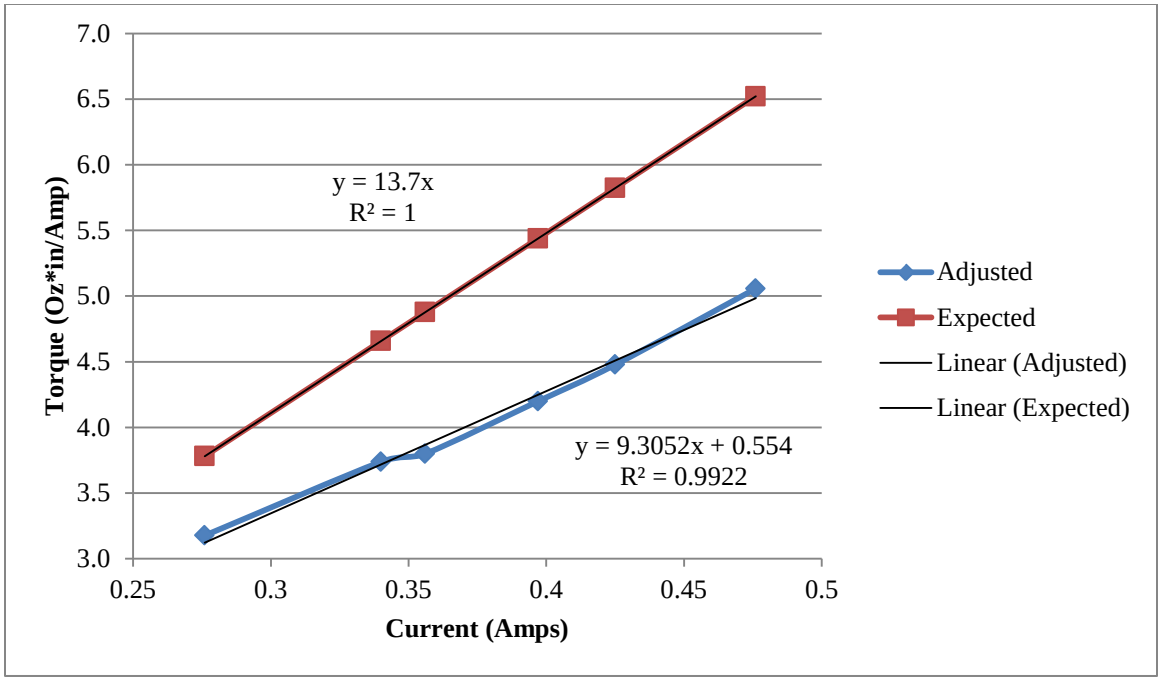

Figure 49: Driver Motor Torque Behavior

The preceding figure shows the behavior of the driver motor torque as a function of input current. The "calculated" data line represents the behavior of shaft angular velocity had the provided manufacturer voltage constant worked.

9.5.3 Generator Testing

The following section outlines the testing results of the generators.

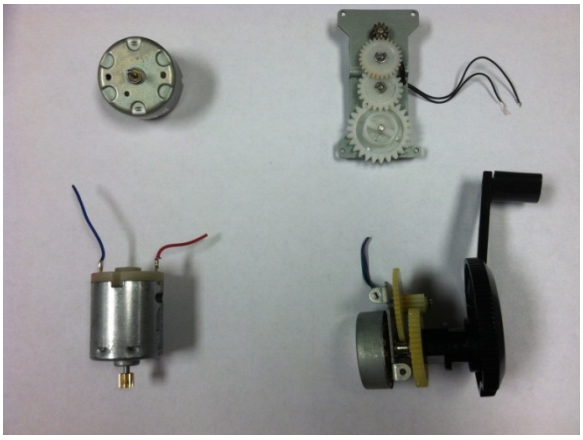

Figure 50: Generators Tested

Beginning from the top-left generator in a clock-wise rotation the nomenclature of the generators assigned was generator1, generator 2, generator 3, and generator 4.

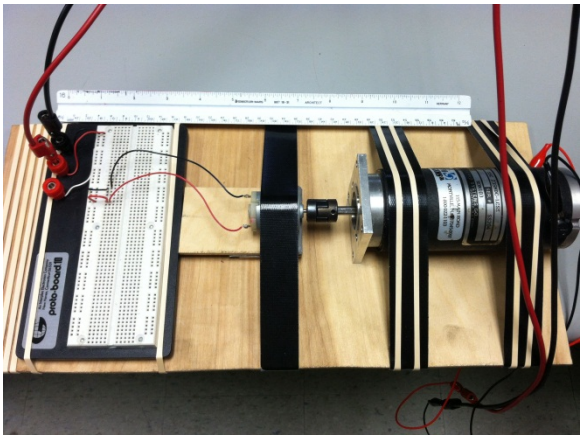

Figure 51: Experimental Set-up Testing of Generators

*The generators were set up and tested asshown in the preceding figure. *Note: the testing circuitry pictured is not representative of the actual circuitry used; please refer to subsequent figures for the circuit.*

Table 18: Generator 1 Testing Data (100 Ω Load)

Motor Drive						*Electromagnetic Generator*		
Voltage (Volts)	**Amperage (Amps)**	**Angular Velocity (RPM)**	**Torque (oz-in)**	**Angular Velocity (rad/s)**	**Torque (N*m)**	**Voltage (Volts)**	**Current (Amps)**	**Efficiency, η**
4.994	0.259	588.650	2.964	61.643	419.718	0.599	0.169	7.84%
9.989	0.304	1232.955	3.383	129.115	479.012	1.258	0.355	14.70%
14.987	0.342	1877.647	3.736	196.627	529.082	1.913	0.540	20.16%
19.981	0.374	2521.823	4.034	264.085	571.247	2.566	0.721	24.76%
24.981	0.403	3166.773	4.304	331.624	609.458	3.217	0.907	28.99%
29.977	0.433	3811.207	4.583	399.109	648.988	3.869	1.082	32.25%

*The preceding table outlines the data recovered when testing generator 1. Voltage and current were supplied to the driver motor by an external power supply, while the resulting voltage and current from the generator were recorded. *Note: An electrical load of 100 Ω was applied to the generator for the duration of data collection of this data.*

Table 19: Generator 2 Testing Data (100 Ω Load)

Motor Drive						*Electromagnetic Generator*		
Voltage (Volts)	**Amperage (Amps)**	**Angular Velocity (RPM)**	**Torque (oz-in)**	**Angular Velocity (rad/s)**	**Torque (N*m)**	**Voltage (Volts)**	**Current (Amps)**	**Efficiency, η**
4.995	0.289	588.779	3.243	61.657	459.247	0.539	0.152	5.68%
9.991	0.330	1233.213	3.625	129.142	513.270	1.146	0.323	11.23%
14.987	0.379	1877.647	4.081	196.627	577.835	1.754	0.494	15.27%
19.984	0.415	2522.210	4.416	264.125	625.270	2.355	0.663	18.82%
24.981	0.444	3166.773	4.686	331.624	663.482	2.957	0.834	22.22%
29.977	0.470	3811.207	4.927	399.109	697.741	3.561	1.006	25.42%

*Above is a data table recovered when testing generator 2. Identical data recovery procedures were employed as in testing generator one. *Note: An electrical load of 100 Ω was applied to the generator for the duration of data collection of this data.*

Table 20: Generator 3 Testing Data (100 Ω Load)

Motor Drive						*Electromagnetic Generator*			
Voltage (Volts)	**Amperage (Amps)**	**Angular Velocity (RPM)**	**Torque (oz.-in.)**	**Angular Velocity (rad/s)**	**Torque (N*m)**	**Voltage (Volts)**	**Current (Amps)**	**Power (W)**	**Efficiency, η**
4.999	0.257	589.295	2.945	61.711	417.082	1.409	1.481	2.087	0.01%
9.960	0.311	1229.214	3.448	128.723	488.235	3.023	3.443	10.408	336.01%
14.992	0.346	1878.292	3.774	196.694	534.353	4.579	5.391	24.685	475.89%
19.990	0.400	2522.984	4.276	264.206	605.506	6.126	7.368	45.136	564.49%
24.989	0.413	3167.805	4.397	331.732	622.635	7.653	9.318	71.311	690.96%
29.986	0.472	3812.368	4.946	399.230	700.376	9.191	11.162	102.590	724.84%

*The table outlines the data recovered when testing generator 3. The generator was identified as an AC system; therefore, appropriate measures were taken to measure AC values. *Note: An electrical load of 100 Ω was applied to the generator for the duration of data collection of this data.*

Although the efficiency calculations from generator three were identified as incorrect the electrical production values were greater compared to those produced by the competitive generators; therefore, further testing of generator three at 500, 1000, 1500 ohms were conducted.

Table 21: Generator 3 Testing Data (500 Ω Load)

Motor Drive						*Electromagnetic Generator*			
Voltage (Volts)	**Amperage (Amps)**	**Angular Velocity (RPM)**	**Torque (Oz*in)**	**Angular Velocity (rad/s)**	**Torque (N*m)**	**Voltage (Volts)**	**Current (Amps)**	**Power (W)**	**Efficiency, η**
4.999	0.267	589.295	3.038	61.711	430.259	1.412	0.223	0.315	23.59%
9.995	0.312	1233.729	3.457	129.196	489.553	2.980	0.558	1.663	53.32%
14.992	0.354	1878.292	3.848	196.694	544.894	4.517	0.934	4.219	79.49%
19.990	0.389	2522.984	4.174	264.206	591.011	6.048	1.330	8.044	103.44%
24.989	0.417	3167.805	4.434	331.732	627.905	7.618	1.752	13.347	128.08%
29.987	0.449	3812.497	4.732	399.244	670.070	9.168	2.167	19.867	147.56%

The table outlines the data recovered when testing generator 3 during an electrical loading of 500 Ω as an AC system.

Table 22: Generator 3 Testing Data (1000 Ω Load)

Motor Drive						*Electromagnetic Generator*			
Voltage (Volts)	**Amperage (Amps)**	**Angular Velocity (RPM)**	**Torque (Oz*in)**	**Angular Velocity (rad/s)**	**Torque (N*m)**	**Voltage (Volts)**	**Current (Amps)**	**Power (W)**	**Efficiency, η**
4.999	0.272	589.295	3.085	61.711	436.847	1.402	0.119	0.167	12.27%
9.997	0.324	1233.987	3.569	129.223	505.365	2.971	0.253	0.752	23.21%
14.992	0.366	1878.292	3.960	196.694	560.706	4.507	0.419	1.888	34.42%
19.990	0.404	2522.984	4.313	264.206	610.776	6.037	0.605	3.652	45.23%
24.991	0.425	3168.063	4.509	331.759	638.447	7.558	0.797	6.024	56.71%
29.998	0.461	3813.916	4.844	399.392	685.882	9.105	1.000	9.105	65.84%

The table outlines the data recovered when testing generator 3 during an electrical loading of 1000 Ω as an AC system.

Table 23: Generator 3 Testing Data (1500 Ω Load)

Motor Drive						*Electromagnetic Generator*			
Voltage (Volts)	**Amperage (Amps)**	**Angular Velocity (RPM)**	**Torque (Oz*in)**	**Angular Velocity (rad/s)**	**Torque (N*m)**	**Voltage (Volts)**	**Current (Amps)**	**Power (W)**	**Efficiency, η**
4.998	0.255	589.166	2.927	61.697	414.447	1.437	0.089	0.128	10.03%
9.995	0.297	1233.729	3.318	129.196	469.788	3.014	0.162	0.488	16.45%
14.992	0.333	1878.292	3.653	196.694	517.223	4.564	0.260	1.187	23.77%
19.990	0.367	2522.984	3.969	264.206	562.023	6.110	0.374	2.285	31.15%
24.989	0.399	3167.805	4.267	331.732	604.188	7.647	0.490	3.747	37.58%
29.986	0.434	3812.368	4.592	399.230	650.305	9.187	0.612	5.622	43.20%

The table outlines the data recovered when testing generator 3 during an electrical loading of 1500 Ω as an AC system.

9.5.4 Development of Power Curves

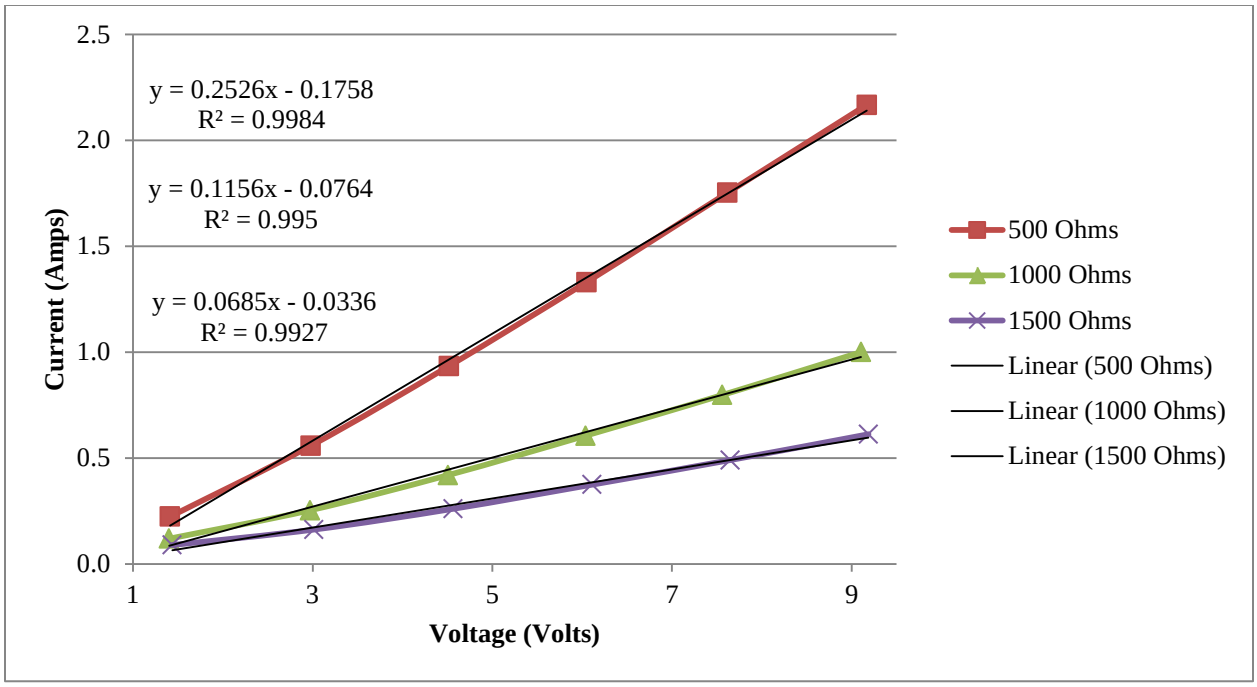

Figure 52: Current Flow Relative to Voltage and Electrical Loading (Generator 3)

Generator three was tested at three electrical loading conditions of 500, 1000, and 1500 ohms; the curve shows the interrelationship of the generator voltage output with respect to current output.

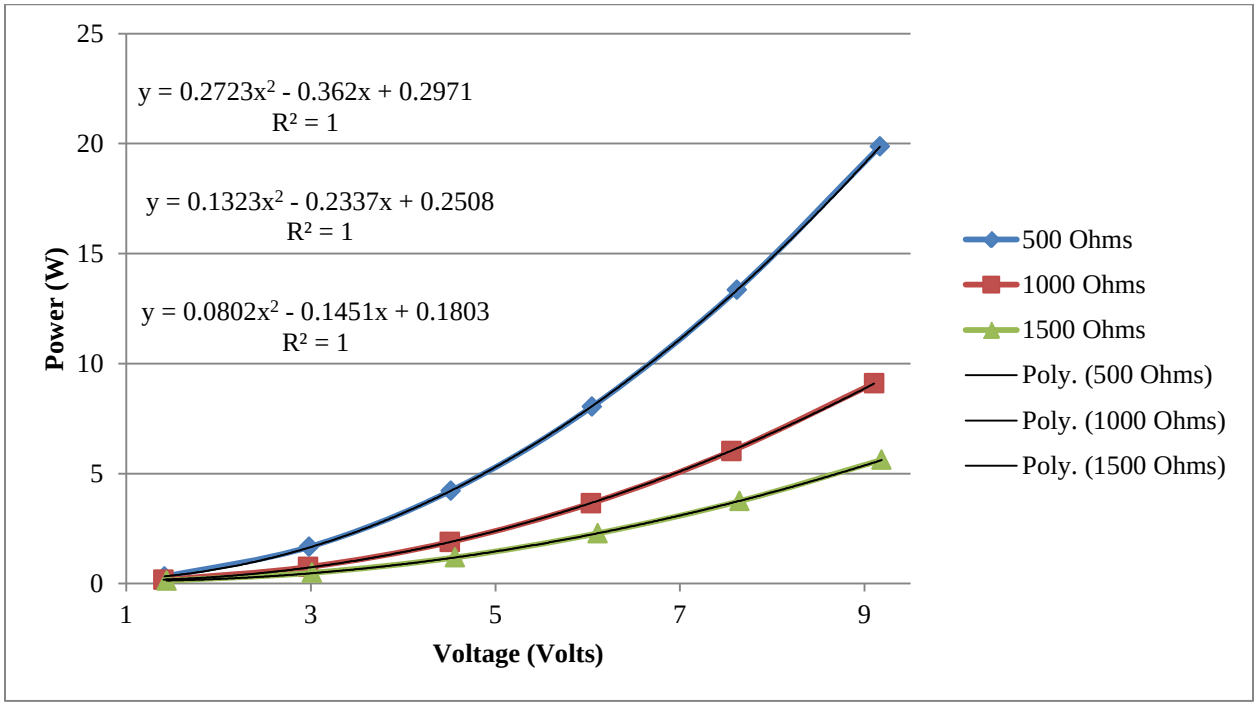

Figure 53: Power Production Relative to Voltage and Electrical Loading (Generator 3)

The preceding curves were derived from the Current vs. Voltage Interrelationship graph depicted above by utilizing the

9.6 Electrical Conditioning System

In this section the group will outline the steps utilized for design and development of the electrical conditioning system.

9.6.1 Generator Information Prompt

The following is the script, verbatim, from Mr. Allen Kelly outlining the general information required to design the electrical conditioning system for the project:

> *Somewhere in the exercise I know you have defined the following. Put the parameters below into a spreadsheet and I can have a reasonable BOM done rather quickly (actually a basic design) including some reasonable BOM costs for projections of up to about 100 units.*
>
> *You have to tell me a **due date** since I am busy I want to hit the due date to give you time to review and apply the data to your study.*
>
> ***Power Supply Input Parameters:***
>
> *1. Maximum Generator Voltage Available: … Vin_{max}*
>
> *2. Minimum useable Generator Voltage. … Vin_{min}*
>
> *3. Maximum Generator Current Available at the (above) Minimum Generator Voltage: …Iin_{Vmin}*
>
> *4. Maximum Generator Current Available at Maximum Voltage:Iin_{vmax}*
>
> *5. Power curves (if you can produce them) showing current versus voltage interrelationships.*
>
> ***Power Supply Output Parameters:***
>
> *1. Is a Hiccup mode desired during low generator production? A mode where capacitive storage and threshold detection can be used to store energy in capacitors until thresholds are met that will deliver a burst of well-regulated full power for a short period and shut down until such time as another cache of energy is built up into a capacitor.*
>
> *2. Desired **Minimum ON time** for hiccup mode. … T_{opmin}*
>
> ***3. Maximum output current**.. Example USB 1 = 150ma USB2 = 500ma **… $Iout_{max}$***
>
> *4. **Maximum output current limit** (this is different from the above in that the above is an operating limit, this is a cut-off limit) … **$Iout_{lim}$***
>
> ***5.** Voltage output requirements example: 5 Volts ±0.5 **… V_{out}***
>
> ***Power Supply Environmental Parameters:***
>
> *Operating temperatures Min and Max.*

Is package a completely water proof coating required?

Is power supply board structurally integrated (subject to operational mechanical stress) or structurally protected? Is there a designated location?

9.7Computer Aided Design (CAD) of System

The computer aided design (CAD) of the system knee brace was drafted utilizing Pro/ENGINEER Wildfire 5.0 while subsequent dimensioning and drawing depictions were rendered utilizing Dassault Systèmes, S. A. SolidWorks 2012.

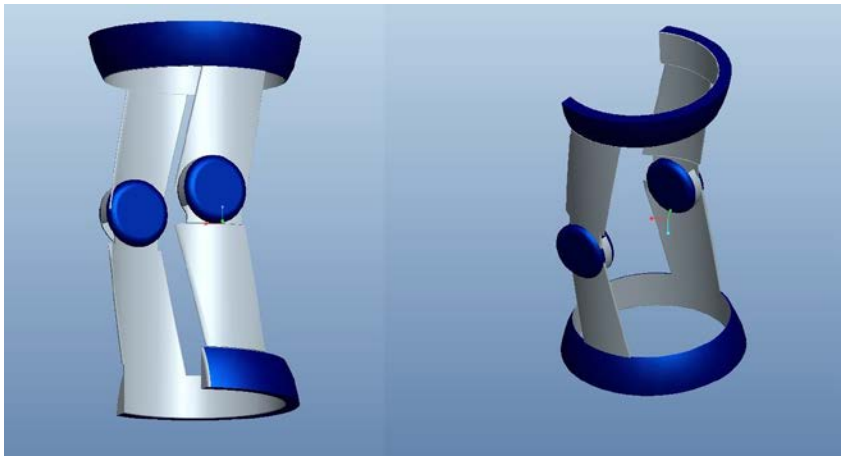

Figure 54: Pro/ENGINEER Preliminary 3D Solid Model

Figure 54 *shows an early and crude CAD model view of the bioenergy harvester*.

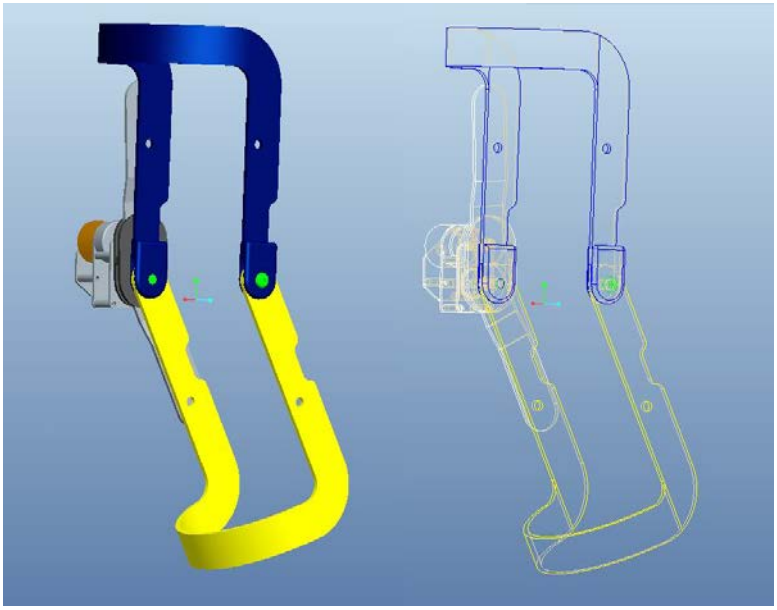

Figure 55: Pro/ENGINEER Secondary 3D Solid Model & Wireframe Front View

Figure 55 *shows a more refined design assembled axillary front view of the bioenergy harvester with the 3D solid model and wireframe depictions. *Note: Although the design is better refined, it still lacks the double hinge mechanism ultimately incorporated in the final design.*

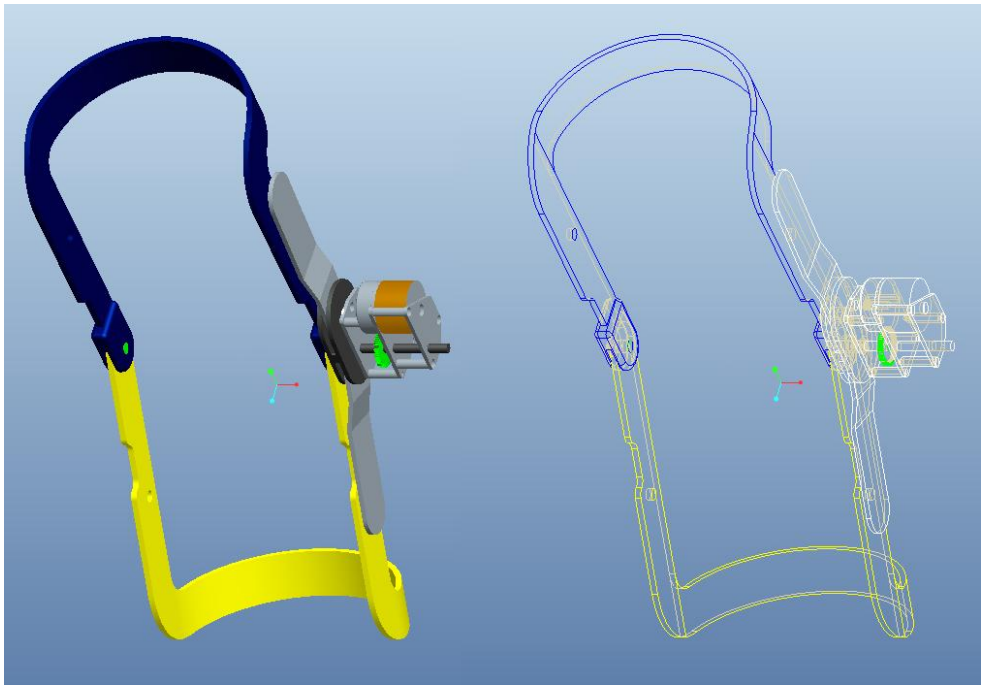

Figure 56: Pro/ENGINEER Secondary 3D Solid Model & Wireframe Back View

Figure 56 *shows the assembled axillaryback view of the bioenergy harvester with the 3D solid model and wireframe depictions.*

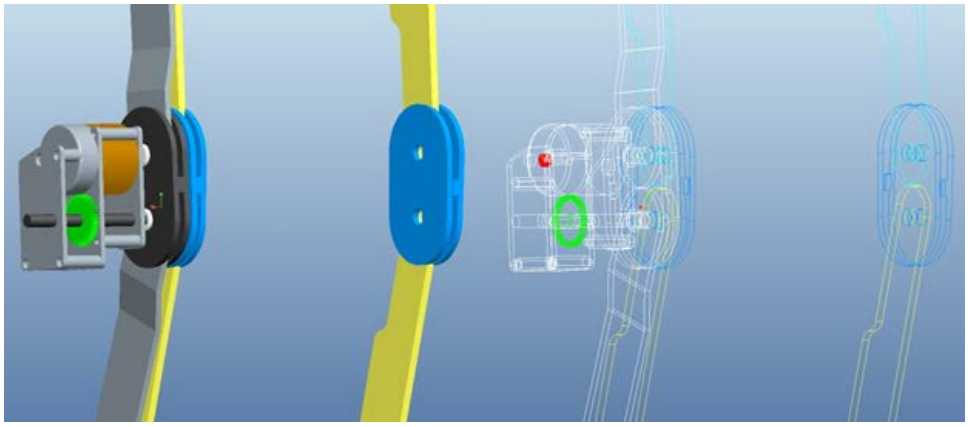

Figure 57: Pro/ENGINEER Front 3D Solid Model & Wireframe Views

Figure 57*shows the assembled auxiliary front view of the bioenergy harvester with the 3D solid model and wireframe depictions.*Note: CAD model has now reached final design incorporating a double hinge mechanism more closely resembling that of the final physical prototype.*

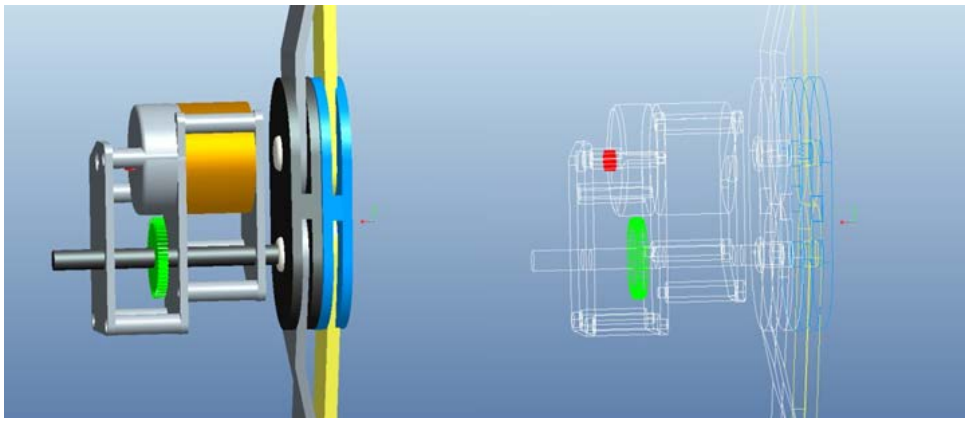

Figure 58: Pro/Engineer Transmission Close-up 3D Solid Model & Wireframe Views

Figure 58 *shows a close-up assembled front view of the bioenergy harvester.*
**Note: Several gearing components haven't been included for this modeling due to lack of final gearing ratio selection during modeling process.*

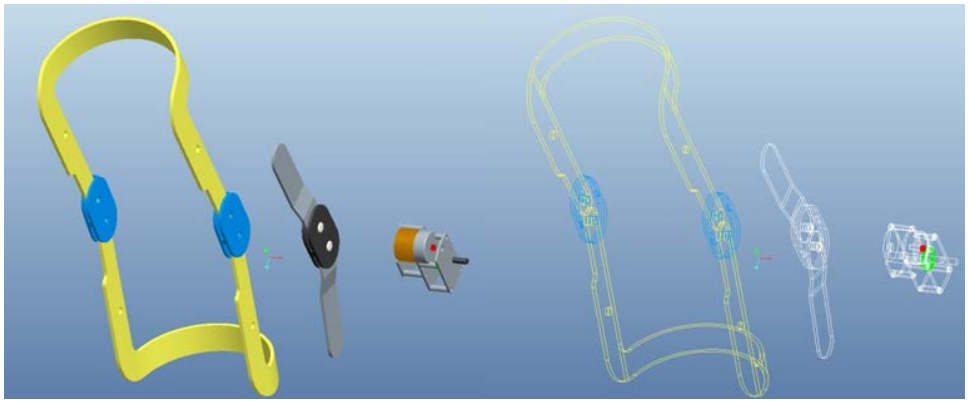

Figure 59: Pro/Engineer Back Exploded 3D Solid Model & Wireframe Views

Figure 58Figure 59 *shows an auxiliary back view of the bioenergy harvester with the 3D solid model and wireframe depictions.*

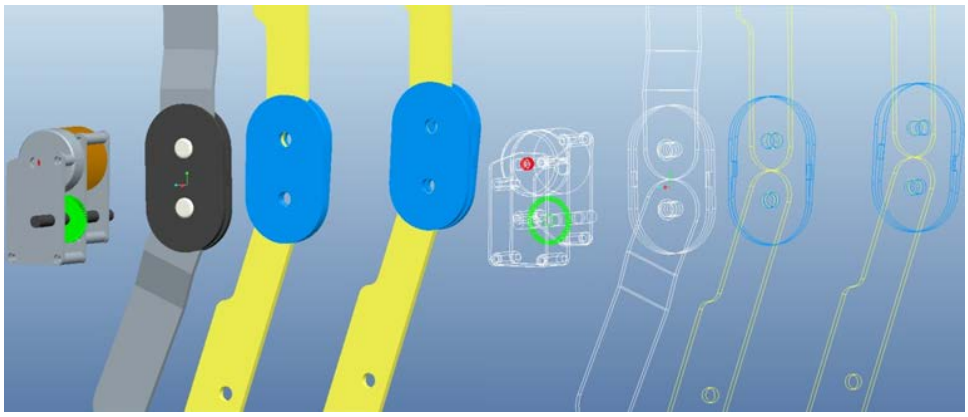

Figure 60: Pro/Engineer Exploded Subsystems Solid Model & Wireframe Views

Figure 60 *shows an exploded view of the generator/transmission, polycentric hinge, and brace subsystems.*

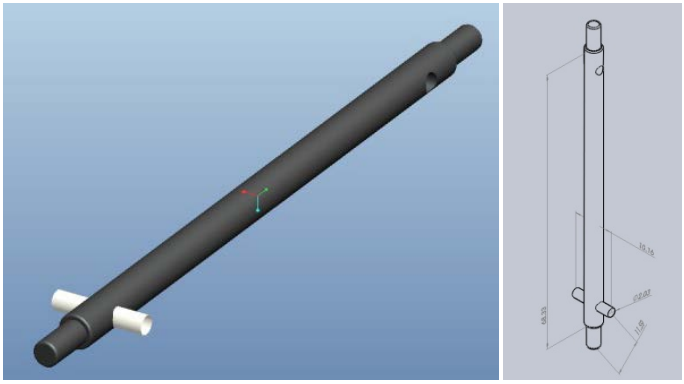

Figure 61: SolidWorks Solid Model & Wireframe Views of the Shaft and Pin Assembly

*Figure 61 shows a solid and wireframe view of the shaft/pin assembly.*Note: For shaft dimensions please view section*

The following section shows several drawings which were drafted Dimensioning and drawing depictions were rendered utilizing Dassault Systèmes, S. A. SolidWorks 2012.

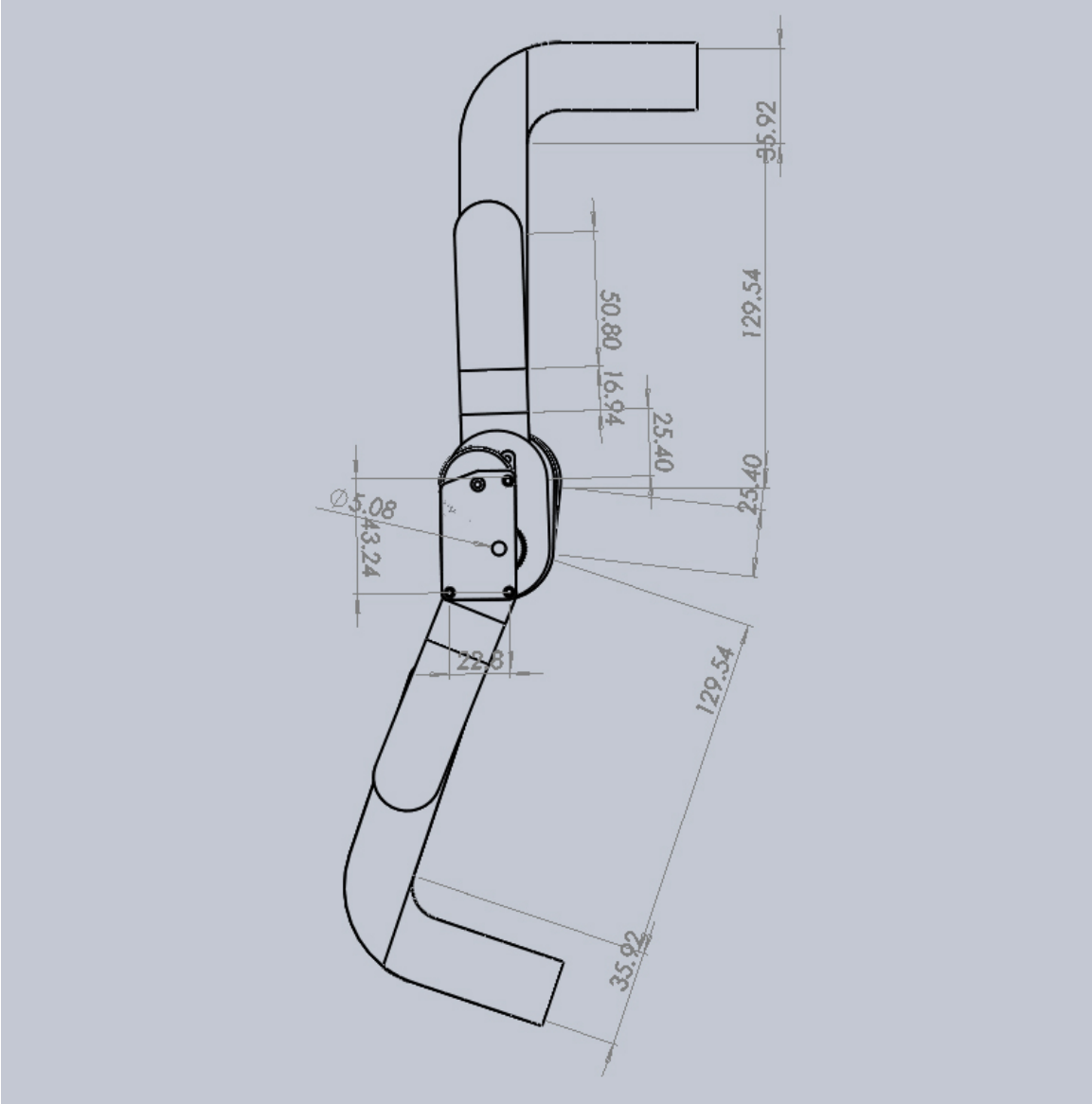

Figure 62: SolidWorks Solid Model Left View of the Knee Brace Assembly

*The preceding figure shows a left view of the bioenergy harvester with wireframe and dimension depictions. *Note: Units are in Inches*

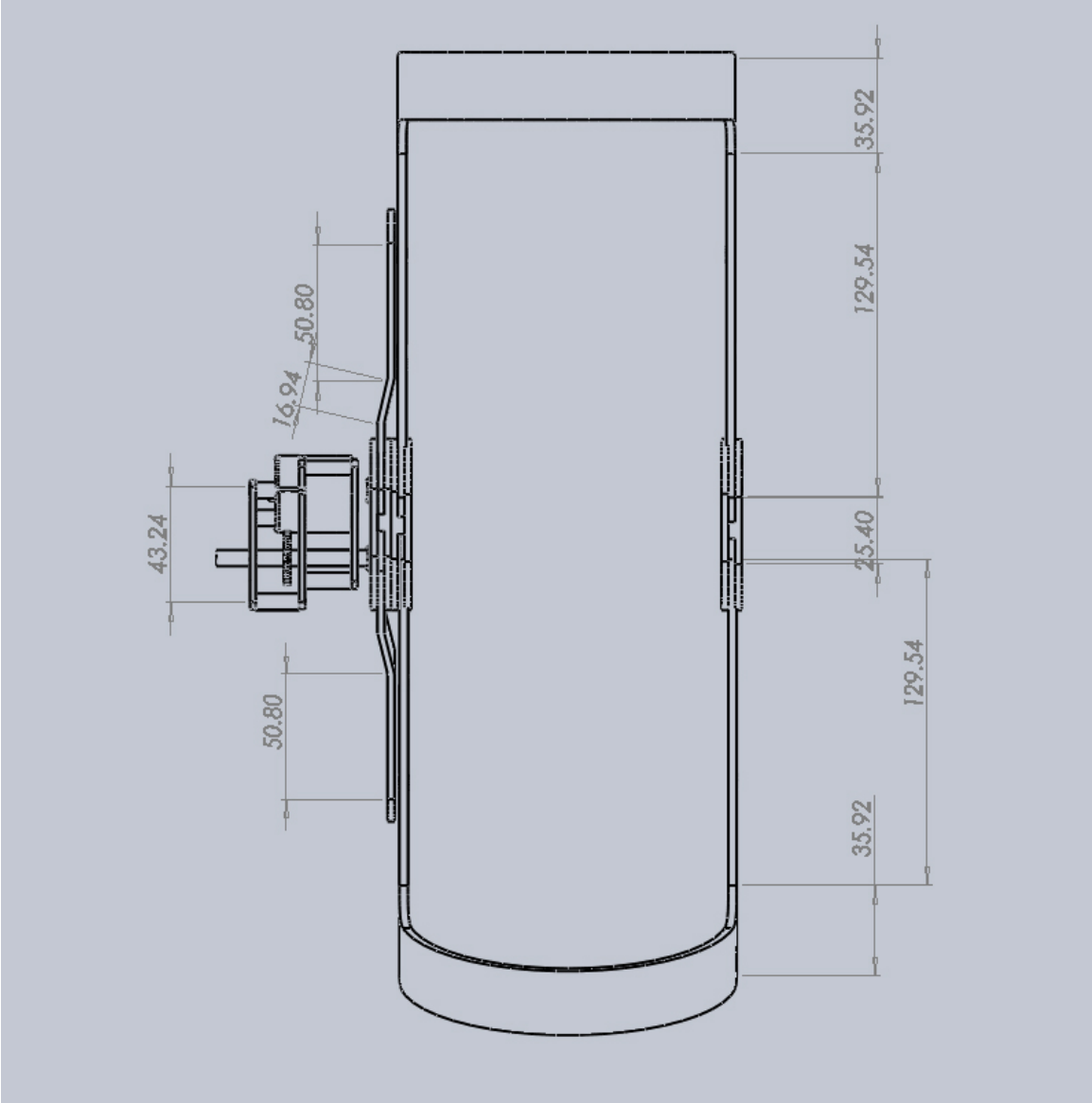

Figure 63: SolidWorks Solid Model Front View of the Knee Brace Assembly

*Figure 63 shows a front view of the bioenergy harvester with wireframe and dimension depictions. *Note: Units are in Inches*

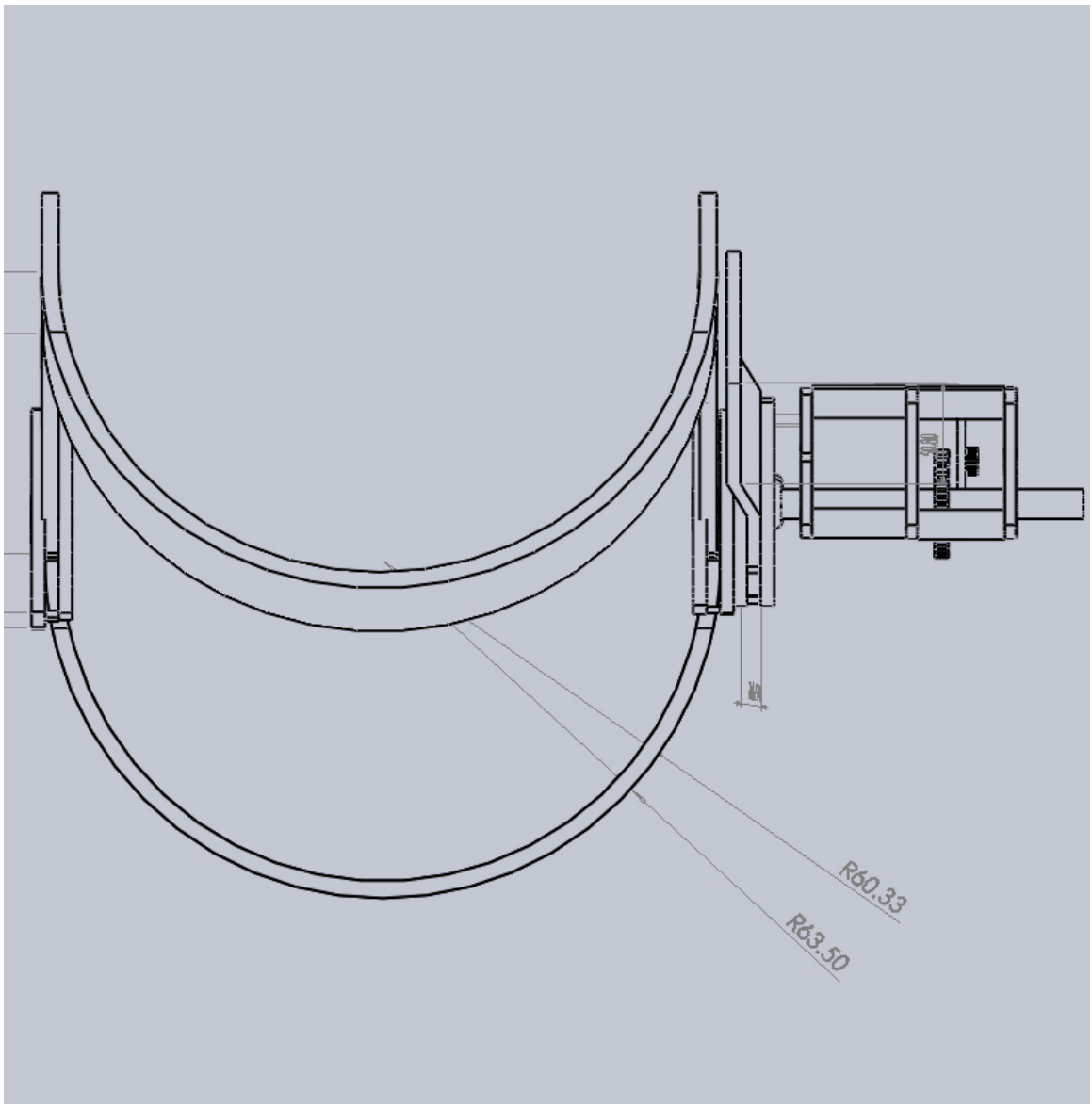

Figure 64: SolidWorks Solid Model Top View of the Knee Brace Assembly

*The previous figure shows a top view of the bioenergy harvester with wireframe and dimension depictions. *Note: Units are in Inches*

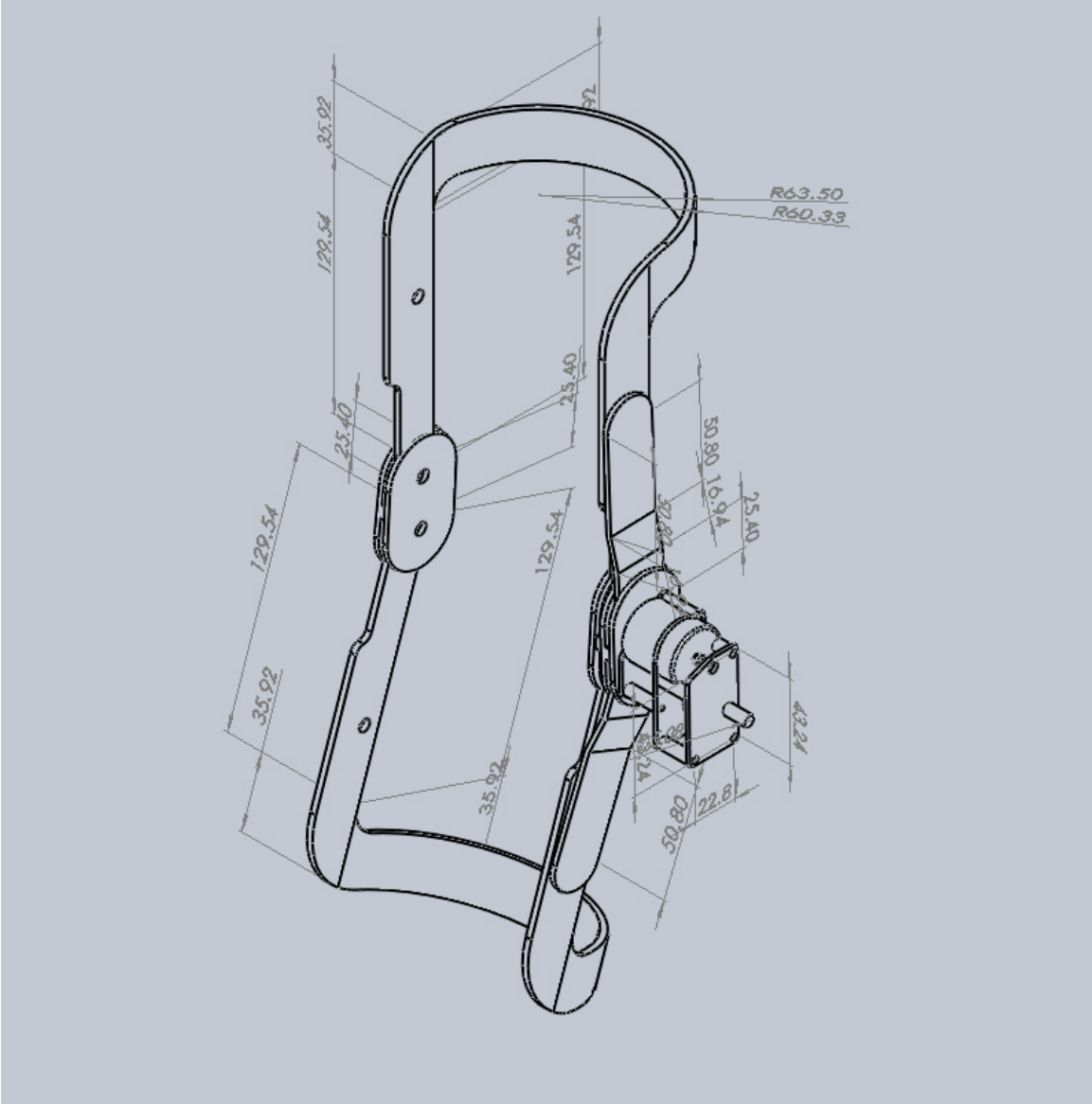

Figure 65: SolidWorks Solid Model 3-Dimensional View of the Knee Brace Assembly

*Figure 65 shows a 3-dimensional view of the bioenergy harvester with wireframe and dimension depictions. *Note: Units are in Inches*

10.0 Construction of System

The following section reviews several of the steps taken by the design group to construct the system.

10.1 Final Parts List

For the production of this prototype system the design team opted to utilize several off the shelf items. These items were chosen for multiple reasons and the favorable characteristics of the transmission, hinge, and brace systems can be reviewed in sections 9.4.4 Selection of Transmission System, 9.3.3 Selection of Knee Brace System, and 9.3.4 Secondary Selection of Knee Brace System, respectively.

Figure 66: Final Component Sub-assemblies

The above figure shows the component sub-assembly systems chosen for the bio-energy knee brace. Left to right: Bledsoe Axiom knee brace, Tamiya High Power gear train system, and Mueller polycentric hinge system.

10.2 Shaft/Hinge Assembly

After several design considerations for transmission of knee angular deflection to the transmission system the design team finally settled on the following attachment method.

By selective disassembly of one arm of the hinge system the design team was able to mill a one-eight diametric slot for placement of the transmission shaft axel. In doing this the transmission shaft axel then became rigidly connected to the hinge arm; therefore, acting as the pivot point of the arm and undergoing the angular motion of its mating part.

Figure 67: Hinged Arm with Mating Pinned Transmission Shaft

The above figure shows the hinged arm component post machining of the slotted channel way for fitting of the pinned transmission axel.

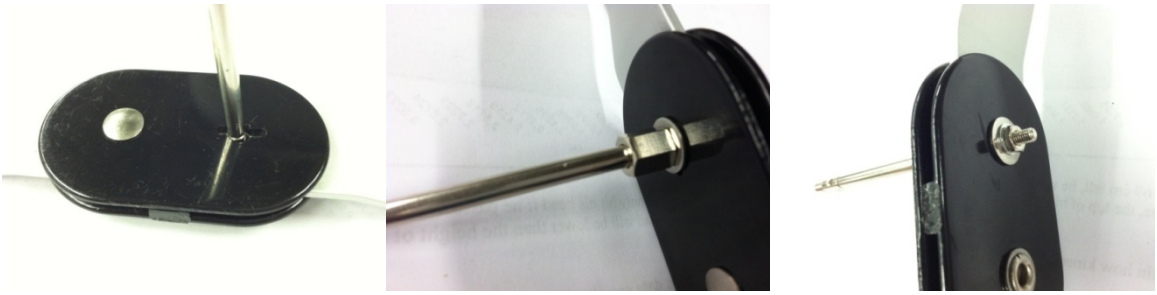

Figure 68: Pictorial Process of Shaft to Hinge Assembly

Figure 68 depicts the process of attachment of the transmission shaft to the hinge system. Left to right: shaft was inserted through arm and base plate channel ways, inserted shaft was fitted with a spacing nut for subsequent transmission mounting, a locking nut is added to the shaft end for placement.

10.3 Gear Box Mounting

After retrofitting of the shaft to the hinge system, subsequent placement of the transmission was conducted. The frame of the transmission was fitted onto the base of the hinge by way of custom brackets. Once these brackets were in place use of a *Loctite Instant Mix 5 Minute Epoxy* was utilized for attachment.

10.3 Final Assembly Details

Elastic bands were used to allow for the epoxy to cure overnight. At first glance, the epoxy seemed a fitting way of attaching the gear box to the hinge mechanism, however later test trials proved otherwise. Shortly after a mechanical failure during one of the test runs, the epoxy failed detaching the gear system from the polycentric hinge mechanism. The decision was made to use mechanical bolts to secure the gear box rather than reuse epoxy.

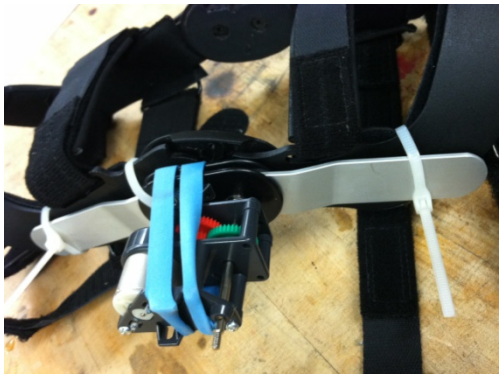

Figure 69: Impromptu Flexion/Extension Prototype Testing

Figure 69 shows the initial mounting, shortly after assembly, of the bio-mechanical energy harvester to a human subject. During this situation a member of the design team demonstrated the of the prototype to flex and extend: mirroring the motion of the knee joint movements.

10.3 Reinforcement Changes

As previously mentioned after initial testing, adhesion failure of the epoxy/resin system which held the transmission to the base plate of the polycentric hinge system was noticed. In order to re-attach and mediate further detachments four UNC # 1 self-tapping screws were utilized to screw the transmission brackets to the upper base plate of the hinge.

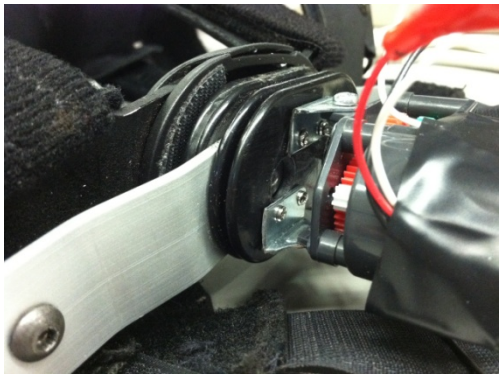

Figure 70: Transmission Attachment Depicting Alternative Screw Attachment Method

The preceding picture shows the alternative attachment method selected for attaching the transmission and generator subsystem to the hinge component.

11.0 Prototype Testing

In the proceeding section the method of testing the prototype will be explained. The data gathered from the experimental testing will be analyzed as well.

11.1 Experimental Setup

A treadmill containing a speedometer was obtained in order to test the prototype. A subject utilized the treadmill at 3, 5, and 7 MPH with the prototype strapped on.

The 3 MPH testing rate was chosen to produce a comparable set of data to that of the paper published by Donelan and his research group. Since, Donelan's subject testing rate corresponded to 1.3 m/sec or 2.91 MPH we elected to test at 3 MPH. (J. M. Donelan, 2008)

An additional testing rate of 5 MPH was chosen based on literature research on "average speed walker data"; while, 7 MPH testing rates was derived based on data provided by *Pace Calculator* for the average running speed of a 23 year old male. (Myer, 2012) (Pace Calculator) The following equation was used to determine the average pace for the above mentioned demographic:

$$5K\ Pace\ (MPH) = \frac{1\ (Hr)}{Average\ Mile\ Time\ (Hr)}$$

Derived from Pace calculator the average mile time of a 23 year old male was 09:09:16 per mile or 6.56 MPH, which was rounded to 7 MPH for subsequent testing.

A data acquisition system was connected to the prototype in order to transfer data onto a PC. Utilizing National Instruments LabVIEW software, the voltages produced by the prototype were graphed and recorded. Multiple subjects were gathered in order to have sufficient data to analyze.

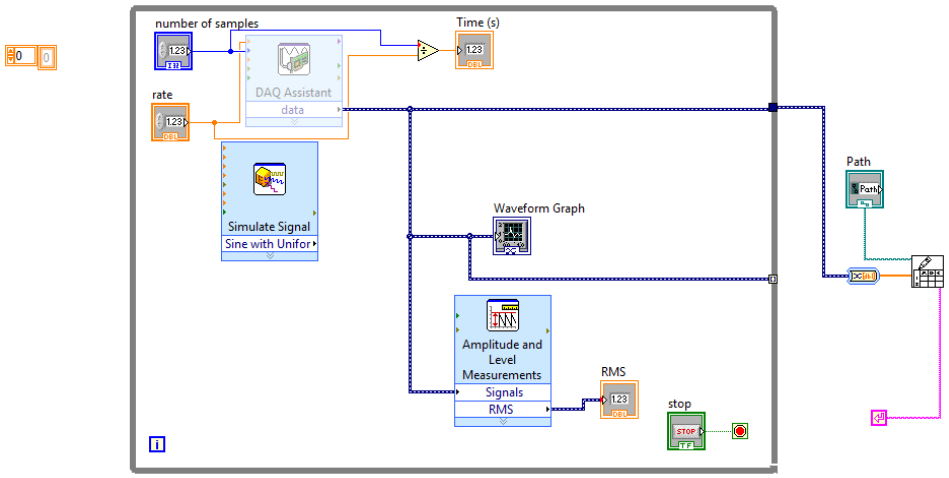

Figure 71: LabView Block Diagram for Prototype Analysis

The preceding figure shows the block diagram path the data acquisition system follows in collecting input signaling from the harvester's electromagnetic generator.

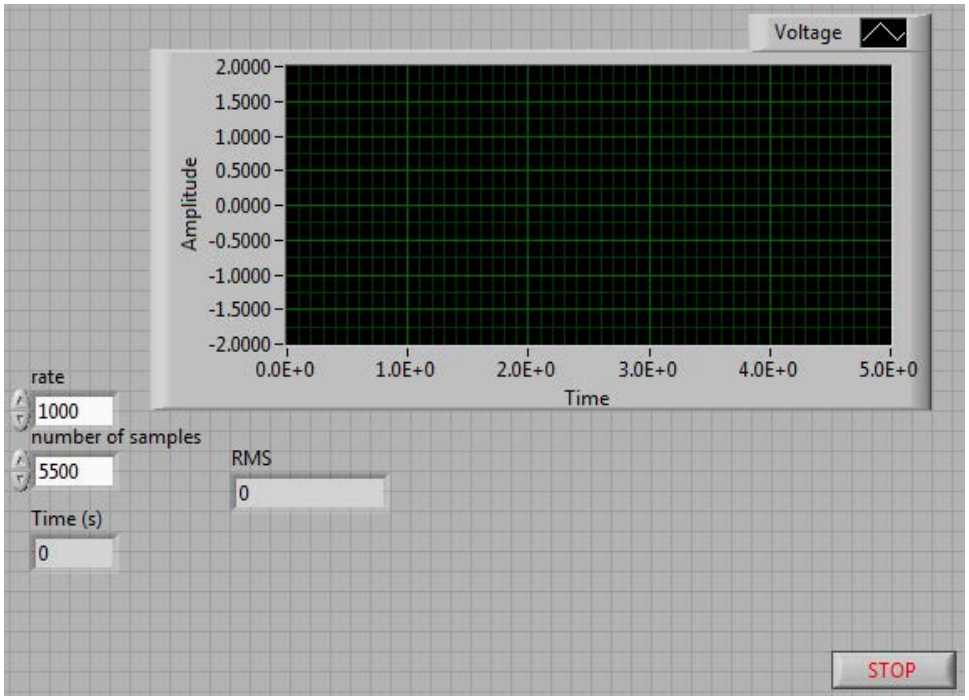

Figure 72: LabVIEW Front Panel for Project Analysis

Figure 58*The above figure shows the front panel view of the data acquisition system. A time variant waveform is displayed of the input signal, were the amplitude of the waveform is the time dependent voltage and the x-axis corresponds to the cycle time-step.*

The LabVIEW Front Panel display acts as a user interface for starting/stopping data acquisition, altering the sampling rate and the number of samples taken. Our sampling rate and number of samples were taken to correspond closely to the data parameters presented in previous literature. The paper by Riemer and Shapiro, states that their test data was collected at a test speed of 1.3 m/s, which we approximated to 3 MPH, and cycle frequency of 0.9 Hz. (Raziel Riemer, 2011)

$$Time\ (t) = \frac{1}{frequency\ (f)}$$

From the preceding equation the design team calculated the test time per cycle to be ~1.1 seconds; we multiplied the cycle time by a factor of five to obtain anour data collection cycle of ~5.5 seconds.

$$Data\ Collection\ Cycle = \frac{Rate}{Number\ of\ Samples}$$

From the preceding equation we chose the rate and number of samples to be 1,000 samples/sec. and 5,000 samples, respectively.

11. 2 Data Collection

The tables below contain only a small portion of all the voltage readings garnered during different trials. An RMS calculation, whose formula can be seen below, was done for each trial and the average RMS value for all the trials was obtained.

$$V_{RMS} = \sqrt{\frac{1}{n}(V_1^2 + V_2^2 + \cdots + V_n^2)}$$

Using the average RMS value we were able to calculate the average power and current RMS values. The following shows the interrelationship formula used to derive the average power and current RMS:

$$Average\ Power\ (P_{Avg.}) = \frac{(V_{RMS})^2}{R} \overset{also}{\Longrightarrow} V_{RMS} \times I_{RMS}$$

11.2.1 Subject 1 Data

The following section presents the data collected from Subject 1 during testing of the performance of the biomechanical energy harvesting brace.

Table 24: Subject 1 Treadmill Data (3 MPH)

3 MPH							
Trial 1	Trial 2	Trial 3	Trial 4	Trial 5			V_{RMS} (Volts)
-0.341	0.000	-0.446	0.004	0.009		Trial 1	0.201
-0.486	0.000	-0.484	0.004	0.008		Trial 2	0.175
-0.501	0.000	-0.472	0.005	0.006		Trial 3	0.165
-0.462	0.000	-0.411	0.007	0.004		Trial 4	0.192
-0.371	0.000	-0.326	0.007	0.000		Trial 5	0.204
-0.442	0.000	-0.457	0.008	-0.001			
-0.478	0.000	-0.477	0.009	0.000		Avg. V_{RMS} (Volts)	0.187
-0.47	0.000	-0.456	0.011	0.000		Avg. P_{RMS} (Watts)	0.0001
-0.42	0.000	-0.391	0.011	0.000		Avg. I_{RMS} (Amps)	0.0004
-0.331	0.000	-0.313	0.012	0.000			

*The preceding table contains the average RMS values for voltage, current and power at three miles per hour.*Note: Subject 1 was a male with a height and weight of 5'8" (1.73 m) and 158 lbs. (71.67 kg), respectively.*

Table 25: Subject 1 Treadmill Data (5 MPH)

5 MPH							
Trial 1	Trial 2	Trial 3	Trial 4	Trial 5			V_{RMS} (Volts)
0.022	0.784	0.892	-0.014	-0.525		Trial 1	0.342
0.022	0.717	0.612	-0.01	-0.538		Trial 2	0.335
0.021	0.651	0.856	-0.007	-0.494		Trial 3	0.366
0.021	0.769	0.831	-0.004	-0.388		Trial 4	0.354
0.022	0.707	0.735	-0.003	-0.491		Trial 5	0.336
0.023	0.62	0.879	-0.003	-0.528			
0.024	0.738	0.66	-0.001	-0.5		Avg. V_{RMS} (Volts)	0.347
0.026	0.677	0.806	0.001	-0.408		Avg. P_{RMS} (Watts)	0.0002
0.028	0.59	0.855	0.002	-0.472		Avg. I_{RMS} (Amps)	0.0007
0.03	0.715	0.645	0.003	-0.52			

The table above contains the average RMS values for voltage, current and power at five miles per hour.

Table 26: Subject 1 Treadmill Data (7 MPH)

7 MPH							
Trial 1	Trial 2	Trial 3	Trial 4	Trial 5			V_{RMS} (Volts)
0.522	0.997	0.73	-0.092	0.189		Trial 1	0.444
0.667	1.087	0.809	-0.089	0.179		Trial 2	0.453
0.672	0.989	0.685	-0.086	0.168		Trial 3	0.460
0.438	1.102	0.651	-0.084	0.156		Trial 4	0.498
0.57	1.006	0.697	-0.08	0.116		Trial 5	0.442
0.613	1.129	0.597	-0.076	0.122			
0.565	1.002	0.495	-0.072	0.128		Avg. V_{RMS} (Volts)	0.459
0.402	1.121	0.554	-0.069	0.134		Avg. P_{RMS} (Watts)	0.0004
0.493	1.036	0.52	-0.065	0.136		Avg. I_{RMS} (Amps)	0.0009
0.516	1.135	0.435	-0.061	0.136			

The above table contains the average RMS values for voltage, current and power at seven miles per hour.

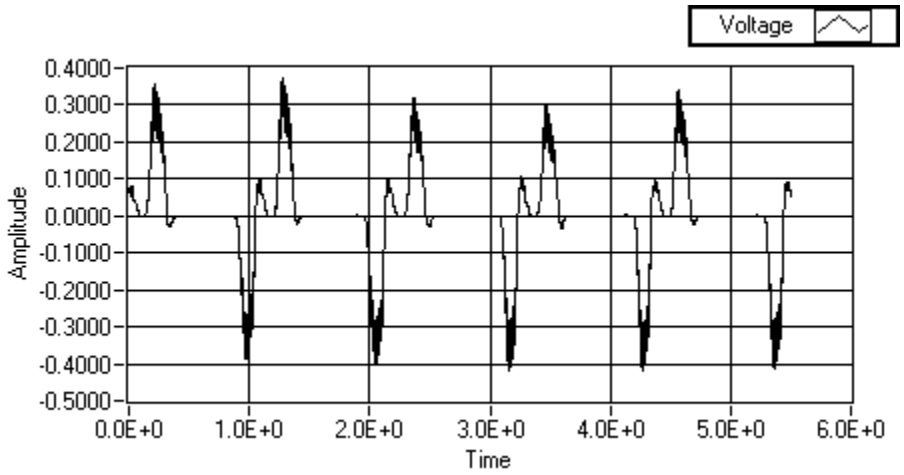

Figure 73: Subject 1 LabVIEW Waveform Data (3 MPH)

The preceding figure shows the voltage waveform production of Subject 1 during trial 1 of 5 at 3 MPH.

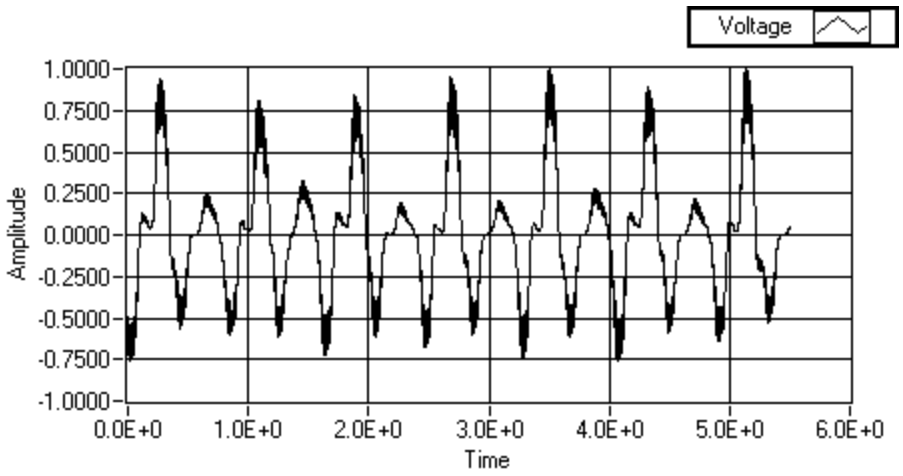

Figure 74: Subject 1 LabVIEW Waveform Data (5 MPH)

The preceding figure shows the voltage waveform production of Subject 1 during trial 1 of 5 at 5 MPH.

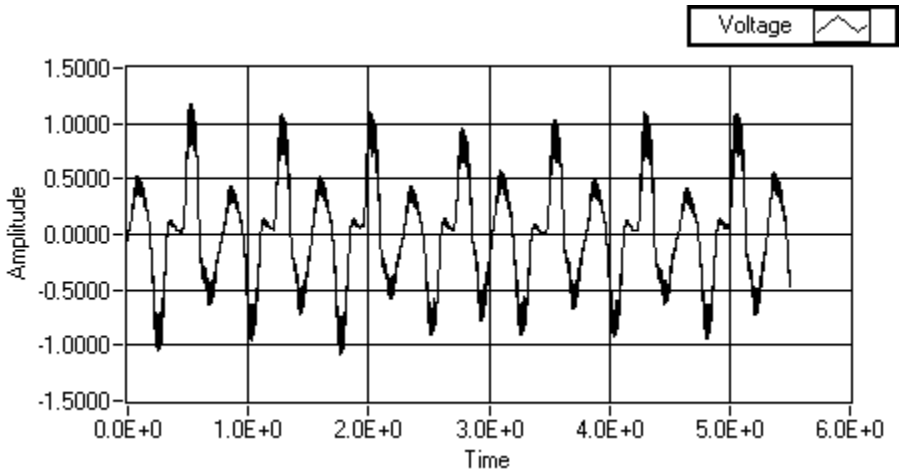

Figure 75: Subject 1 LabVIEW Waveform Data (7 MPH)

The preceding figure shows the voltage waveform production of Subject 1 during trial 1 of 5 at 7 MPH.

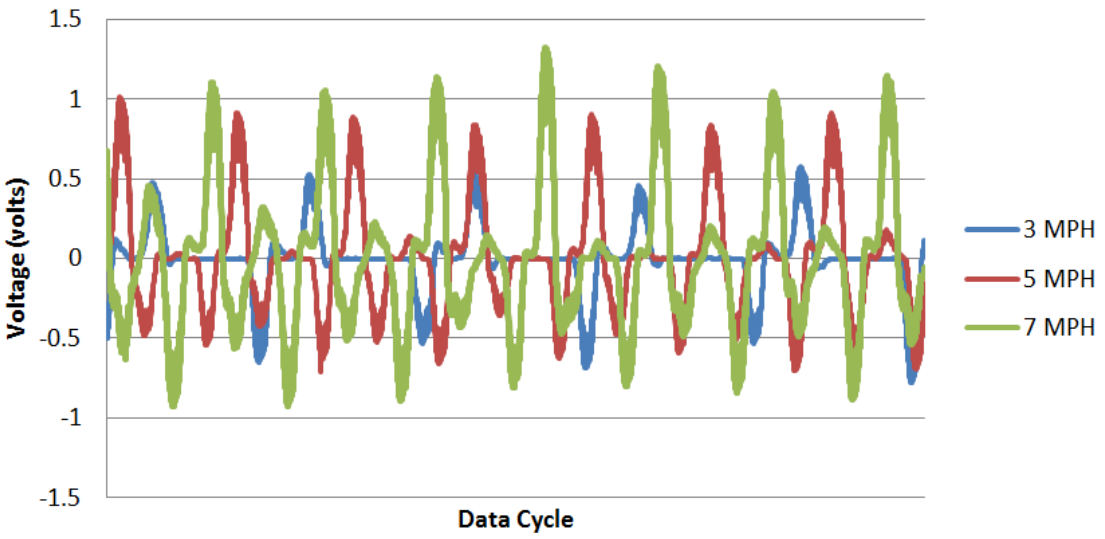

Figure 76: Subject 1 Coalesced Treadmill Data

The graph displayed above shows how the voltage readings changed with respect to time. All the data points recorded for one trial at each of three different velocities were graphed together in order to compare the voltage readings.

11.2.2 Subject 2 Data

The following section presents the treadmill data gathered when Subject 2 was fitted to undergo testing with the bio-energy harvester.

Table 27: Subject 2 Treadmill Data (3 MPH)

3 MPH							
Trial 1	Trial 2	Trial 3	Trial 4	Trial 5			V_{RMS} (Volts)
-0.11	0.173	0	0.622	0		Trial 1	0.169
-0.11	0.166	0	0.512	0		Trial 2	0.248
-0.11	0.159	0	0.567	0		Trial 3	0.240
-0.109	0.216	0	0.625	0		Trial 4	0.242
-0.107	0.244	0	0.59	0		Trial 5	0.169
-0.106	0.27	0	0.458	0			
-0.103	0.287	0	0.579	0		Avg. V_{RMS} (Volts)	0.214
-0.101	0.293	0	0.616	0		Avg. P_{RMS} (Watts)	0.00009
-0.099	0.286	0	0.554	0		Avg. I_{RMS} (Amps)	0.00043
-0.096	0.261	0	0.418	0			

*The preceding table contains the average RMS values for voltage, current and power at three miles per hour.*Note: Subject 2 was a female with a height and weight of 5'2" (1.57 m) and 117 lbs. (53.07 kg), respectively.*

Table 28: Subject 2 Treadmill Data (5 MPH)

5 MPH							
Trial 1	Trial 2	Trial 3	Trial 4	Trial 5			V_{RMS} (Volts)
0.259	0.568	-0.435	-0.301	0.456		Trial 1	0.338
0.22	0.569	-0.468	-0.308	0.49		Trial 2	0.381
0.302	0.501	-0.457	-0.296	0.478		Trial 3	0.345
0.311	0.378	-0.373	-0.3	0.407		Trial 4	0.388
0.305	0.51	-0.496	-0.375	0.446		Trial 5	0.361
0.291	0.521	-0.569	-0.435	0.513			
0.265	0.469	-0.574	-0.463	0.522		Avg. V_{RMS} (Volts)	0.363
0.233	0.367	-0.443	-0.448	0.467		Avg. P_{RMS} (Watts)	0.0003
0.196	0.427	-0.603	-0.39	0.367		Avg. I_{RMS} (Amps)	0.0007
0.221	0.452	-0.677	-0.509	0.521			

The above table contains the average RMS values for voltage, current and power at five miles per hour.

Table 29: Subject 2 Treadmill Data (7 MPH)

7 MPH							
Trial 1	Trial 2	Trial 3	Trial 4	Trial 5			V_{RMS} (Volts)
-0.943	-0.594	-0.001	0.157	0.004		Trial 1	0.399
-0.896	-0.495	-0.001	0.152	0.005		Trial 2	0.393
-0.863	-0.606	0	0.146	0.003		Trial 3	0.070
-0.959	-0.617	-0.001	0.112	-0.003		Trial 4	0.094
-0.72	-0.537	-0.001	0.12	-0.003		Trial 5	0.044
-0.954	-0.496	-0.002	0.129	-0.004			
-0.824	-0.577	-0.003	0.139	-0.004		Avg. V_{RMS} (Volts)	0.200
-0.896	-0.568	-0.004	0.146	-0.004		Avg. P_{RMS} (Watts)	8.00272E-05
-0.922	-0.482	-0.005	0.152	-0.003		Avg. I_{RMS} (Amps)	0.000400068
-0.766	-0.473	-0.004	0.156	-0.003			

Table 29 *contains the average RMS values for voltage, current and power at seven miles per hour. *Note: Trials 3-5 should be noted to have significant variance from trials 1-2 from the same subject.*

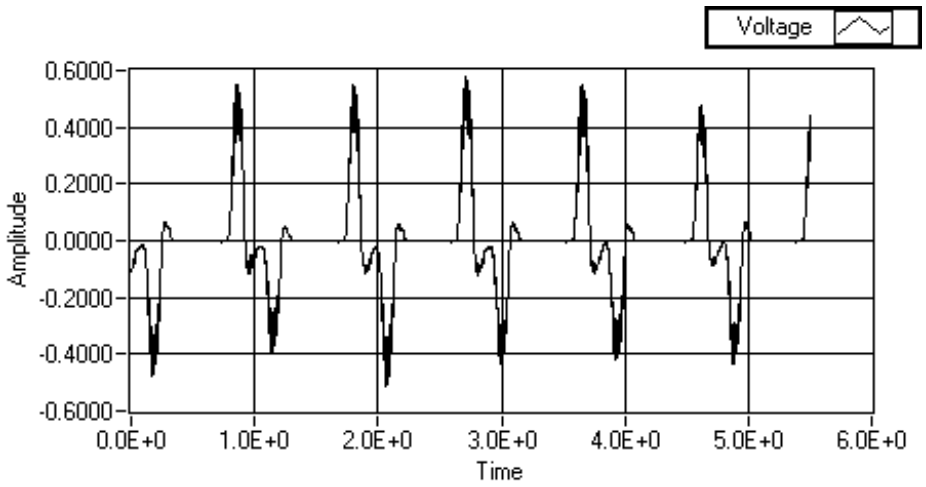

Figure 77: Subject 2 LabVIEW Waveform Data (3 MPH)

The preceding figure shows the voltage waveform production of Subject 2 during trial 1 of 5 at 3 MPH.

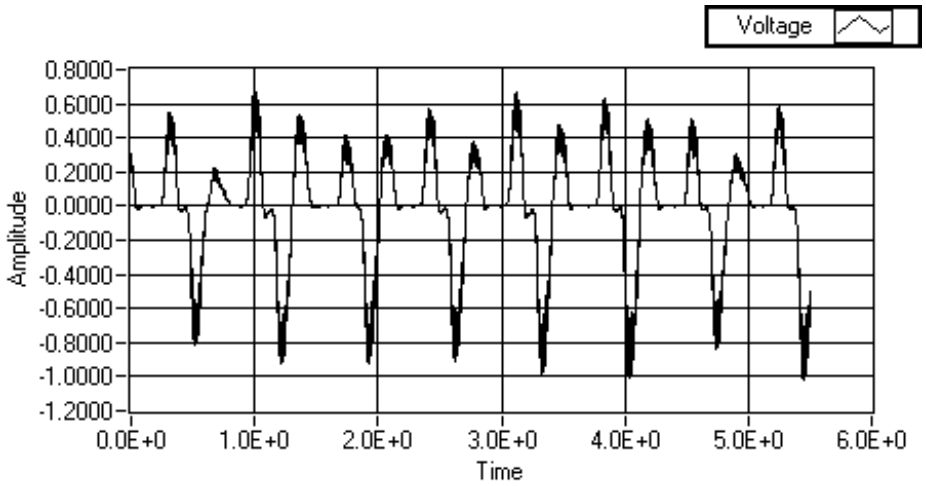

Figure 78: Subject 2 LabVIEW Waveform Data (5 MPH)

The preceding figure shows the voltage waveform production of Subject 2 during trial 1 of 5 at 5 MPH.

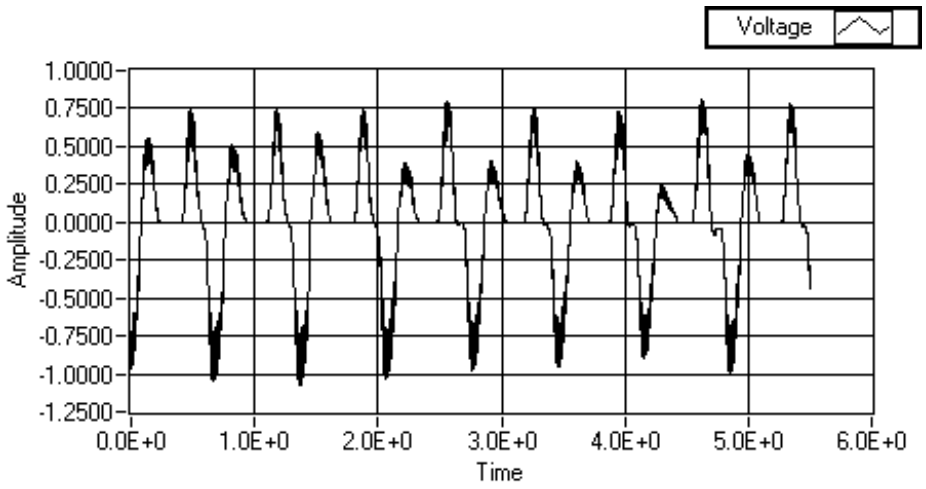

Figure 79: Subject 2 LabVIEW Waveform Data (7 MPH)

The preceding figure shows the voltage waveform production of Subject 1 during trial 1 of 5 at 7 MPH.

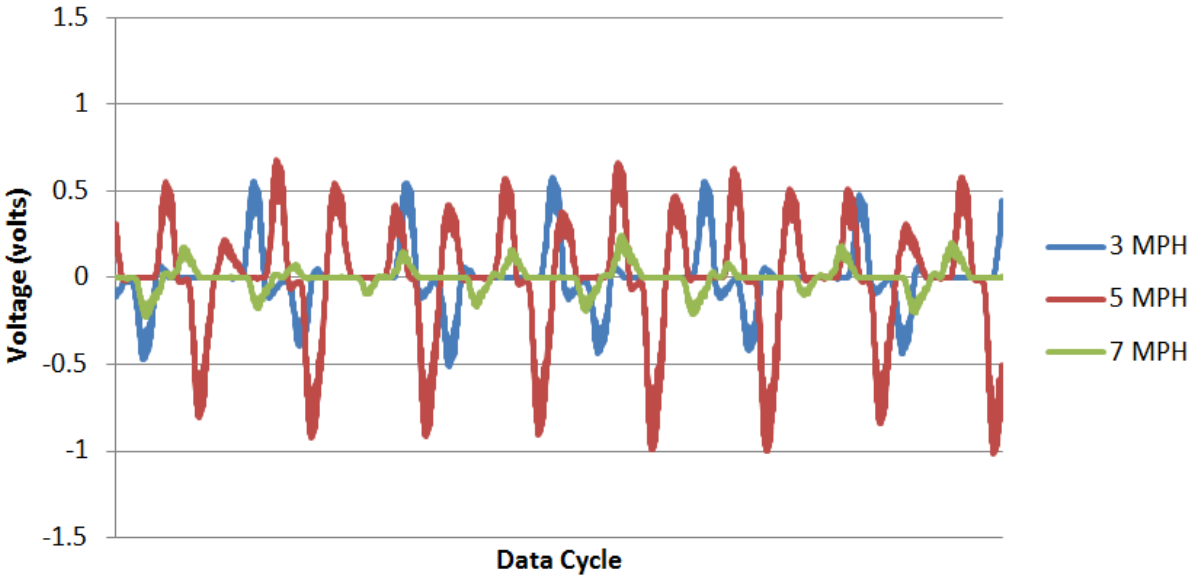

Figure 80: Subject 2 Coalesced Treadmill Data

The graph displayed above shows how the voltage readings changed with respect to time. All the data points recorded for one trial at each of three different velocities were graphed together in order to compare the voltage readings.

Due to abnormal experimental data produced by Subject 2 the mechanisms of failure were needed to be addressed in order for a secondary round of data collection to be conducted. In

order to view descriptions of prototype failure and subsequent analysis and redesign please view section 11.3 Prototype Failure and it's respective sub-headings.

11.3 Prototype Failure

The data gathered from Subject 2 during trials 3-5 at 7 MPH did not correspond to the data garnered during trials 1-2 at the same speed. This seemed a bit awkward to the team so we began inspecting the prototype for any damage.

When we disconnected the transmission shaft from the polycentric hinge system the connecting pin fell out in two pieces. When rotating the transmission shaft the hollow pin experienced greater shear stresses than it could handle and failed. This resulted in limited power transmission from the host to the generator and the production of the misleading data recorded for subject 2 at 7 MPH.

Figure 81: Pin Failure due to Shear

The figure above shows the transmission shaft and the connecting pin after it failed under shear loading. As pictured above, the pin is not only hollow but is seemed to be meshed into a cylindrical shape. Besides the pin material, these factors can be said to have contributed to its failure.

11.3.1 Pin Failure Analysis & Redesign

In order to prevent further failure of the pinning system for the transmission analytical calculations along with finite elemental analysis (FEA) were performed on the pin structure.

An analytical analysis of the loadings the axle shaft and pin assembly experienced was performed by first assuming an input moment on the axle shaft of 40 Nm. (Raziel Riemer, 2011)

By assuming a worst case scenario, where the full 40 Nm moment of the knee was transmitted to the shaft connected to a locked gearbox system, force was calculated by dividing the input moment of 40 Nm by the outermost radial distance of the shaft.

$$Force\ (F) = \frac{Torque\ (T)}{Radial\ Distance(\rho)}$$

However, since our pin structure is assembled in such a manner that two shear surfaces must be considered the following equation was utilized to obtain the shear loading condition. (Hibbler, 2008)

$$Shear\ Force\ (V) = Force\ (F)/2$$

Two equations for determining the shear stress experienced by the pin were utilized.

The followingaverage shear stress equation simplifies the loading case to an example of simple/direct shear. (Hibbler, 2008)

$$Average\ Shear\ Stress(\tau_{Avg}) = \frac{Shear\ Force(V)}{Area\ (A)}$$

Two pin types were analyzed: a hollow pin, which depicts the original pin used, and a solid pin. Please see sectionA.3 Handwritten Calculations for review of calculations performed.

A secondary equation, referred to as the shear formula, was utilized to find the shear stress in the pin member's transverse axis of the cross-sectional area. (Hibbler, 2008)

$$\tau = \frac{VQ}{It}\ where\ Q = \int_{A'}^{\infty} ydA' = \bar{y}'A'$$

Again, an analysis for the shear stress was performed on two models: a hollow and solid pin. The solutions derived correspond to the maximum shear stress experienced in the pins: for review of the calculations please see section A.3 Handwritten Calculations.

$$Factor\ of\ Safety\ (F.S.) = \frac{Failure\ Shear\ (\tau_{Fail})}{Allowable\ Shear\ \ (\tau_{Allow})}$$

The preceding equation is the equation the design team utilized for deriving the factor of safety. A factor of safety was calculated from the shear analysis performed and may be seen in section A.3 Handwritten Calculations.

Proceeding the analytical calculations of the pin failure, Algor Autodesk mechanical simulation software was utilized for validation and optimization of the shear pin.

The FEA of both the pin and the shaft were modeled in a worst case scenario environment in which the gearing mechanism would lock; therefore, exerting the greatest amount of forces possible onto the system.

For both the pin and the shaft, there were several load cases analyzed using FEA software, in this case Algor. The structural failure of the hollow pin was the initial motivation to proceed with the FEA yet; further analysis was done on a solid pin and the shaft.

Below is a description of the different load scenarios for the various parts.

Hollow Pin (Point Loading)

The key to utilizing Algor in an efficient way is to figure out the correct boundary conditions. When calculating the worst case scenario and for practicality purposes, the load across the hollow pin was converted into a single point load placed where the stress concentrations should be. This single point load was calculated to be 10,000N. The analysis was done with a semi-fine mesh which was constructed with about 3000 elements using a brick element type, and the material selected for this analysis was AISI 1045 Hot Rolled Steel. The boundary conditions were set according to a realistic approach in which the pin was completely fixed at the center and semi-fixed at the ends with the only allowable motion in the x direction to simulate shear. The maximum stress results given by the simulation were of $1.24\ X\ 10^9 \text{N}/m^2$, using Tresca, which coincide with our hand calculations and seem to be reasonable. Below is a graphical representation of the simulation along with the corresponding stress levels.

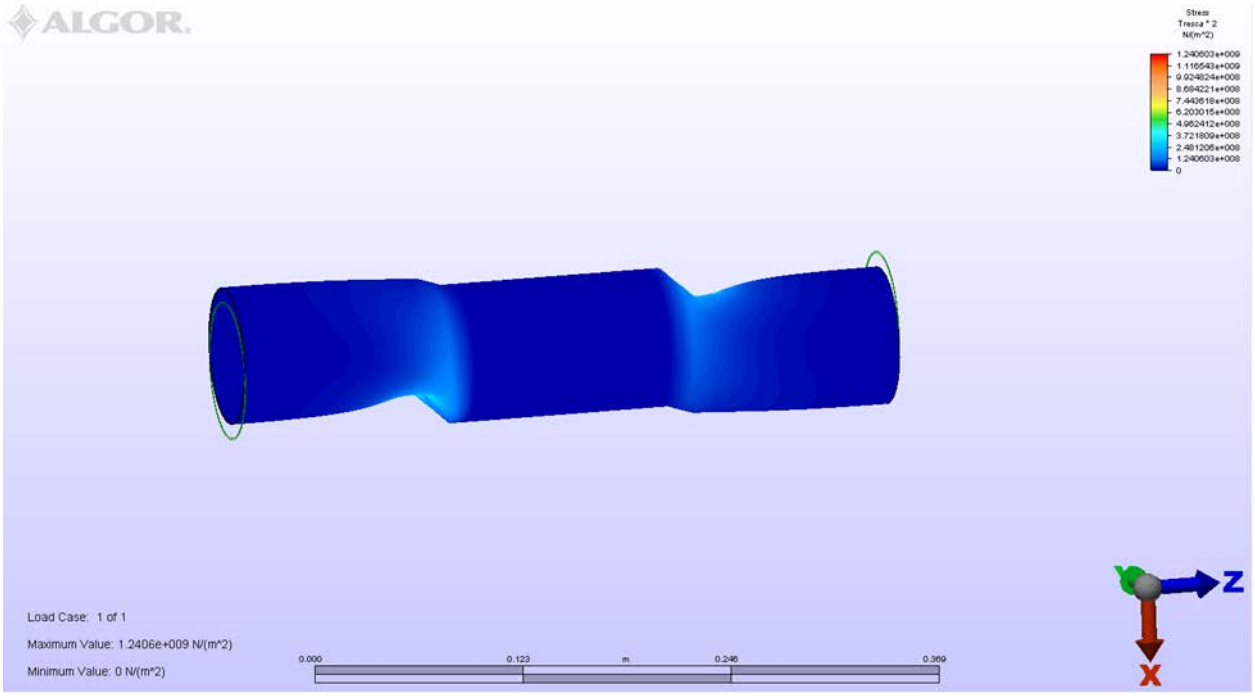

Figure 82: Hollow Pin Model with Point Loading

Figure 82 shows hollow pin modeled with AISI 1045 steel material properties - brick type element FEA with Tresca max/min Stress values.

The apparent deformation of the pin, although not completely accurate, is reasonable within the given boundary conditions and can be utilized as guidelines to real world scenarios.

Hollow Pin (Distributed Loading)

This load case was utilized in an attempt to make the simulation more realistic according to loading conditions. The mesh formation, element type, boundary conditions, and material specifications are identical to Load Case 1 varying only in the way the load was applied. For this case the force of 10,000N was distributed across half of the corresponding surface making it a more realistic distributed load. The amount of nodes on each surface was about 195, therefore $\frac{10000N}{195}$ = 51.28N per node approximately. The maximum stress value, in Tresca, was given to be $1.569\ X\ 10^8 \text{N}/m^2$ according to simulation results. This value is still within the reasonable scale of stress values therefore considering the simulation a success. When compared to Load Case 1, the max stress value given by the distributed load case is one order of magnitude smaller. This makes sense because now the load is distributed over an entire surface therefore having more area and less stress concentration. Below is a graphical representation of the simulation along with the corresponding stress values.

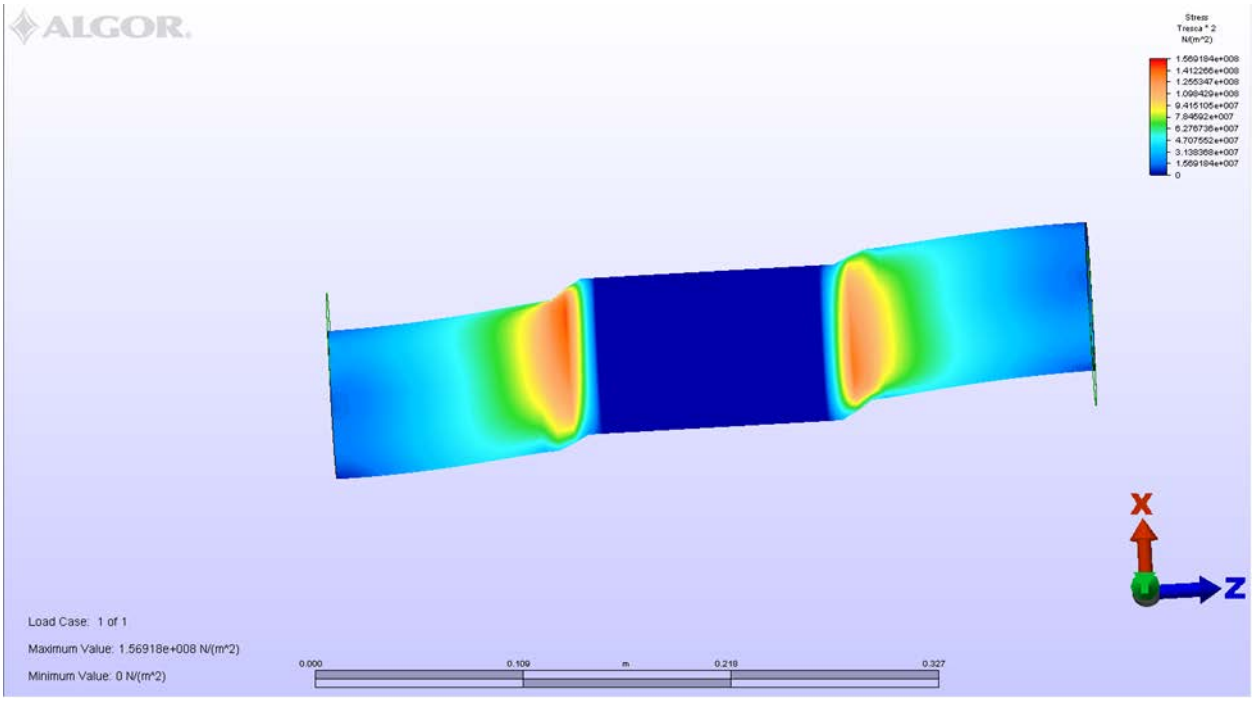

Figure 83: Hollow Pin with Distributed Loading

Shows hollow pin AISI 1045 Steel - brick type element FEA with Tresca max/min Stress values utilizing distributed load conditions.

The deformation in this case has a more distributed approach as well, showing more of a linear difference in deformation between each node of the affected regions. Stress concentration regions are still clearly visible and appear to be accurate as well.

Solid Pin (Point Loading)

In this modeling scenario, the same approach was used as in the Hollow Pin (Point Load) case; in which the load was reduced to a point load applied at the concentrated stress regions for practicality. Again the point load is found to be 10,000N placed on symmetrically opposite sides of the structure. The model was made with brick element type, AISI 1045 Hot Rolled Steel with a semi-fine mesh containing about 5,000 elements. The boundary conditions were set as realistic as possible with a fixed center and semi-fixed edges allowing movement only in the x axis to simulate pure shear. The maximum stress result given in this case was of $2.66\ X\ 10^8$ N/m^2. When compared to the first case of the hollow pin, the maximum stress is one order of magnitude less; this is more than likely due to the face that the stress is differently distributed across the structure since it is now a solid structure. Again, these results seem reasonable within our given parameters. Below is a graphical representation of the simulation along with the corresponding regional stresses.

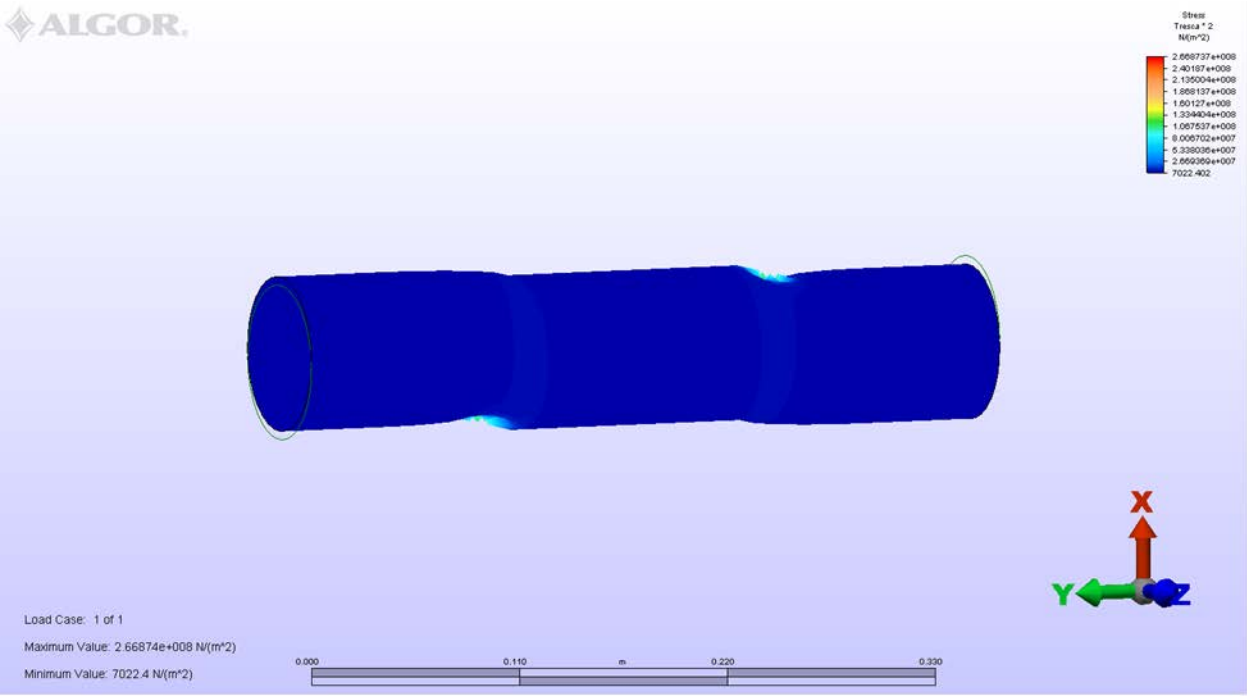

Figure 84: Solid Pin Model with Point Loading

Shows solid pin AISI 1045 Steel - brick type element FEA with Tresca max/min Stress values utilizing point load conditions.

The deformation results when compared to the hollow pin scenario make sense because less deformation was expected out of the solid pin due to more material being affected. We can clearly see how the outer regions of the pin have been constrained to have movement only in the x axis simulating pure shear.

Solid Pin (Distributed Loading)

When analyzing the solid pin distributed loading scenario, all boundary, material, and element type conditions remain constant with the exception of the way the load was applied. In this scenario, the 10,000N force was distributed across the surface of contact. With the surface containing about 195 nodes the force of 10,000N was then divided by the number of nodes giving us approximately 51.28N per node. The maximum stress value using Tresca was given as $5.37\ X10^6 N/m^2$. Notice how the value of this case when compared to the Solid Pin Load Case 1 is much lower by 2 orders of magnitude. This could possibly be explained by the distributed load although there could be unforeseen discrepancies due to the utilization of the program. Below is a graphical representation of the analysis with its corresponding regional stress values.

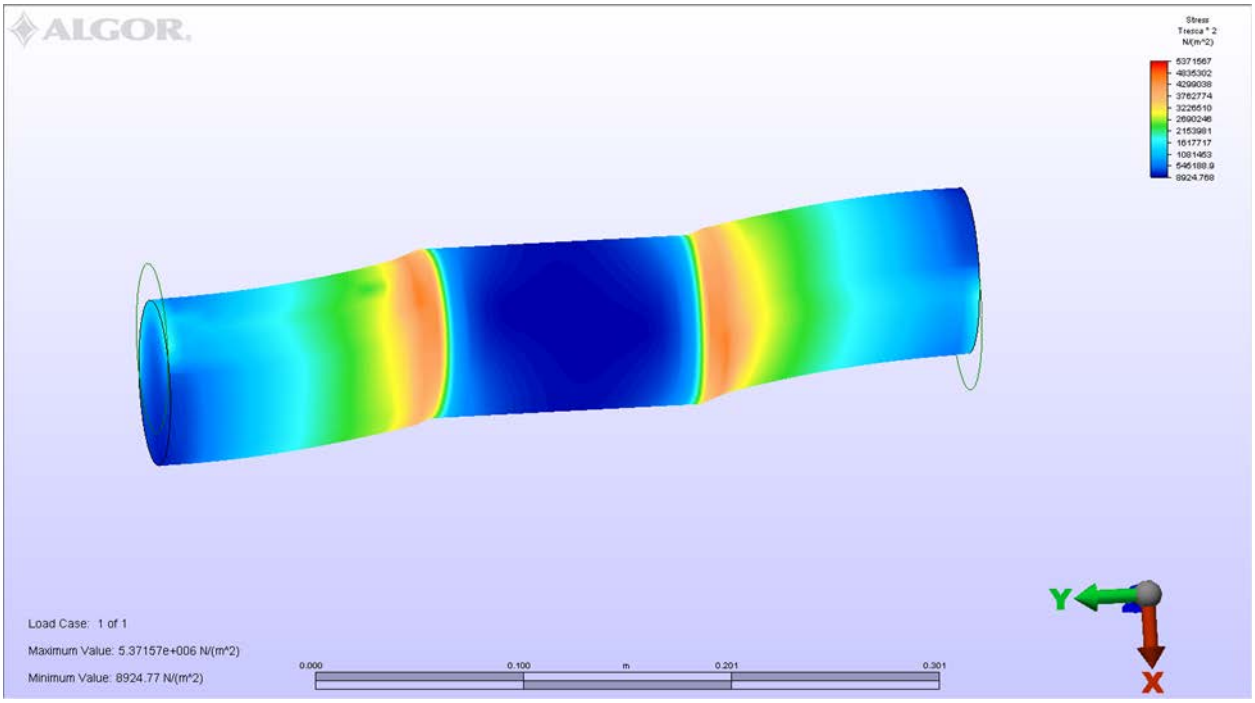

Figure 85: Solid Pin Model with Distributed Loading

Shows solid pin AISI 1045 Steel - brick type element FEA with Tresca max/min Stress values utilizing distributed load conditions.

Although the stress levels may be suspicious, the deformation shown seems to be consistent with the distributed load conditions, therefore giving good insight on the possible shear of this pin.

Solid Pin (Central Distributed Loading)

This load case was made in an attempt to model the analysis from a completely different point of view while still simulating accurate results. In this scenario, element type and material selection remain constant. The only changes made were the applied boundary conditions along with the applied load distribution. In case 3 we attempt to apply boundary conditions that although are not

graphically realistic, they could be more realistic when given the final results. In this scenario the center part of the pin is partially fixed with allowable movement only on the z axis. The two outer regions of the pin are modeled as completely fixed. This was done in an attempt to model a more realistic interpretation of shear. The magnitude of the force is doubled since it is applied at the center region giving us 20,000N, in this scenario the load is distributed across the center region in a linear orientation. This central linear region was composed of 16 nodes giving us 1250N of force per node. Below is a graphical representation of the analysis along with the corresponding regional stresses.

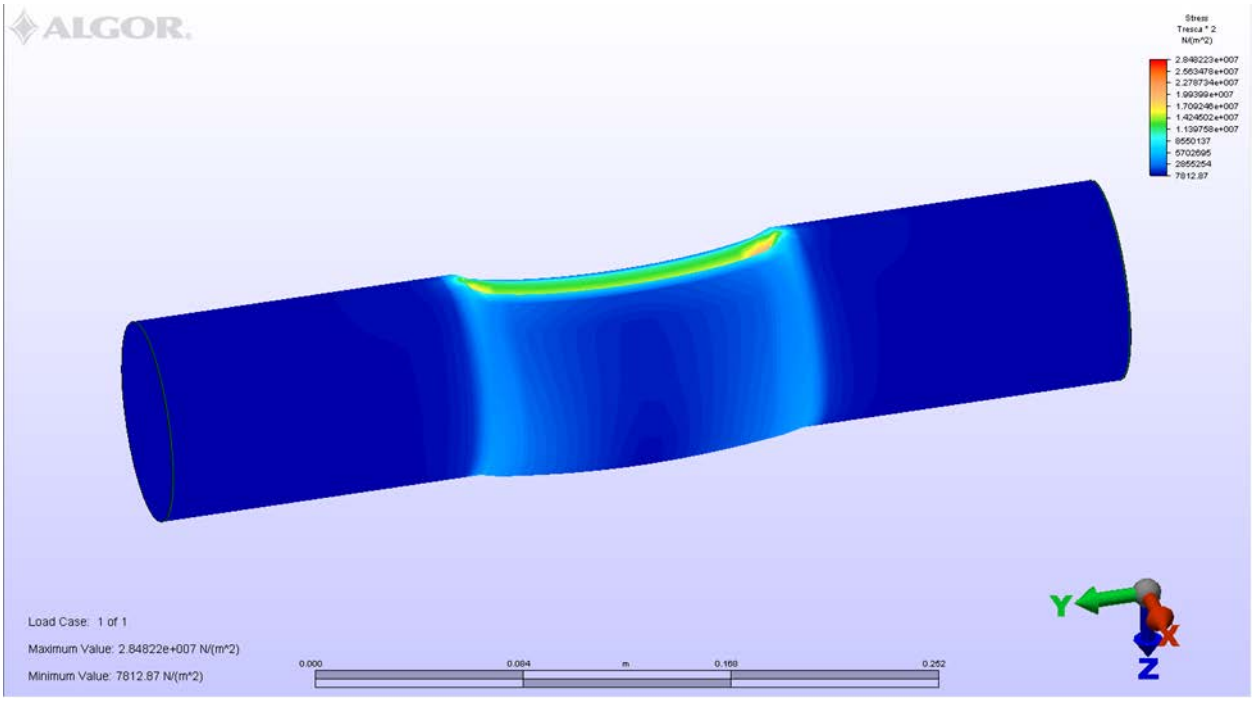

Figure 86: Solid Pin with Central Distributed Loading Conditions

Shows solid pin AISI 1045 Steel - brick type element FEA with Tresca max/min Stress values utilizing distributed center load conditions.

The deformation shown in this analysis is reasonable within our given parameters giving us a new look and insight in the possible shear analysis.

Shaft Loading Analysis

The shaft FEA was done in order to give us insight on the behavior of the shaft and possible deformation once the pin loads were applied. When looking at the shaft we find that we can model the forces acting on it as two counteracting moments of$40N * m$. The first moment can be applied in the region where the pin should be located and the second can be applied where the gear will be located in the shaft. The modeling of the shaft had to be done in a more indirect approach due restrictions to model moments around whole structures in Algor. In order to solve this problem the moments were simulated with linear vector forces applied in their

corresponding directions. The forces utilized were of 10,000N each. The boundary conditions used for the shaft although unconventional were useful to model accurate displacement results. The shaft was composed of brick element type and AISI 1045 Hot Rolled Steel with a semi-fine mesh size of about 6000 elements. Below is a graphical representation of the possible displacement of the shaft.

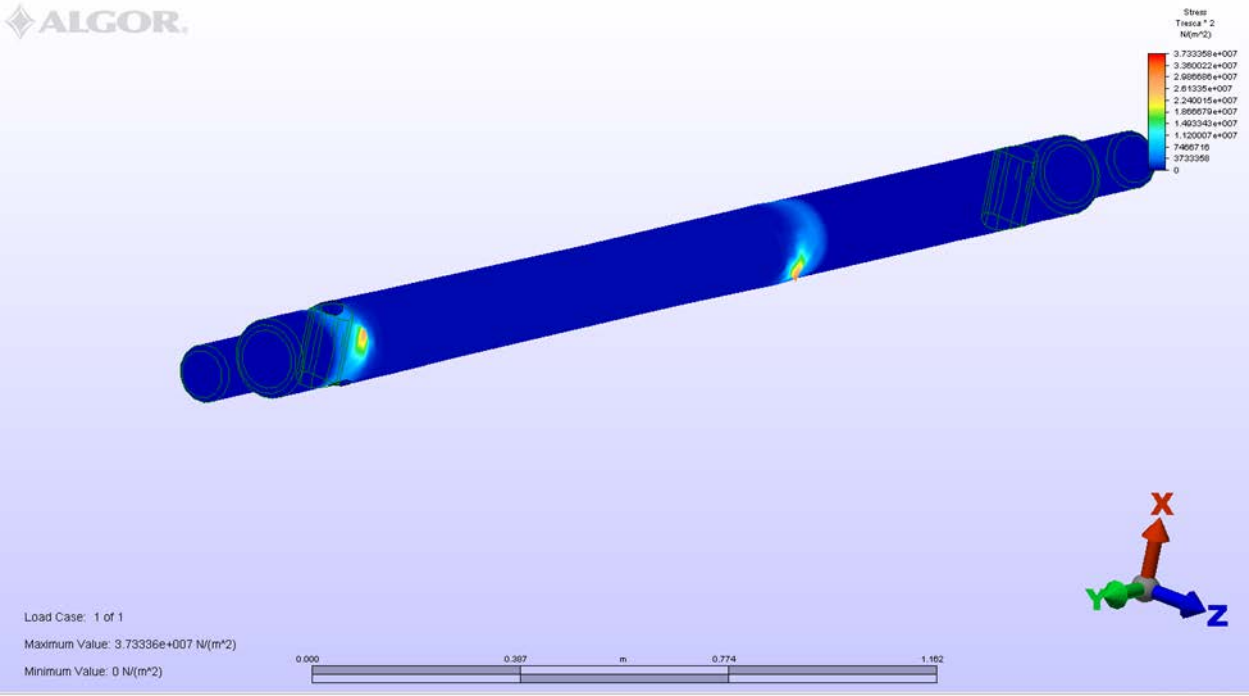

Figure 87: Shaft Model with Point Loads for Simulation of Moment Conditions

Shows shaft AISI 1045 Steel - brick type element FEA with Tresca max/min displacement values utilizing moment load conditions.

The displacement of the shaft shows the direction and the magnitude of the possible deformation that could occur giving extreme conditions.

11.4 Secondary Data Collection

Once prototype refinement was collected and the mechanisms of failure were addressed a secondary round of data collection was conducted.

The tables below contain only a small portion of all the voltage readings garnered during different trials. An RMS calculation, whose formula can be seen below in section 11.1 Experimental Setup, was done for each trial and the average RMS value for all the trials were obtained. Identical testing parameters were conducted relative to those undertook for subjects one and two.

11.4.1 Subject 3 Data

The following section presents the data collected from Subject 3 during testing of the performance of the biomechanical energy harvesting brace.

Table 30: Subject 3 Treadmill Data (3 MPH)

3 MPH							
Trial 1	Trial 2	Trial 3	Trial 4	Trial 5			V_{RMS} (Volts)
-0.153	-0.484	-0.144	0.006	-0.222		Trial 1	0.279
-0.143	-0.473	-0.134	0.003	-0.224		Trial 2	0.289
-0.131	-0.416	-0.124	0.002	-0.22		Trial 3	0.289
-0.117	-0.329	-0.114	0.001	-0.211		Trial 4	0.316
-0.106	-0.461	-0.103	0	-0.198		Trial 5	0.282
-0.098	-0.484	-0.092	0	-0.177			
-0.121	-0.465	-0.083	0	-0.161		Avg. V_{RMS} (Volts)	0.291
-0.122	-0.403	-0.075	0	-0.211		Avg. P_{RMS} (Watts)	0.0002
-0.122	-0.396	-0.068	0	-0.224		Avg. I_{RMS} (Amps)	0.0006
-0.121	-0.455	-0.086	0	-0.236			

*The preceding table contains the average RMS values for voltage, current and power at three miles per hour.*Note: Subject 3 was a male with a height and weight of 5'7" (1.70 m) and 140 lbs. (63.50 kg), respectively.*

Table 31: Subject 3 Treadmill Data (5 MPH)

5 MPH							
Trial 1	Trial 2	Trial 3	Trial 4	Trial 5			V_{RMS} (Volts)
0.051	0.622	0.864	-0.759	-0.752		Trial 1	0.479
0.051	0.405	0.698	-0.639	-1.073		Trial 2	0.503
0.049	0.5	0.885	-0.68	-0.847		Trial 3	0.520
0.048	0.524	0.808	-0.736	-1.041		Trial 4	0.516
0.046	0.482	0.773	-0.632	-0.896		Trial 5	0.543
0.042	0.399	0.862	-0.674	-1.025			
0.038	0.31	0.614	-0.745	-0.975		Avg. V_{RMS} (Volts)	0.512
0.035	0.319	0.849	-0.667	-0.955		Avg. P_{RMS} (Watts)	0.0005
0.031	0.294	0.841	-0.634	-0.997		Avg. I_{RMS} (Amps)	0.0010
0.027	0.248	0.679	-0.728	-0.891			

The above table contains the average RMS values for voltage, current and power at five miles per hour.

Table 32: Subject 3 Treadmill Data (7 MPH)

7 MPH							
Trial 1	Trial 2	Trial 3	Trial 4	Trial 5			V_{RMS} (Volts)
0.163	0.135	-0.9	-0.727	1.073		Trial 1	0.576
0.164	0.131	-1.151	-0.529	1.106		Trial 2	0.596
0.166	0.126	-0.946	-0.814	1.113		Trial 3	0.594
0.164	0.118	-1.137	-0.749	1.217		Trial 4	0.616
0.124	0.11	-0.921	-0.713	1.116		Trial 5	0.601
0.14	0.103	-1.148	-0.815	1.281			
0.16	0.094	-0.96	-0.7	0.995		Avg. V_{RMS} (Volts)	0.597
0.182	0.084	-1.133	-0.778	1.357		Avg. P_{RMS} (Watts)	0.0007
0.199	0.075	-0.932	-0.841	1.197		Avg. I_{RMS} (Amps)	0.0012
0.215	0.065	-1.147	-0.666	1.295			

The above table contains the average RMS values for voltage, current and power at seven miles per hour.

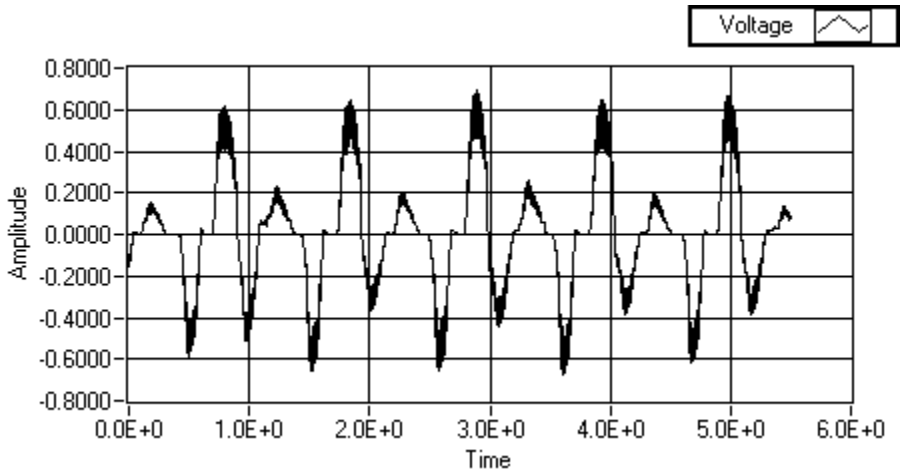

Figure 88: Subject 3 LabVIEW Waveform Data (3 MPH)

The preceding figure shows the voltage waveform production of Subject 3 during trial 1 of 5 at 3 MPH.

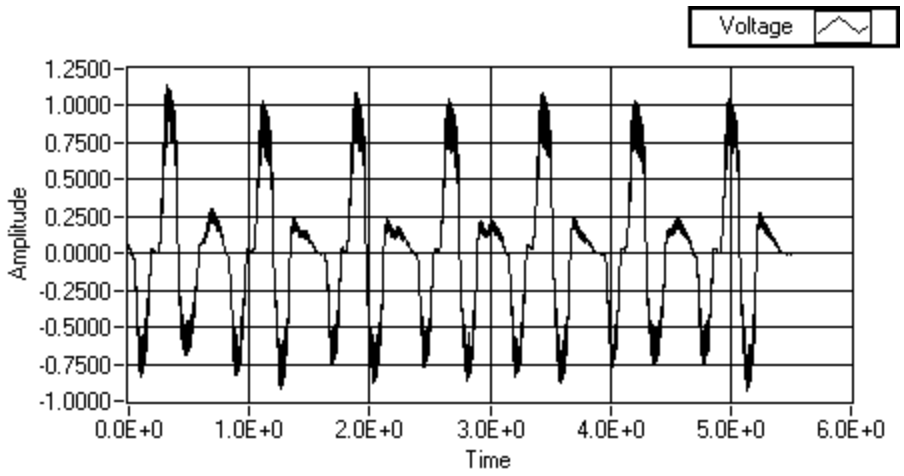

Figure 89: Subject 3 LabVIEW Waveform Data (5 MPH)

The preceding figure shows the voltage waveform production of Subject 3 during trial 1 of 5 at 5 MPH.

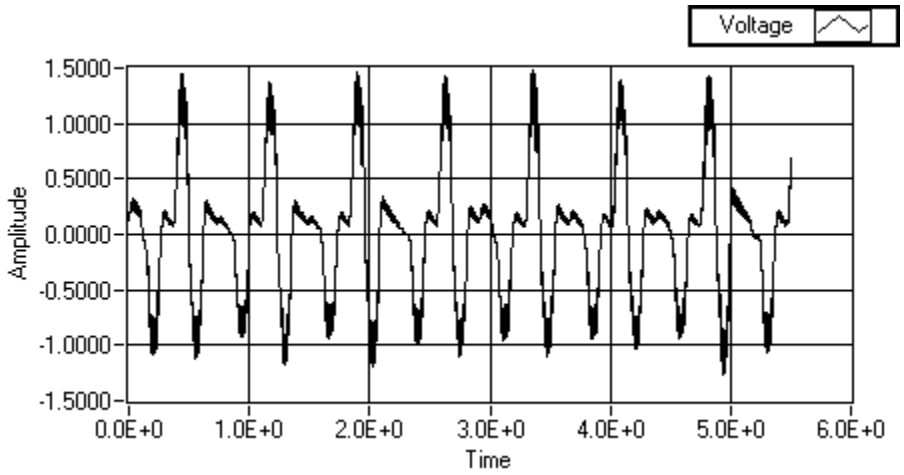

Figure 90: Subject 3 LabVIEW Waveform Data (7 MPH)

The preceding figure shows the voltage waveform production of Subject 3 during trial 1 of 5 at 7 MPH.

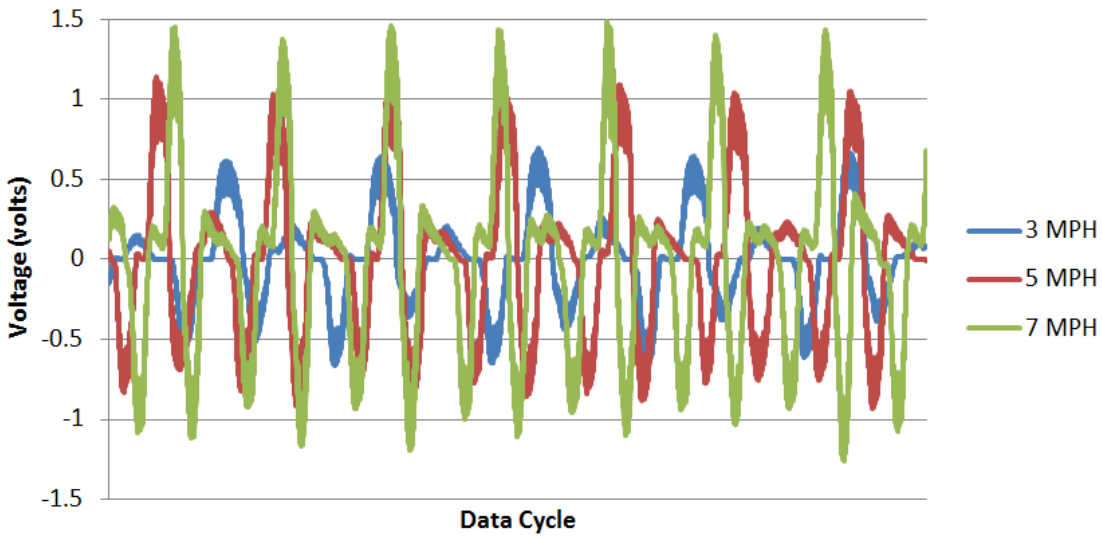

Figure 91: Subject 3 Coalesced Treadmill Data

The graph displayed above shows how the voltage readings changed with respect to time. All the data points recorded for one trial at each of three different velocities were graphed together in order to compare the voltage readings.

11.4.2 Subject 4 Data

The following section presents the data collected from Subject 4 during testing of the performance of the biomechanical energy harvesting brace.

Table 33: Subject 4 Treadmill Data (3 MPH)

3 MPH							
Trial 1	Trial 2	Trial 3	Trial 4	Trial 5			V_{RMS} (Volts)
0	0	-0.334	-0.46	0.461		Trial 1	0.214
0	0	-0.47	-0.487	0.446		Trial 2	0.188
0	0	-0.507	-0.462	0.396		Trial 3	0.224
0	0	-0.494	-0.39	0.359		Trial 4	0.203
0.001	0	-0.417	-0.313	0.422		Trial 5	0.201
0.002	0	-0.468	-0.448	0.447			
0.002	0	-0.538	-0.455	0.432		Avg. V_{RMS} (Volts)	0.206
0.002	0	-0.542	-0.428	0.383		Avg. P_{RMS} (Watts)	8.5E-05
0.002	0	-0.47	-0.366	0.348		Avg. I_{RMS} (Amps)	0.0004
0.002	0	-0.491	-0.344	0.41			

*The preceding table contains the average RMS values for voltage, current and power at three miles per hour.*Note: Subject43 was a male with a height and weight of 5'7" (1.70 m) and 151 lbs. (68.50 kg), respectively.*

Table 34: Subject 4 Treadmill Data (5 MPH)

5 MPH							
Trial 1	Trial 2	Trial 3	Trial 4	Trial 5			V_{RMS} (Volts)
0.615	-0.071	0.843	0.003	-0.112		Trial 1	0.313
0.558	-0.066	0.76	0.004	-0.107		Trial 2	0.318
0.529	-0.06	0.772	0.004	-0.102		Trial 3	0.344
0.639	-0.055	0.847	0.004	-0.096		Trial 4	0.349
0.64	-0.049	0.569	0.005	-0.09		Trial 5	0.351
0.462	-0.043	0.793	0.006	-0.083			
0.619	-0.037	0.817	0.006	-0.076		Avg. V_{RMS} (Volts)	0.335
0.677	-0.031	0.643	0.007	-0.07		Avg. P_{RMS} (Watts)	0.0002
0.604	-0.025	0.833	0.008	-0.065		Avg. I_{RMS} (Amps)	0.0007
0.595	-0.019	0.79	0.009	-0.077			

The above table contains the average RMS values for voltage, current and power at five miles per hour.

Table 35: Subject 4 Treadmill Data (7 MPH)

7 MPH							
Trial 1	Trial 2	Trial 3	Trial 4	Trial 5			V_{RMS} (Volts)
0.009	-0.159	-0.022	-0.016	0.123		Trial 1	0.436
0.009	-0.159	-0.016	-0.015	0.123		Trial 2	0.416
0.009	-0.155	-0.008	-0.008	0.122		Trial 3	0.433
0.008	-0.151	-0.001	-0.001	0.119		Trial 4	0.432
0.008	-0.145	0.004	0.003	0.093		Trial 5	0.434
0.008	-0.135	0.009	0.005	0.101			
0.008	-0.125	0.012	0.008	0.109		Avg. V_{RMS} (Volts)	0.430
0.008	-0.119	0.013	0.01	0.12		Avg. P_{RMS} (Watts)	0.00037045
0.008	-0.149	0.012	0.011	0.129		Avg. I_{RMS} (Amps)	0.00086076
0.007	-0.157	0.014	0.013	0.137			

The above table contains the average RMS values for voltage, current and power at seven miles per hour.

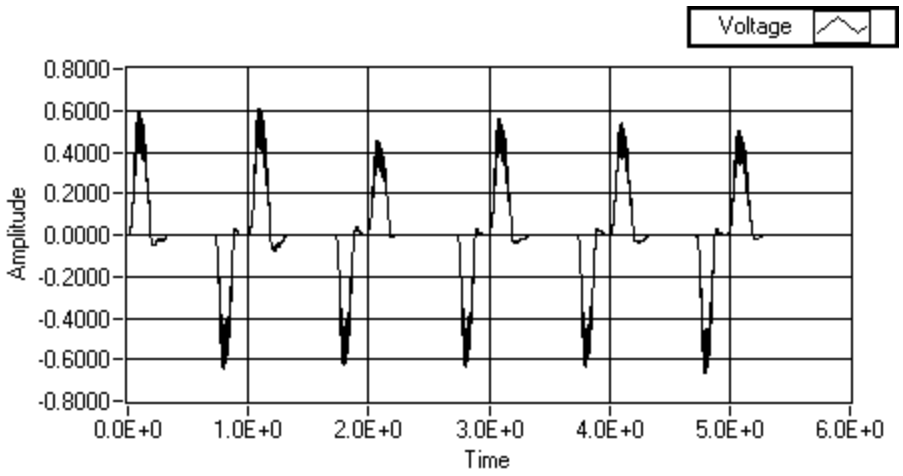

Figure 92: Subject 4 LabVIEW Waveform Data (3 MPH)

The preceding figure shows the voltage waveform production of Subject 4 during trial 1 of 5 at 3 MPH.

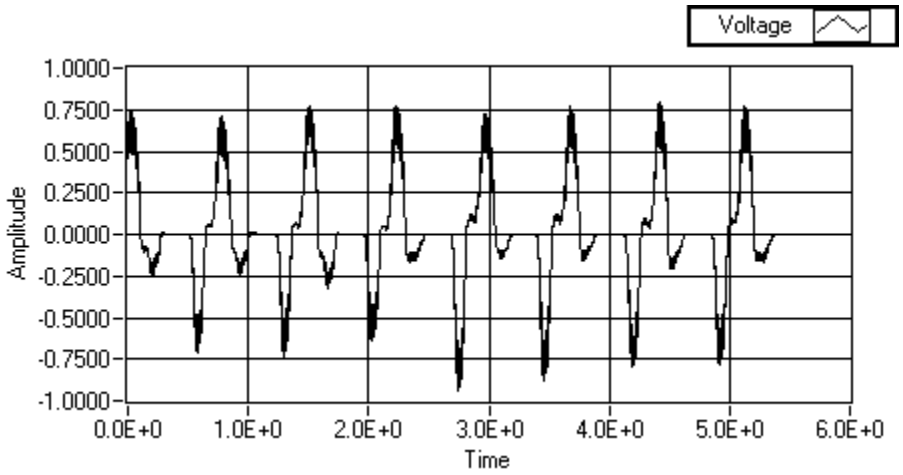

Figure 93: Subject 4 LabVIEW Waveform Data (5 MPH)

The preceding figure shows the voltage waveform production of Subject 4 during trial 1 of 5 at 5 MPH.

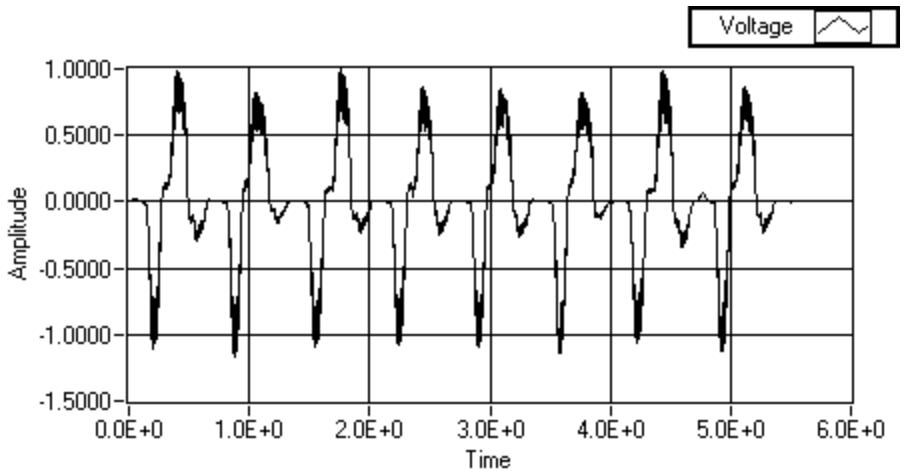

Figure 94: Subject 4 LabVIEW Waveform Data (7 MPH)

The preceding figure shows the voltage waveform production of Subject 4 during trial 1 of 5 at 7 MPH.

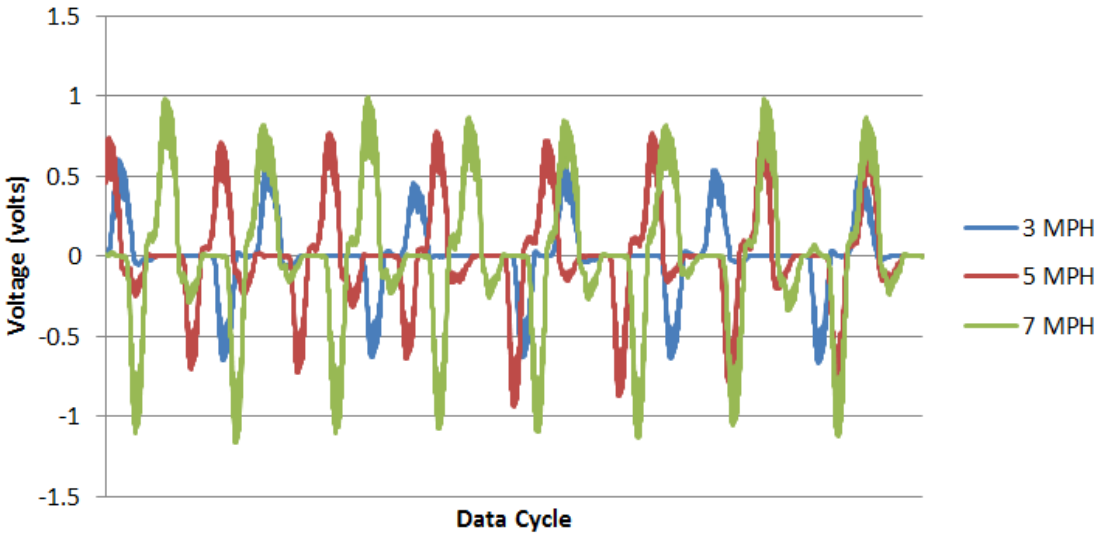

Figure 95: Subject 4 Coalesced Treadmill Data

The graph displayed above shows how the voltage readings changed with respect to time. All the data points recorded for one trial at each of three different velocities were graphed together in order to compare the voltage readings.

11.4.3 Subject 5 Data

The following section presents the data collected from Subject 5 during testing of the performance of the biomechanical energy harvesting brace.

Table 36: Subject 5 Treadmill Data (3 MPH)

3 MPH							
Trial 1	Trial 2	Trial 3	Trial 4	Trial 5			V_{RMS} (Volts)
0.001	0.031	0	0	0		Trial 1	0.219
0.001	0.029	-0.001	0	0		Trial 2	0.253
0.001	0.027	-0.002	0	0		Trial 3	0.225
0.001	0.025	-0.001	0	0		Trial 4	0.223
0.001	0.023	-0.001	0	0		Trial 5	0.234
0.001	0.02	-0.001	0	0			
0.001	0.018	-0.001	0	0		Avg. V_{RMS} (Volts)	0.2307
0.001	0.015	-0.001	0	0		Avg. P_{RMS} (Watts)	0.0001
0.001	0.013	-0.001	0	0		Avg. I_{RMS} (Amps)	0.0005
0.001	0.011	-0.001	0	0			

*The preceding table contains the average RMS values for voltage, current and power at three miles per hour.*Note: Subject43 was a male with a height and weight of 5'7" (1.70 m) and 151 lbs. (68.50 kg), respectively.*

Table 37: Subject 5 Treadmill Data (5 MPH)

5 MPH							
Trial 1	Trial 2	Trial 3	Trial 4	Trial 5			V_{RMS} (Volts)
0	0.389	0	0.534	0.044		Trial 1	0.388
0	0.368	0	0.68	0.053		Trial 2	0.396
-0.001	0.325	-0.001	0.696	0.064		Trial 3	0.359
-0.001	0.272	0	0.525	0.075		Trial 4	0.377
-0.001	0.212	0.001	0.723	0.087		Trial 5	0.403
-0.001	0.156	0.001	0.771	0.095			
-0.001	0.135	-0.001	0.603	0.086		Avg. V_{RMS} (Volts)	0.3844
-0.002	0.105	-0.003	0.818	0.103		Avg. P_{RMS} (Watts)	0.0003
-0.002	0.068	-0.002	0.817	0.125		Avg. I_{RMS} (Amps)	0.0008
0.001	0.027	0	0.699	0.152			

The above table contains the average RMS values for voltage, current and power at five miles per hour.

Table 38: Subject 5 Treadmill Data (7 MPH)

7 MPH							
Trial 1	Trial 2	Trial 3	Trial 4	Trial 5			V_{RMS} (Volts)
0.155	0.115	-0.861	0.095	-0.12		Trial 1	0.494
0.175	0.115	-1.109	0.104	-0.091		Trial 2	0.484
0.193	0.114	-0.856	0.111	-0.063		Trial 3	0.474
0.209	0.112	-1.12	0.118	-0.036		Trial 4	0.452
0.22	0.11	-0.923	0.123	-0.01		Trial 5	0.457
0.229	0.107	-1.089	0.126	0.01			
0.231	0.103	-0.928	0.126	0.024		Avg. V_{RMS} (Volts)	0.4722
0.225	0.099	-1.093	0.126	0.037		Avg. P_{RMS} (Watts)	0.0004
0.215	0.096	-0.99	0.126	0.049		Avg. I_{RMS} (Amps)	0.0009
0.192	0.092	-1.054	0.124	0.061			

The above table contains the average RMS values for voltage, current and power at seven miles per hour.

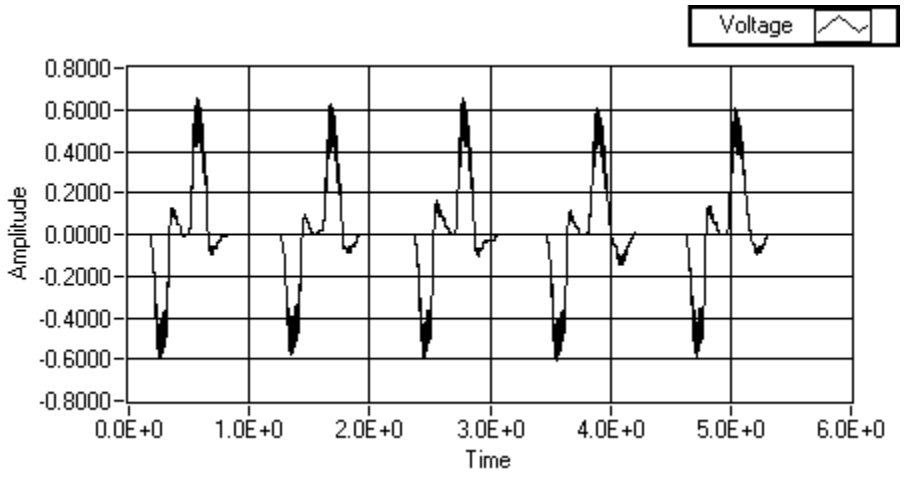

Figure 96: Subject 5 LabVIEW Waveform Data (3 MPH)

The preceding figure shows the voltage waveform production of Subject 5 during trial 1 of 5 at 3 MPH.

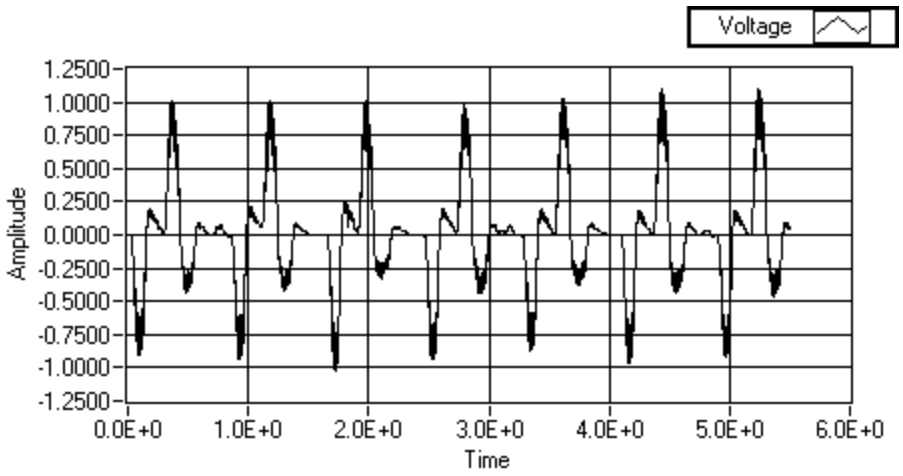

Figure 97: Subject 5 LabVIEW Waveform Data (5 MPH)

The preceding figure shows the voltage waveform production of Subject 5 during trial 1 of 5 at 5 MPH.

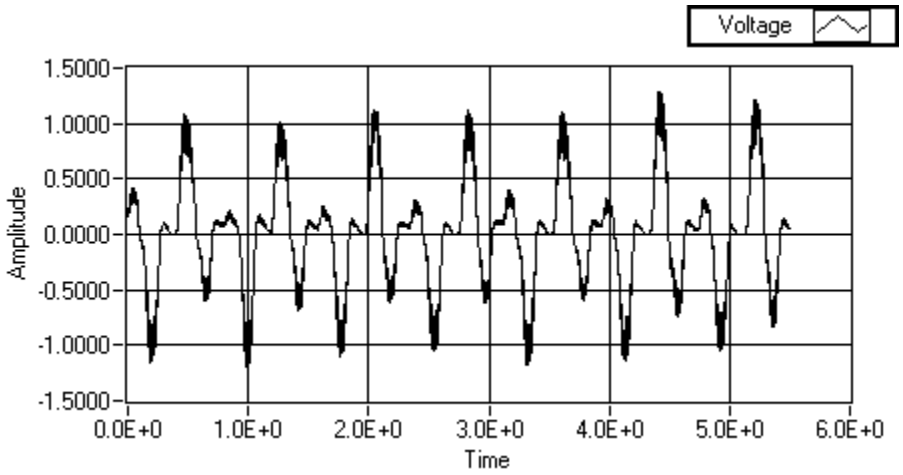

Figure 98: Subject 5 LabVIEW Waveform Data (7 MPH)

The preceding figure shows the voltage waveform production of Subject 5 during trial 1 of 5 at 7 MPH.

Figure 99: Subject 5 Coalesced Treadmill Data

The graph displayed above shows how the voltage readings changed with respect to time. All the data points recorded for one trial at each of three different velocities were graphed together in order to compare the voltage readings.

11.4.4 Subject 6 Data

The following section presents the data collected from Subject 5 during testing of the performance of the biomechanical energy harvesting brace.

Table 39: Subject 6 Treadmill Data (3 MPH)

3 MPH							
Trial 1	Trial 2	Trial 3	Trial 4	Trial 5			V_{RMS} (Volts)
0.044	0.204	0.34	0	0		Trial 1	0.157
0.033	0.221	0.313	0	0		Trial 2	0.148
0.023	0.234	0.248	0	0		Trial 3	0.165
0.012	0.241	0.295	0	0		Trial 4	0.174
0.003	0.243	0.326	0	0		Trial 5	0.175
-0.005	0.237	0.343	0	0			
-0.01	0.226	0.341	0	0		Avg. V_{RMS} (Volts)	0.1636
-0.014	0.177	0.321	0	0		Avg. P_{RMS} (Watts)	0.0001
-0.019	0.201	0.287	-0.001	0		Avg. I_{RMS} (Amps)	0.0003
-0.022	0.226	0.262	0	0			

*The preceding table contains the average RMS values for voltage, current and power at three miles per hour.*Note: Subject 6 was a male with a height and weight of 5'10" (1.78 m) and 145 lbs. (65.77 kg), respectively.*

Table 40: Subject 6 Treadmill Data (5 MPH)

5 MPH							
Trial 1	Trial 2	Trial 3	Trial 4	Trial 5			V_{RMS} (Volts)
0.077	-0.049	0.378	0	0		Trial 1	0.191
0.064	-0.05	0.379	0	0		Trial 2	0.231
0.064	-0.049	0.355	0	0		Trial 3	0.229
0.065	-0.049	0.338	0	0		Trial 4	0.254
0.067	-0.048	0.409	0	0		Trial 5	0.253
0.068	-0.048	0.456	0	0			
0.068	-0.047	0.465	0	0		Avg. V_{RMS} (Volts)	0.2315
0.069	-0.061	0.435	-0.001	0		Avg. P_{RMS} (Watts)	0.0001
0.069	-0.06	0.375	0	0		Avg. I_{RMS} (Amps)	0.0005
0.068	-0.062	0.464	0	0			

The above table contains the average RMS values for voltage, current and power at five miles per hour.

Table 41: Subject 6 Treadmill Data (7 MPH)

7 MPH							
Trial 1	Trial 2	Trial 3	Trial 4	Trial 5			V_{RMS} (Volts)
0.151	-0.81	-0.032	-0.001	0		Trial 1	0.329
0.152	-0.768	-0.031	0	0		Trial 2	0.347
0.152	-0.883	-0.03	0	0		Trial 3	0.342
0.151	-0.745	-0.028	0	0		Trial 4	0.353
0.148	-0.815	-0.027	0	0.001		Trial 5	0.336
0.143	-0.845	-0.025	0	0			
0.138	-0.616	-0.024	-0.001	0		Avg. V_{RMS} (Volts)	0.3413
0.132	-0.858	-0.023	0	0.001		Avg. P_{RMS} (Watts)	0.0002
0.126	-0.805	-0.022	0	0		Avg. I_{RMS} (Amps)	0.0007
0.091	-0.737	-0.02	0	0			

The above table contains the average RMS values for voltage, current and power at seven miles per hour.

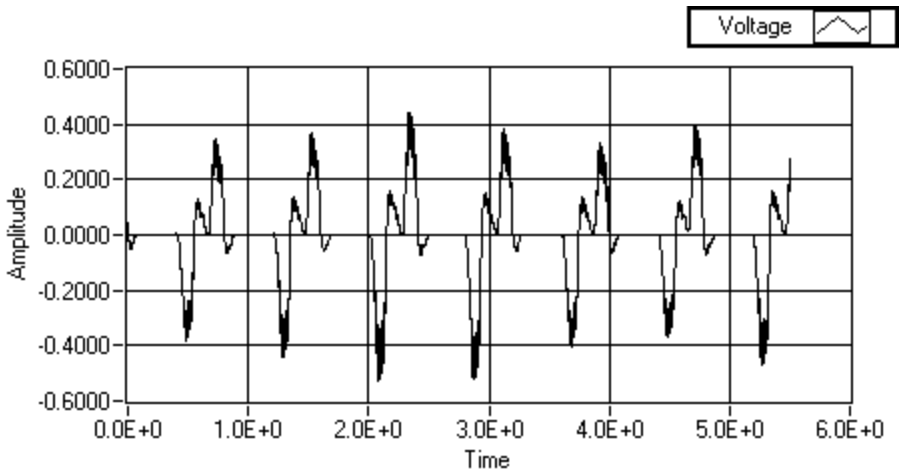

Figure 100: Subject 6 LabVIEW Waveform Data (3 MPH)

The preceding figure shows the voltage waveform production of Subject 6 during trial 1 of 5 at 3 MPH.

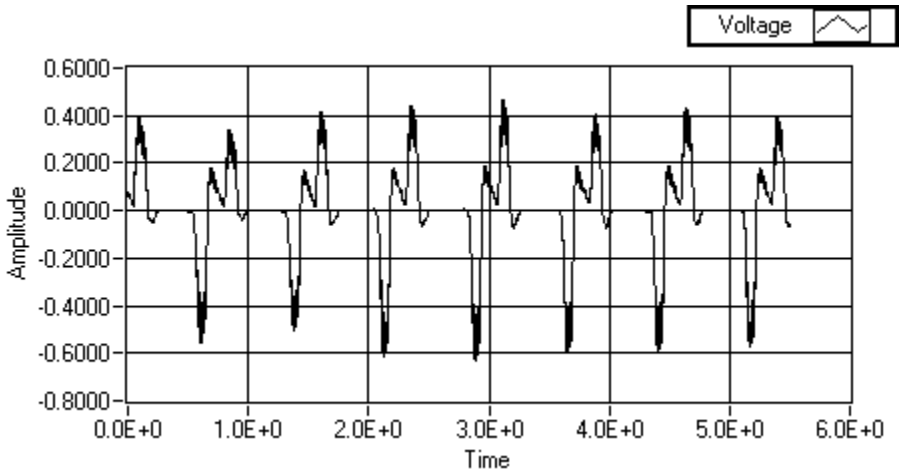

Figure 101: Subject 6 LabVIEW Waveform Data (5 MPH)

The preceding figure shows the voltage waveform production of Subject 6 during trial 1 of 5 at 5 MPH.

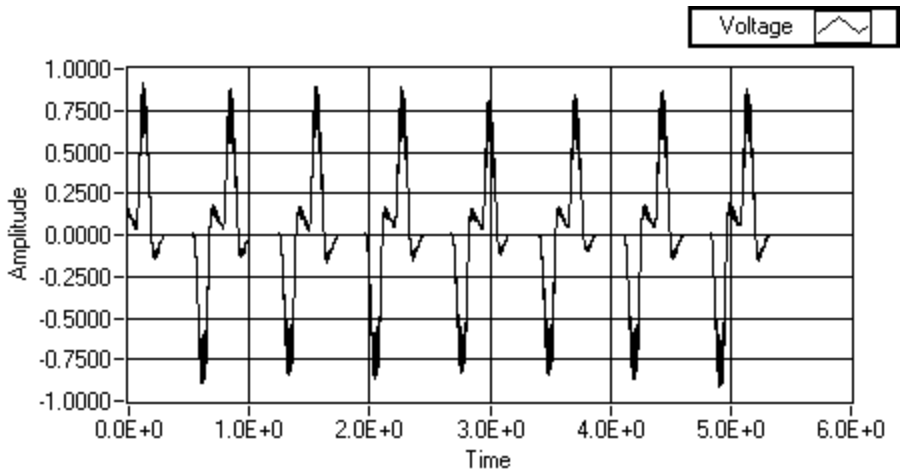

Figure 102: Subject 6 LabVIEW Waveform Data (7 MPH)

The preceding figure shows the voltage waveform production of Subject 6 during trial 1 of 5 at 7 MPH.

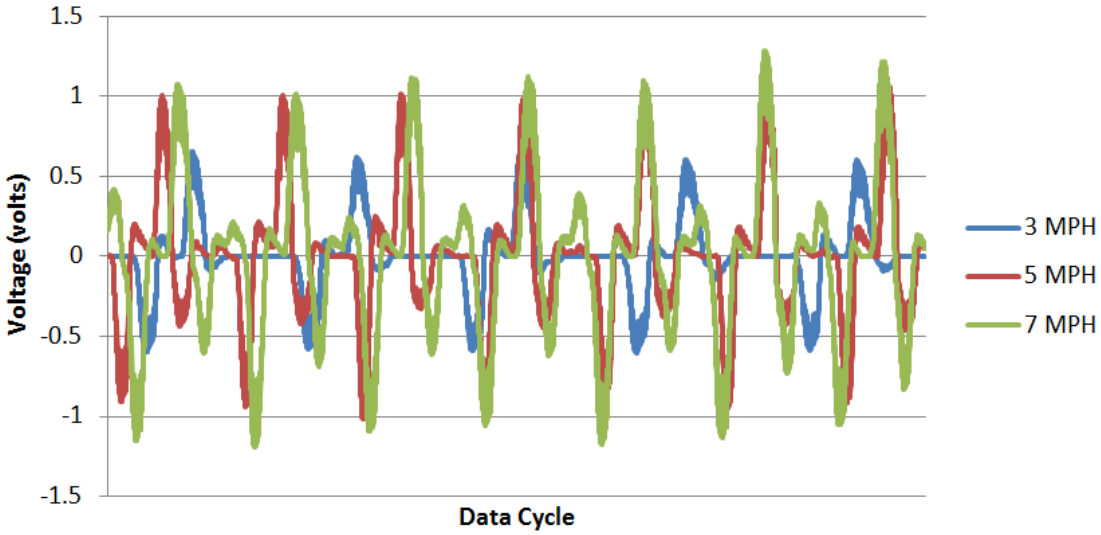

Figure 103: Subject 6 Coalesced Treadmill Data

The graph displayed above shows how the voltage readings changed with respect to time. All the data points recorded for one trial at each of three different velocities were graphed together in order to compare the voltage readings.

12.0 Product Comparison

In the preceding section a comparison between our product and the PowerWalk M-Series will be analyzed. Although all detailed information about the PowerWalk M-Series design could not be obtained, a proper analysis of the product was conducted.

Table 42: Dimensions & Sizes Product Comparison

	Dimensions			Sizes						
	Weight (g)	Length (in)	Width (in)	Custom	X-Small	Small	Large	X-Large	2X-Large	3X-Large
PowerWalk M-Series	750	N/A	N/A	X		X	X	X		
Our Product	750	16	9	X	X	X	X	X	X	

*The table above shows a comparison for dimensions & sizes between the PowerWalk M-Series and our product. Only the weight of the PowerWalk M-Series was available and further dimensions were not found. An **X** indicates what size of knee brace is available for each product.*

Table 43: Material Selection & Generator Type Product Comparison

	Material Selection				Generator Type		
	Knee Brace	Gears	Transmission Shaft	Transmission Chassis	Magnetic	Piezo	Static
PowerWalk M-Series	Carbon Fiber	N/A	N/A	Aluminum	X		
Our Product	Magnesium Alloy	Polyacetal Resin		Injection-Molded ABS	X		

*The table above shows a comparison for material selection & generator type between the PowerWalk M-Series and our product. Only the knee brace and transmission chassis materials of the PowerWalk M-Series were available. Other component materials were not found. An **X** indicates what generator type each product contains.*

Table 44: Gear Type & Clutch System Product Comparison

	Gear Type				Clutch System		
	External Spur	Rack and Pinion	Helical	Bevel	N/A	One Way	Manual
PowerWalk M-Series	X					X	
Our Product	X				X		

*The table above shows a comparison of gear type & clutch system between the PowerWalk M-Series and our product. An **X** indicates the type of component each product contains.*

Table 45: Electrical Storage & Operational Speed Product Comparison

	Electrical Storage				Operational Speed			
	N/A	Battery	Capacitor	Hybrid System	1 MPH	3 MPH	5 MPH	7 MPH
PowerWalk M-Series		Li Ion Cells			X	X	X	X
Our Product	X				X	X	X	X

*The table above shows a comparison of electrical storage & operational speed between the PowerWalk M-Series and our product. An **X** indicates the selection made for each category.*

Table 46: System Power & Current Outputs

	Nominal Power Output	Maximum Power Output	Output Voltage	Max Output Current
PowerWalk M-Series	8 to 14	25	5 to 16.8	5
Our Product	0.07 to 0.5	0.5	0.1 to 0.5	0.9

The table above shows a comparison of power and current production between the PowerWalk M-Series and our product. Units for power, voltage, and current are watss, volts, and amps.

12.1 Energy Harvesting Method

Both the PowerWalk M-Series and our product harvest the bio-mechanical energy produced by the knee.

Although, the PowerWalk M-Series only utilizes the knee extension phase to harvest energy. It acts under similar principles as those employed in the braking mechanism found in many electrical cars by assisting muscles perform negative work and harvesting the energy produced.

Our product utilizes the full range of motion of the knee in the gait cycle. The material selection of our transmission allows the user to utilize the knee brace without feeling any interrupting forces.

12.2 System Dimensioning

Our prototype resulted with dimensions of width: 9”, length: 16” and a weight of 750 grams.

In general, the dimensions of both products will rely on the user’s dimensions. Custom knee braces must be constructed for each user or general sizes (e.g. small, large, etc.) can be produced to accommodate different dimension ranges.

Overall, one characteristic is shared by both products and that’s a weight of approximately 750 grams.

12.3 Material Selection

The PowerWalk M-Series consists of a carbon fiber knee brace and an aluminum chassis in the transmission system. The knee brace material allows for a high strength-to-volume ratio making it strong for its size. It also allows for a high temperature tolerance. The chassis material allows for minimal weight addition to the product. Since aluminum is not magnetic, it will not interfere with the generator magnets.

Our product consists of a magnesium alloy knee brace and an injection-molded ABS chassis in the transmission. The knee brace material allows our product to resist impact by deforming instead of cracking, unlike carbon fiber. This allows us to notice and fix signs of possible failure instead of immediately failing. The chassis material is also able to sustain impact without deformation adding to the security of the product. The gear material chosen for our product is a polyacetal resin. The material allows the gears to function with less mechanical noise than metal gears. The transmission shaft is made of 1045 steel hot-rolled. This material adds to the security of the product allowing for high stresses to act on the shaft without failure.

12.4 Transmission System

Both the PowerWalk M-Series and our product contain a transmission system composed of a driving shaft and external spur gears but characteristics, such as the number of gears and their gear ratio, vary.

The PowerWalk M-Series contains a three stage gear train with a maximum gear ratio of 113:1. (Qingguo Li, 2009)

Our product contains a three stage high power gear train with a maximum gear ration of 64.8:1. Once the gear box is assembled, it measures approximately 60mm x 80mm x 28mm.

12.5 Generator

Both the PowerWalk M-Series and our product contain a brushless DC rotary magnetic generator. Specific data such as the magnet size and the number of coil turns for the PowerWalk M-Series generator could not be obtained.

Our product contains a metal-brush motor manufactured by Mabuchi Motors. The motor is utilized in reverse, whereby mechanical power is inputted through the shaft, thus generating electricity. At maximum efficiency the motor can run at an angular velocity of 5040 rev/min producing a current of 0.64 Amps. Maximum efficiency can be achieved by applying a torque of 0.98 mN*m on the motor. The motor has an operating range of 1.5~3.0 Volts and a nominal 1.5 Volts constant.

12.6 Clutch System

The PowerWalk M-Series contains a passive one-way clutch mounted on the first gear of the product's transmission system. This allows for the transmission to engage during knee extension while allowing the input shaft to freely rotate during knee flexion. This product also contains an

electrical switch that works simultaneously with the clutch system to control the opening and closing of the power generation cycle.

Our product does not contain a clutch system or an electrical switch. This allows for our product to generate power at both the flexion and extension of the knee.

12.7 Electrical Storage

The PowerWalk M-Series utilizes Li Ion Cell batteries to store the electrical energy produce by the generator.

We were not able to integrate any circuitry or electrical storage system into our product. The electricity produced by the generator in our product can only be directly inputted into a device.

13.0 Conclusion

According to the publication put forth by Riemer and Shapiro there are several disadvantages with the PowerWalk M-Series. First, the M-Series only works at the swing phase; thus, all the phases of negative work during the gait cycle are not utilized. (Raziel Riemer, 2011) Due to the fact that the M-series utilizes a complex control system to engage/disengage power acquired from the knee based upon the gait phase, design of the system is further complicated.

Our device simplifies the prototype design by allowing the power acquisition phase to be enacted throughout the entire gait cycle. The benefits of this are twofold: first, prototype cost is maintained low due to forgoing implementation of an advance motion controller and secondly by disallowing periodic altering of the walking gait. (Qingguo Li, 2009)

As reported in the paper by Qingguo Li, due to the periodic engaging and disengaging of power acquisition the M-Series prototype precursor altered the stride of the test subjects; therefore, it was the goal of the design team to mitigate this scenario. The design team first decided to allow power collection from the knee throughout the entire gait cycle as a means of applying a consistent reactant moment; subsequently, this allows for a more fluid walking form. Secondly, the design team also chose to decrease the total reactant moment imposed by the knee brace. We reduced the gearing ratio from 113:1 to 64.8:1 in order to reduce the primary reactant force.

Final subject testing and data analysis shows that the change in gearing ratios prevents the hindering of the normal walking gait, while at the same time meeting the customer's power requirements of 0.5 watts at speeds of 5 and 7 MPH for all test subjects. Since proof of concept has been done it is the recommendation of this design group to proceed with further refinement of the design.

14.0 Future Work

Although, significant work was done by the design team there continues to be an expansive amount of future work to be performed. The design team has identified the following list of goals as worthy topics for expansion of the project:

- Redesign of transmission shaft connection to knee actuation hinge system for increased Factor of Safety (FS)
- Development of electrical conditioning system, i.e.: rectifier and DC-DC up-stepping transformer
- Redesign of transmission system for compaction of profile dimensions.
- Implementation of a coil spring system for storage of mechanical energy; thereby, allowing for a semi-constant power supplementation to the input of the transmission system.
- Identification and implementation of an electrical energy storage cell, e.g.: lithium ion-polymer battery, high capacity capacitor, hybrid storage system, etc.
- Development of CAD system casing for external protection of transmission/generator system, followed by production on the Pan American in-house 3D Viper Si2 Rapid Prototyping Machine.
- Implementation of high mechanical to electrical energy conversion generator.

With continued divergent research, compared to that produced by Donelan et al., into the device design of this biomechanical energy harvester it is not unfathomable that future technologies may come together to produce a system of optimal efficiencies and performance.

Appendices

A.1 Decision Matrices

A.1.1 Transducers

	Design Criteria vs. Objectives									
	Cost	Power Requirements	# of Parts	Size	Atachability	Safety	Weight	Reliability	User Interface	# of Relations
Low Cost	X	X	X	X			X			5
High Power Output	X	X						X		4
Low Power Input	X	X	X				X		X	6
Easy to Install			X	X	X			X	X	5
User Friendly			X	X	X					3
Safe						X		X	X	3
Appearance	X			X						2
Minimum # of Parts	X		X	X			X		X	5
Small	X	X	X	X			X		X	6
Low Weight	X		X	X			X		X	5
Reliable		X			X			X		3

	Design Criteria Weighing Matrix: 0-1 Scale										
	Cost	Power Requirement	# of Parts	Size	Atachability	Safety	Weight	Reliability	User Interface	Score	Weight
Cost	X	0	1	0	0	0	0	0	0	1	0.03
Power Requirement	1	X	0	1	0	0	0	1	1	4	0.13
# of Parts	1	0	X	1	0	0	1	0	1	4	0.13
Size	0	1	1	X	0	0	1	0	1	4	0.13
Atachability	0	0	1	0	X	0	0	1	1	3	0.10
Safety	0	0	0	0	0	X	0	1	1	2	0.07
Weight	0	0	1	1	0	0	X	0	1	3	0.10
Reliability	0	1	0	0	1	1	0	X	0	3	0.10
User Interface	0	0	1	1	1	1	1	1	X	6	0.20
	Total Number of Comparisons									30	
	Weight = Score/(Sum of the Scores)										1.00

	Selection Matrix									
	Cost	Power Requirement	# of Parts	Size	Atachability	Safety	Weight	Reliability	User Interface	Score
Electromagnetic	0.0056	0.0667	0.0000	0.0000	0.0167	0.0190	0.0000	0.0500	0.1000	0.2579
Electrostatic	0.0056	0.0444	0.0222	0.0222	0.0000	0.0095	0.0333	0.0333	0.0667	0.2373
Piezoelectric	0.0167	0.0000	0.0667	0.0667	0.0333	0.0286	0.0500	0.0167	0.0000	0.2786
Electro Active Polymer	0.0056	0.0222	0.0444	0.0444	0.0500	0.0095	0.0167	0.0000	0.0333	0.2262

Design Variant Ranking with Respect to Cost						
Design Cost	Electromagnetic	Electrostatic	Piezoelectric	Electro Active Polymer	Score = Row Sum	Norm. Score
Electromagnetic	X	0	0	1	1	0.167
Electrostatic	1	X	0	0	1	0.167
Piezoelectric	1	1	X	1	3	0.500
Electro Active Polymer	0	1	0	X	1	0.167
Column Sum	2	2	0	2	6	
Sum of Normalized Scores						1.000

Design Variant with Respect to Power Requirement						
Power Requirements	Electromagnetic	Electrostatic	Piezoelectric	Electro Active Polymer	Score = Row Sum	Norm. Score
Electromagnetic	X	1	1	1	3	0.500
Electrostatic	0	X	1	1	2	0.333
Piezoelectric	0	0	X	0	0	0.000
Electro Active Polymer	0	0	1	X	1	0.167
Column Sum	0	1	3	2	6	
Sum of Normalized Scores						1.000

Design Variant with Respect to Number of Parts						
Number of Parts	Electromagnetic	Electrostatic	Piezoelectric	Electro Active Polymer	Score = Row Sum	Norm. Score
Electromagnetic	X	0	0	0	0	0.000
Electrostatic	1	X	0	0	1	0.167
Piezoelectric	1	1	X	1	3	0.500
Electro Active Polymer	1	1	0	X	2	0.333
Column Sum	3	2	0	1	6	
Sum of Normalized Scores						1.000

Design Variant with Respect to Size						
Size	Electromagnetic	Electrostatic	Piezoelectric	Electro Active Polymer	Score = Row Sum	Norm. Score
Electromagnetic	X	0	0	0	0	0.000
Electrostatic	1	X	0	0	1	0.167
Piezoelectric	1	1	X	1	3	0.500
Electro Active Polymer	1	1	0	X	2	0.333
Column Sum	3	2	0	1	6	
Sum of Normalized Scores						1.000

Design Variant with Respect to Attachability						
Attachability	Electromagnetic	Electrostatic	Piezoelectric	Electro Active Polymer	Score = Row Sum	Norm. Score
Electromagnetic	X	1	0	0	1	0.167
Electrostatic	0	X	0	0	0	0.000
Piezoelectric	1	1	X	0	2	0.333
Electro Active Polymer	1	1	1	X	3	0.500
Column Sum	2	3	1	0	6	
Sum of Normalized Scores						1.000

Design Variant with Respect to Safety						
Safety	Electromagnetic	Electrostatic	Piezoelectric	Electro Active Polymer	Score = Row Sum	Norm. Score
Electromagnetic	X	1	0	1	2	0.286
Electrostatic	0	X	0	1	1	0.143
Piezoelectric	1	1	X	1	3	0.429
Electro Active Polymer	0	1	0	X	1	0.143
Column Sum	1	3	0	3	7	
Sum of Normalized Scores						1.000

Design Variant with Respect to Weight						
Weight	Electromagnetic	Electrostatic	Piezoelectric	Electro Active Polymer	Score = Row Sum	Norm. Score
Electromagnetic	X	0	0	0	0	0.000
Electrostatic	1	X	0	1	2	0.333
Piezoelectric	1	1	X	1	3	0.500
Electro Active Polymer	1	0	0	X	1	0.167
Column Sum	3	1	0	2	6	
Sum of Normalized Scores						1.000

Design Variant with Respect to Reliability						
Reliability	Electromagnetic	Electrostatic	Piezoelectric	Electro Active Polymer	Score = Row Sum	Norm. Score
Electromagnetic	X	1	1	1	3	0.5
Electrostatic	0	X	1	1	2	0.33333333
Piezoelectric	0	0	X	1	1	0.16666667
Electro Active Polymer	0	0	0	X	0	0
Column Sum	0	1	2	3	6	
Sum of Normalized Scores						1

Design Variant with Respect to User Interface						
Interface	Electromagnetic	Electrostatic	Piezoelectric	Electro Active Polymer	Score = Row Sum	Norm. Score
Electromagnetic	X	1	1	1	3	0.5
Electrostatic	0	X	1	1	2	0.33333333
Piezoelectric	0	0	X	0	0	0
Electro Active Polymer	0	0	1	X	1	0.16666667
Column Sum	0	1	3	2	6	
Sum of Normalized Scores						1

A.1.2 Energy Source

	Design Criteria vs. Objectives									
	Cost	Power Requirements	# of Parts	Size	Attachability	Safety	Weight	Reliability	User Interface	# of Relations
Low Cost	X	X	X							3
High Power Output	X	X	X				X		X	5
Low Power Input	X	X	X	X			X			5
Easy to Install			X		X					2
User Friendly		X	X				X		X	4
Safe		X	X	X		X	X			5
Appearance										0
Minimum # of Parts	X	X	X	X		X	X		X	7
Small	X	X	X	X		X	X			6
Low Weight	X	X	X	X		X	X		X	7
Reliable	X							X	X	3

	Design Criteria Weighing Matrix: 0-1 Scale										
	Cost	Power Requirement	# of Parts	Size	Attachability	Safety	Weight	Reliability	User Interface	Score	Weight
Cost	X	1	1	1	0	0	0	0	0	3	0.10
Power Requirement	1	X	1	0	1	0	1	0	1	5	0.16
# of Parts	1	1	X	1	1	1	1	1	1	8	0.26
Size	1	0	0	X	1	1	1	0	0	4	0.13
Atachability	1	1	1	1	X	0	0	0	0	4	0.13
Safety	0	0	0	0	0	X	1	0	0	1	0.03
Weight	0	0	1	1	1	0	X	0	0	3	0.10
Reliability	0	0	0	0	0	1	1	X	0	2	0.06
User Interface	0	1	0	0	0	0	0	0	X	1	0.03
	Total Number of Comparisons									31	
	Weight = Score/(Sum of the Scores)										1.00

	Selection Matrix									
	Cost	Power Requirement	# of Parts	Size	Attachability	Safety	Weight	Reliability	User Interface	Score
Center of Mass	0.0000	0.0269	0.1290	0.0000	0.0215	0.0161	0.0000	0.0000	0.0108	0.2043
Heel Strike	0.0484	0.0000	0.0000	0.0645	0.0645	0.0000	0.0484	0.0323	0.0161	0.2742
Knee	0.0161	0.0538	0.0860	0.0215	0.0430	0.0108	0.0161	0.0215	0.0000	0.2688
Ankle	0.0323	0.0806	0.0430	0.0430	0.0000	0.0054	0.0323	0.0108	0.0054	0.2527

Design Variant Ranking with Respect to Cost						
Design Cost	Center of Mass	Heel Strike	Knee	Ankle	Score = Row Sum	Norm. Score
Center of Mass	X	0	0	0	0	0.000
Heel Strike	1	X	1	1	3	0.500
Knee	1	0	X	0	1	0.167
Ankle	1	0	1	X	2	0.333
Column Sum	3	0	2	1	6	
Sum of Normalized Scores						1.000

Design Variant Ranking with Respect to Power Requirement						
Power Requirements	Center of Mass	Heel Strike	Knee	Ankle	Score = Row Sum	Norm. Score
Center of Mass	X	1	0	0	1	0.167
Heel Strike	0	X	0	0	0	0.000
Knee	1	1	X	0	2	0.333
Ankle	1	1	1	X	3	0.500
Column Sum	2	3	1	0	6	
Sum of Normalized Scores						1.000

Design Variant Ranking with Respect to Size						
Size	Center of Mass	Heel Strike	Knee	Ankle	Score = Row Sum	Norm. Score
Center of Mass	X	0	0	0	0	0.000
Heel Strike	1	X	1	1	3	0.500
Knee	1	0	X	0	1	0.167
Ankle	1	0	1	X	2	0.333
Column Sum	3	0	2	1	6	
Sum of Normalized Scores						1.000

Design Variant Ranking with Respect to Attachability						
Attachability	Center of Mass	Heel Strike	Knee	Ankle	Score = Row Sum	Norm. Score
Center of Mass	X	0	0	1	1	0.167
Heel Strike	1	X	1	1	3	0.500
Knee	1	0	X	1	2	0.333
Ankle	0	0	0	X	0	0.000
Column Sum	2	0	1	3	6	
Sum of Normalized Scores						1.000

Design Variant Ranking with Respect to Safety						
Safety	Center of Mass	Heel Strike	Knee	Ankle	Score = Row Sum	Norm. Score
Center of Mass	X	1	1	1	3	0.500
Heel Strike	0	X	0	0	0	0.000
Knee	0	1	X	1	2	0.333
Ankle	0	1	0	X	1	0.167
Column Sum	0	3	1	2	6	
Sum of Normalized Scores						1.000

Design Variant Ranking with Respect to Weight						
Weight	Center of Mass	Heel Strike	Knee	Ankle	Score = Row Sum	Norm. Score
Center of Mass	X	0	0	0	0	0.000
Heel Strike	1	X	1	1	3	0.500
Knee	1	0	X	0	1	0.167
Ankle	1	0	1	X	2	0.333
Column Sum	3	0	2	1	6	
Sum of Normalized Scores						1.000

Design Variant Ranking with Respect to Reliability						
Reliable	Center of Mass	Heel Strike	Knee	Ankle	Score = Row Sum	Norm. Score
Center of Mass	X	0	0	0	0	0.000
Heel Strike	1	X	1	1	3	0.500
Knee	1	1	X	0	2	0.333
Ankle	1	0	0	X	1	0.167
Column Sum	3	1	1	1	6	
Sum of Normalized Scores						1.000

Design Variant Ranking with Respect to Interface						
Interface	Center of Mass	Heel Strike	Knee	Ankle	Score = Row Sum	Norm. Score
Center of Mass	X	0	1	1	2	0.333
Heel Strike	1	X	1	1	3	0.500
Knee	0	0	X	0	0	0.000
Ankle	0	0	1	X	1	0.167
Column Sum	1	0	3	2	6	
Sum of Normalized Scores						1.000

A.1.3 Case Mount

	Design Criteria vs. Objectives									
	Cost	Power Requirements	# of Parts	Size	Attachability	Safety	Weight	Reliability	User Interface	# of Relations
Low Cost	X	X	X	X	X		X	X		7
High Power Output	X	X	X	X			X		X	6
Low Power Input	X	X	X	X			X		X	6
Easy to Install			X		X	X		X	X	5
User Friendly		X	X	X	X	X	X		X	7
Safe		X	X	X		X	X		X	6
Appearance	X		X	X	X		X			5
Minimum # of Parts	X	X	X	X	X	X	X		X	8
Small	X	X	X	X	X		X		X	7
Low Weight	X	X	X	X			X		X	6
Reliable	X	X						X	X	4

	Design Criteria Weighing Matrix: 0-1 Scale										
	Cost	Power Requirement	# of Parts	Size	Attachability	Safety	Weight	Reliability	User Interface	Score	Weight
Cost	X	0	1	1	0	0	1	0	0	3	0.14
Power Requirement	0	X	0	1	0	0	1	0	0	2	0.09
# of Parts	1	0	X	1	0	0	1	0	0	3	0.14
Size	0	0	1	X	1	0	1	0	1	4	0.18
Atachability	0	0	1	1	X	0	0	0	0	2	0.09
Safety	0	0	0	1	0	X	1	0	0	2	0.09
Weight	1	0	1	1	0	1	X	0	0	4	0.18
Reliability	0	0	0	0	0	0	0	X	0	0	0.00
User Interface	0	0	1	0	1	0	0	0	X	2	0.09
	Total Number of Comparisons									22	
	Weight = Score/(Sum of the Scores)										1.00

	Selection Matrix									
	Cost	Power Requirement	# of Parts	Size	Attachability	Safety	Weight	Reliability	User Interface	Score
Nylon	0.0273	0.0000	0.0273	0.0727	0.0182	0.0182	0.0727	0.0000	0.0182	0.2545
PVC	0.0409	0.0182	0.0409	0.0000	0.0273	0.0273	0.0364	0.0000	0.0273	0.2182
ABS	0.0545	0.0091	0.0545	0.0364	0.0364	0.0364	0.0182	0.0000	0.0364	0.2818
Carbon Fiber	0.0136	0.0273	0.0136	0.0545	0.0091	0.0000	0.0545	0.0000	0.0091	0.1818
Titanium	0.0000	0.0364	0.0000	0.0182	0.0000	0.0091	0.0000	0.0000	0.0000	0.0636

Design Variant Ranking with Respect to Cost							
Design Cost	Nylon	PVC	ABS	Carbon Fiber	Titanium	Score = Row Sum	Norm. Score
Nylon	X	0	0	1	1	2	0.200
PVC	1	X	0	1	1	3	0.300
ABS	1	1	X	1	1	4	0.400
Carbon Fiber	0	0	0	X	1	1	0.100
Titanium	0	0	0	0	X	0	0.000
Column Sum	2	1	0	3	4	10	
Sum of Normalized Scores							1.000

Design Variant Ranking with Respect to Power Requirement							
Power Requirement	Nylon	PVC	ABS	Carbon Fiber	Titanium	Score = Row Sum	Norm. Score
Nylon	X	0	0	0	0	0	0.000
PVC	1	X	1	0	0	2	0.200
ABS	1	0	X	0	0	1	0.100
Carbon Fiber	1	1	1	X	0	3	0.300
Titanium	1	1	1	1	X	4	0.400
Column Sum	4	2	3	1	0	10	
Sum of Normalized Scores							1.000

Design Variant Ranking with Respect to Number of Parts							
Number of Parts	Nylon	PVC	ABS	Carbon Fiber	Titanium	Score = Row Sum	Norm. Score
Nylon	X	0	0	1	1	2	0.200
PVC	1	X	0	1	1	3	0.300
ABS	1	1	X	1	1	4	0.400
Carbon Fiber	0	0	0	X	1	1	0.100
Titanium	0	0	0	0	X	0	0.000
Column Sum	2	1	0	3	4	10	
Sum of Normalized Scores							1.000

Design Variant Ranking with Respect to Size							
Size	Nylon	PVC	ABS	Carbon Fiber	Titanium	Score = Row Sum	Norm. Score
Nylon	X	1	1	1	1	4	0.400
PVC	0	X	0	0	0	0	0.000
ABS	0	1	X	0	1	2	0.200
Carbon Fiber	0	1	1	X	1	3	0.300
Titanium	0	1	0	0	X	1	0.100
Column Sum	0	4	2	1	3	10	
Sum of Normalized Scores							1.000

Design Variant Ranking with Respect to Attachability							
Attachability	Nylon	PVC	ABS	Carbon Fiber	Titanium	Score = Row Sum	Norm. Score
Nylon	X	0	0	1	1	2	0.200
PVC	1	X	0	1	1	3	0.300
ABS	1	1	X	1	1	4	0.400
Carbon Fiber	0	0	0	X	1	1	0.100
Titanium	0	0	0	0	X	0	0.000
Column Sum	2	1	0	3	4	10	
Sum of Normalized Scores							1.000

Design Variant Ranking with Respect to Safety							
Safety	Nylon	PVC	ABS	Carbon Fiber	Titanium	Score = Row Sum	Norm. Score
Nylon	X	0	0	1	1	2	0.200
PVC	1	X	0	1	1	3	0.300
ABS	1	1	X	1	1	4	0.400
Carbon Fiber	0	0	0	X	0	0	0.000
Titanium	0	0	0	1	X	1	0.100
Column Sum	2	1	0	4	3	10	
Sum of Normalized Scores							1.000

Design Variant Ranking with Respect to Weight							
Weight	Nylon	PVC	ABS	Carbon Fiber	Titanium	Score = Row Sum	Norm. Score
Nylon	X	1	1	1	1	4	0.400
PVC	0	X	1	0	1	2	0.200
ABS	0	0	X	0	1	1	0.100
Carbon Fiber	0	1	1	X	1	3	0.300
Titanium	0	0	0	0	X	0	0.000
Column Sum	0	2	3	1	4	10	
Sum of Normalized Scores							1.000

Design Variant Ranking with Respect to Reliability							
Reliability	Nylon	PVC	ABS	Carbon Fiber	Titanium	Score = Row Sum	Norm. Score
Nylon	X	0	0	0	0	0	0.000
PVC	1	X	0	0	0	1	0.100
ABS	1	1	X	1	1	4	0.400
Carbon Fiber	1	1	0	X	0	2	0.200
Titanium	1	1	0	1	X	3	0.300
Column Sum	4	3	0	2	1	10	
Sum of Normalized Scores							1.000

Design Variant Ranking with Respect to Interface							
Interface	Nylon	PVC	ABS	Carbon Fiber	Titanium	Score = Row Sum	Norm. Score
Nylon	X	0	0	1	1	2	0.200
PVC	1	X	0	1	1	3	0.300
ABS	1	1	X	1	1	4	0.400
Carbon Fiber	0	0	0	X	1	1	0.100
Titanium	0	0	0	0	X	0	0.000
Column Sum	2	1	0	3	4	10	
Sum of Normalized Scores							1.000

A.1.4 Energy Storage

	Cost	Power Requirements	# of Parts	Size	Attachability	Safety	Weight	Reliability	User Interface	# of Relations
Low Cost	X	X								2
High Power Output		X		X						2
Low Power Input										0
Easy to Install			X	X	X					3
User Friendly									X	1
Safe						X			X	2
Appearance										0
Minimum # of Parts			X				X			2
Small		X	X							2
Low Weight			X	X			X			3
Reliable								X		1

	Design Criteria Weighing Matrix: 0-1 Scale										
	Cost	Power Requirement	# of Parts	Size	Attachability	Safety	Weight	Reliability	User Interface	Score	Weight
Cost	X	1	1	0	0	0	0	0	0	2	0.12
Power Requirement	1	X	0	1	0	0	0	0	0	2	0.12
# of Parts	1	0	X	1	0	0	1	0	0	3	0.18
Size	0	1	1	X	0	0	1	0	0	3	0.18
Attachability	0	0	0	1	X	0	0	0	1	2	0.12
Safety	0	0	0	0	0	X	0	0	0	0	0.00
Weight	0	1	1	1	1	0	X	0	0	4	0.24
Reliability	0	0	0	0	0	0	0	X	0	0	0.00
User Interface	0	0	0	0	0	0	1	0	X	1	0.06
	Total Number of Comparisons									17	
	Weight = Score/(Sum of the Scores)										1.00

	Selection Matrix									
	Cost	Power Requirement	# of Parts	Size	Attachability	Safety	Weight	Reliability	User Interface	Score
Capacitor	0.0784	0.0000	0.1176	0.1176	0.0392	0.0000	0.1569	0.0000	0.0000	0.5098
Battery	0.0392	0.0392	0.0588	0.0588	0.0784	0.0000	0.0784	0.0000	0.0392	0.3922
Battery/Capacitor Hybrid	0.0000	0.0784	0.0000	0.0000	0.0000	0.0000	0.0000	0.0000	0.0196	0.0980

Design Variant Ranking with Respect to Cost					
Design Cost	Capacitor	Battery	Battery/Capacitor Hybrid	Score = Row Sum	Norm. Score
Capacitor	X	1	1	2	0.667
Battery	0	X	1	1	0.333
Battery/Capacitor Hybrid	0	0	X	0	0.000
Column Sum	0	1	2	3	
Sum of Normalized Scores					1.000

Design Variant with Respect to Power Requirement					
Power Requirement	Capacitor	Battery	Battery/Capacitor Hybrid	Score = Row Sum	Norm. Score
Capacitor	X	0	0	0	0.000
Battery	1	X	0	1	0.333
Battery/Capacitor Hybrid	1	1	X	2	0.667
Column Sum	2	1	0	3	
Sum of Normalized Scores					1.00

Design Variant with Respect to Number of Parts					
Number of Parts	Capacitor	Battery	Battery/Capacitor Hybrid	Score = Row Sum	Norm. Score
Capacitor	X	1	1	2	0.667
Battery	0	X	1	1	0.333
Battery/Capacitor Hybrid	0	0	X	0	0.000
Column Sum	0	1	2	3	
Sum of Normalized Scores					1.00

Design Variant with Respect to Size					
Size	Capacitor	Battery	Battery/Capa	Score = Row	Norm. Score
Capacitor	X	1	1	2	0.667
Battery	0	X	1	1	0.333
Battery/Capacitor Hybrid	0	0	X	0	0.000
Column Sum	0	1	2	3	
Sum of Normalized Scores					1.00

Design Variant with Respect to Number of Attachability					
Attachability	Capacitor	Battery	Battery/Capacitor Hybrid	Score = Row Sum	Norm. Score
Capacitor	X	0	1	1	0.333
Battery	1	X	1	2	0.667
Battery/Capacitor Hybrid	0	0	X	0	0.000
Column Sum	1	0	2	3	
Sum of Normalized Scores					1.00

Design Variant with Respect to Safety					
Safety	Capacitor	Battery	Battery/Capacitor Hybrid	Score = Row Sum	Norm. Score
Capacitor	X	0	1	1	0.333
Battery	1	X	1	2	0.667
Battery/Capacitor Hybrid	0	0	X	0	0.000
Column Sum	1	0	2	3	
Sum of Normalized Scores					1.00

Design Variant with Respect to Weight					
Weight	Capacitor	Battery	Battery/Capacitor Hybrid	Score = Row Sum	Norm. Score
Capacitor	X	1	1	2	0.667
Battery	0	X	1	1	0.333
Battery/Capacitor Hybrid	0	0	X	0	0.000
Column Sum	0	1	2	3	
Sum of Normalized Scores					1.00

Design Variant with Respect to Reliability					
Reliability	Capacitor	Battery	Battery/Capacitor Hybrid	Score = Row Sum	Norm. Score
Capacitor	X	1	1	2	0.667
Battery	0	X	1	1	0.333
Battery/Capacitor Hybrid	0	0	X	0	0.000
Column Sum	0	1	2	3	
Sum of Normalized Scores					1.00

Design Variant with Respect to Interface					
Interface	Capacitor	Battery	Battery/Capacitor Hybrid	Score = Row Sum	Norm. Score
Capacitor	X	0	0	0	0.000
Battery	1	X	1	2	0.667
Battery/Capacitor Hybrid	1	0	X	1	0.333
Column Sum	2	0	1	3	
Sum of Normalized Scores					1.00

A.1.5 Power Delivery Port

	Desing Criteria vs. Objectives									
	Cost	**Power Requirements**	**# of Parts**	**Size**	**Atachability**	**Safety**	**Weight**	**Reliability**	**User Interface**	**# of Relations**
Low Cost	X	X	X		X			X	X	6
High Power Output	X	X	X		X	X		X		6
Low Power Input										0
Easy to Install	X		X	X	X	X			X	6
User Friendly		X	X	X	X	X			X	6
Safe		X			X	X		X	X	5
Apperance	X		X	X	X		X			5
Minimum # of Parts	X	X	X	X	X		X		X	7
Small	X	X	X	X	X		X		X	7
Low Weight	X		X	X	X		X			5
Reliable	X	X				X		X	X	5

	Cost	Power Requirement	# of Parts	Size	Atachability	Safety	Weight	Reliability	User Interface	Score	Weight
Cost	X	1	0	1	1	0	0	0	1	4	0.13
Power Requirement	1	X	0	1	1	1	0	0	1	5	0.17
# of Parts	1	0	X	1	1	0	1	0	0	4	0.13
Size	0	1	0	X	1	0	1	0	0	3	0.10
Atachability	1	0	1	1	X	1	0	0	1	5	0.17
Safety	0	1	0	0	0	X	0	0	0	1	0.03
Weight	0	0	1	1	0	0	X	0	0	2	0.07
Reliability	0	1	0	0	0	0	0	X	0	1	0.03
User Interface	1	1	0	1	1	1	0	0	X	5	0.17
	Total Number of Comparissions									30	
	Weight = Score/(Sum of the Scores)										1.00

	Selection Matrix									
	Cost	Power Requirement	# of Parts	Size	Atachability	Safety	Weight	Reliability	User Interface	Score
USB	0.08888889	0.111111111	0.04444444	0.06666667	0.11111111	0.02222222	0.04444444	0	0.11111111	0.6
Car Lighter	0.04444444	0.055555556	0.08888889	0.03333333	0.05555556	0	0.02222222	0.02222222	0	0.322222222
Electrical Outlet	0	0	0	0	0	0.01111111	0	0.01111111	0.05555556	0.077777778
Decision										USB

Design Variant Ranking with Respect to Cost					
Design Cost	USB	Car Lighter	Electrical Outlet	Score = Row Sum	Norm. Score
USB	X	1	1	2	0.667
Car Lighter	0	X	1	1	0.333
Electrical Outlet	0	0	X	0	0.000
Column Sum	0	1	2	3	
Sum of Normalized Scores					1.000

Design Variant Ranking with Respect to Power Requirement					
Power Requirement	USB	Car Lighter	Electrical Outlet	Score = Row Sum	Norm. Score
USB	X	1	1	2	0.667
Car Lighter	0	X	1	1	0.333
Electrical Outlet	0	0	X	0	0.000

Column Sum	0	1	2	3	
Sum of Normalized Scores					1.000

Design Variant Ranking with Respect to Number of Parts					
Number of Parts	USB	Car Lighter	Electrical Outlet	Score = Row Sum	Norm. Score
USB	X	0	1	1	0.333
Car Lighter	1	X	1	2	0.667
Electrical Outlet	0	0	X	0	0.000
Column Sum	1	0	2	3	
Sum of Normalized Scores					1.000

Design Variant Ranking with Respect to Size					
Size	USB	Car Lighter	Electrical Outlet	Score = Row Sum	Norm. Score
USB	X	1	1	2	0.667
Car Lighter	0	X	1	1	0.333
Electrical Outlet	0	0	X	0	0.000
Column Sum	0	1	2	3	
Sum of Normalized Scores					1.000

Design Variant Ranking with Respect to Attachability					
Attachability	USB	Car Lighter	Electrical Outlet	Score = Row Sum	Norm. Score
USB	X	1	1	2	0.667
Car Lighter	0	X	1	1	0.333
Electrical Outlet	0	0	X	0	0.000
Column Sum	0	1	2	3	
Sum of Normalized Scores					1.000

Design Variant Ranking with Respect to Safety					
Safety	USB	Car Lighter	Electrical Outlet	Score = Row Sum	Norm. Score
USB	X	1	1	2	0.667
Car Lighter	0	X	0	0	0.000
Electrical Outlet	0	1	X	1	0.333
Column Sum	0	2	1	3	
Sum of Normalized Scores					1.000

Design Variant Ranking with Respect to Weight					
Weight	USB	Car Lighter	Electrical Outlet	Score = Row Sum	Norm. Score
USB	X	1	1	2	0.667
Car Lighter	0	X	1	1	0.333
Electrical Outlet	0	0	X	0	0.000
Column Sum	0	1	2	3	
Sum of Normalized Scores					1.000

Design Variant Ranking with Respect to Realiability					
Realiable	USB	Car Lighter	Electrical Outlet	Score = Row Sum	Norm. Score
USB	X	0	0	0	0.000
Car Lighter	1	X	1	2	0.667
Electrical Outlet	0	1	X	1	0.333
Column Sum	1	1	1	3	
Sum of Normalized Scores					1.000

Design Variant Ranking with Respect to Interface					
Interface	USB	Car Lighter	Electrical Outlet	Score = Row Sum	Norm. Score
USB	X	1	1	2	0.667
Car Lighter	0	X	0	0	0.000
Electrical Outlet	0	1	X	1	0.333

Column Sum	0	2	1	3	
Sum of Normalized Scores					1.000

A.2 Project Charts & Graphs

A.2.1 Customer Survey

CUSTOMER SURVEY

Name:	Age:	Gender:
Objective: To produce a wearable mechanism which converts biomechanical motion into storable electrical energy.		

For each question below, circle the number to the right
that best fits your opinion on the importance of the issue.
Use the scale to match your opinion.

Question	Scale of Importance				
	Not at all	Not very	No Opinion	Some-what	Extremely
Physical look of the mechanism	1	2	3	4	5
Device's weight	1	2	3	4	5
Durability and impact resistance	1	2	3	4	5
Flexibility and freedom of movement	1	2	3	4	5
Ergonomics of device	1	2	3	4	5
Ease of attachment	1	2	3	4	5
Power level indicator feature	1	2	3	4	5
Charge rate	1	2	3	4	5
Price	1	2	3	4	5
Inconspicuousness of the device	1	2	3	4	5
Compliance with general safety regulations	1	2	3	4	5

Rate the following according to amount of expected use

Question	Scale of Importance				
	Never	Rarely	Casually	Often	Very often
Environment					
Athletic training	1	2	3	4	5
Water sports	1	2	3	4	5
Daily Commuting	1	2	3	4	5
Continuous wear	1	2	3	4	5
Charge port type					
Micro/mini-usb	1	2	3	4	5
Standard usb	1	2	3	4	5
Car cigarette lighter	1	2	3	4	5
U.S. standard outlet	1	2	3	4	5

A.2.2 QFD Chart

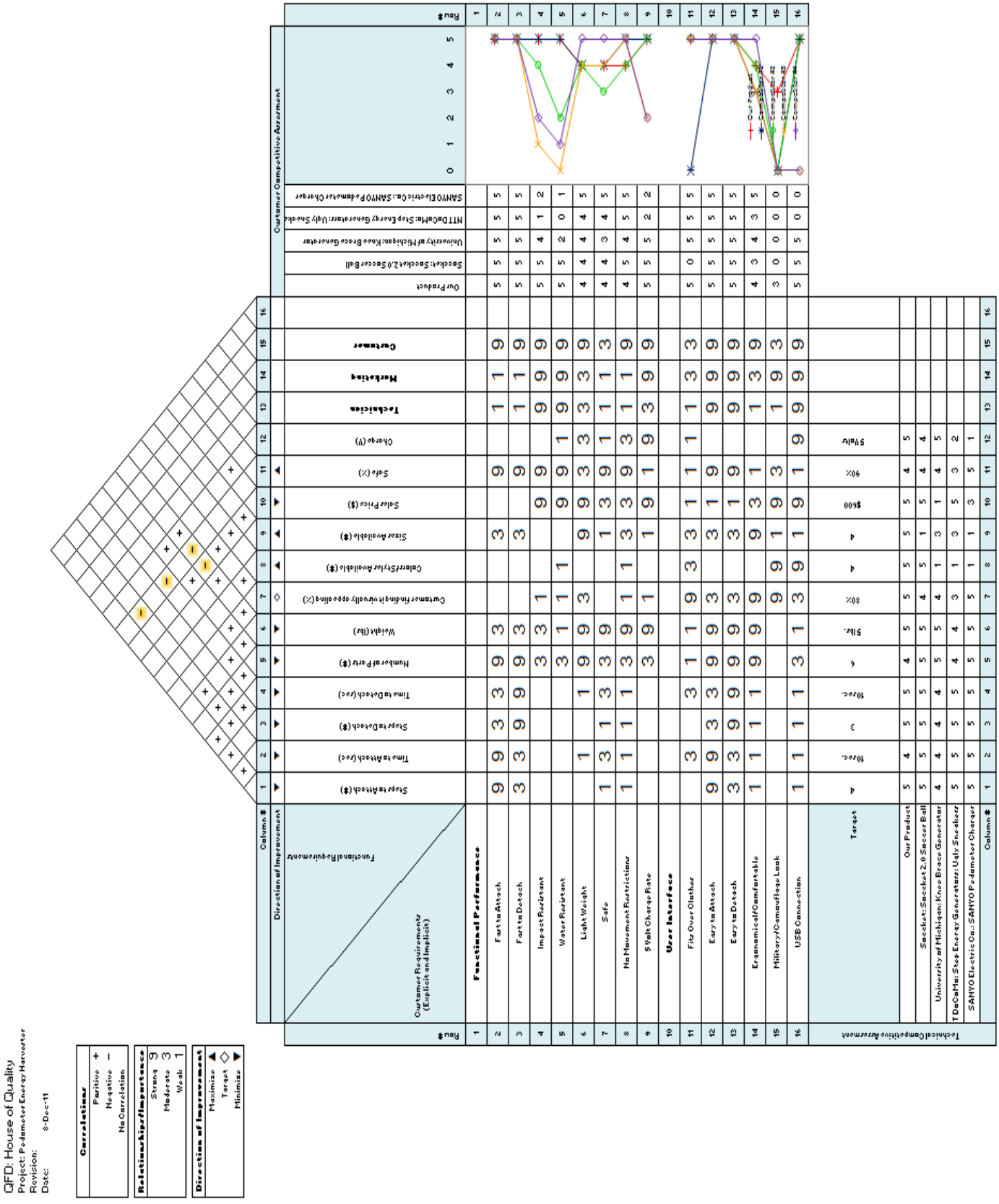

A.2.3 Pareto Analysis

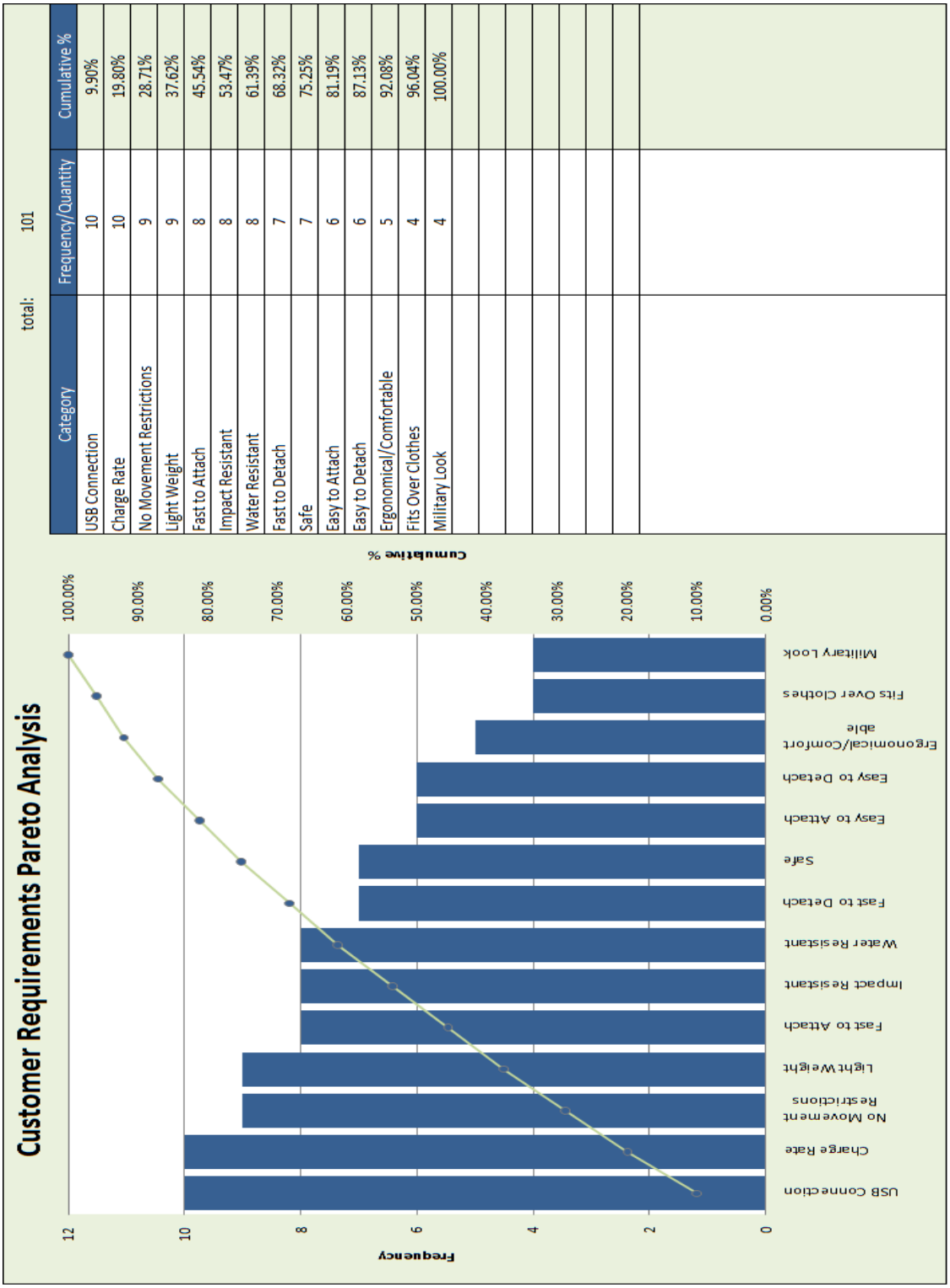

total: 101

Category	Frequency/Quantity	Cumulative %
USB Connection	10	9.90%
Charge Rate	10	19.80%
No Movement Restrictions	9	28.71%
Light Weight	9	37.62%
Fast to Attach	8	45.54%
Impact Resistant	8	53.47%
Water Resistant	8	61.39%
Fast to Detach	7	68.32%
Safe	7	75.25%
Easy to Attach	6	81.19%
Easy to Detach	6	87.13%
Ergonomical/Comfortable	5	92.08%
Fits Over Clothes	4	96.04%
Military Look	4	100.00%

A.3 Handwritten Calculations

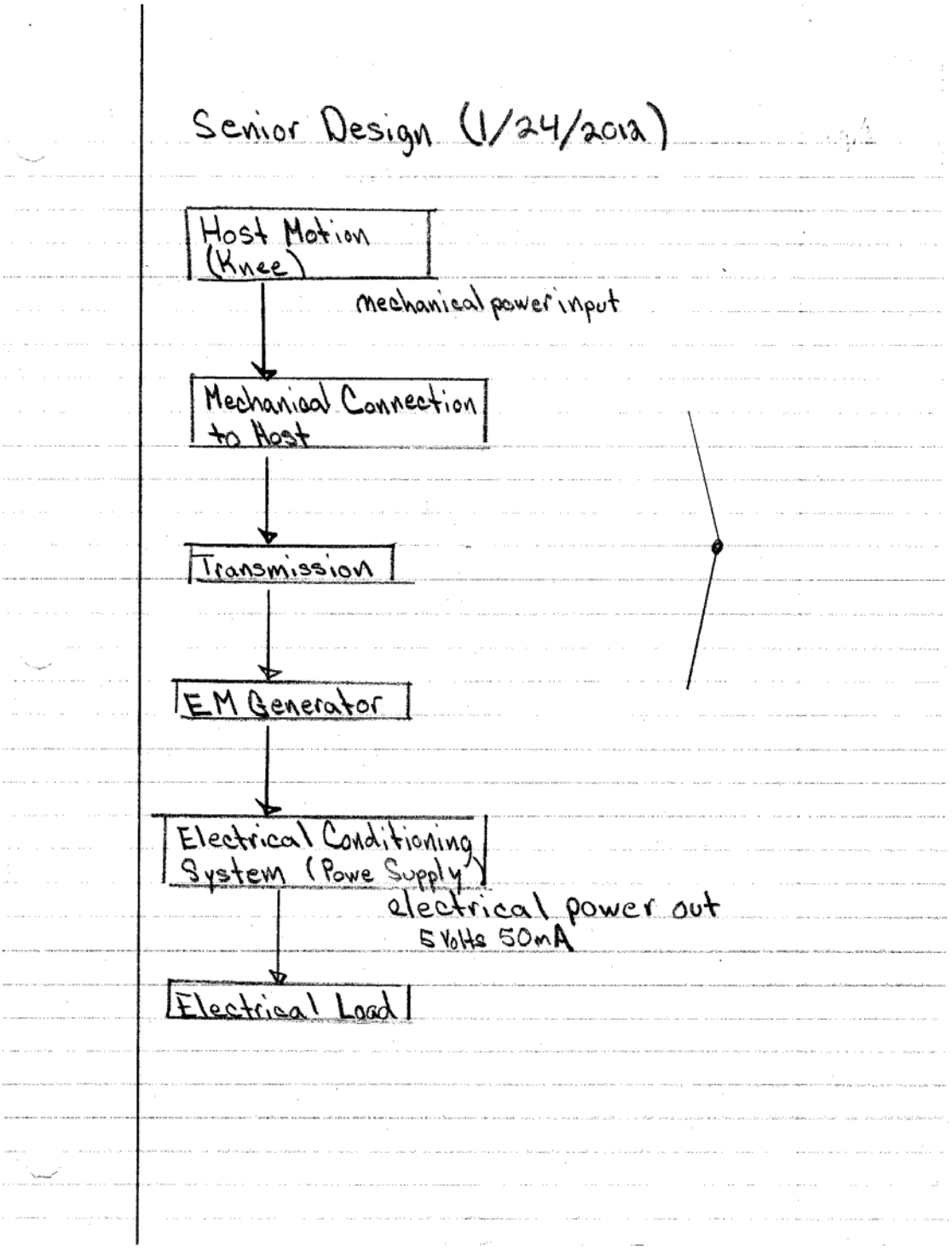

Figure 104: Device System Flowchart

Senior Design (2/17/2012)

pg 1 of 2

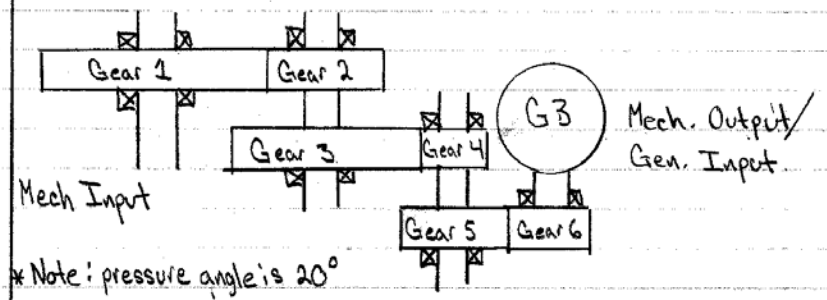

* Note: pressure angle is 20°

$OD_1 = 1.085$ in $N_1 = 26$

$OD_2 = 0.389$ in $N_2 = 8$

$OD_3 = 0.749$ in $N_3 = 22$

$OD_4 = 0.315$ in $N_4 = 8$

$OD_5 = 0.705$ in $N_5 = 28$

$OD_6 = 0.270$ in $N_6 = 10$

In order calculate efficency of gear train we need to calculate the pitch diameter of the gears so:

$PD = N/DP$ where pitch diameter (PD), # of teeth (N), and diametal pitch (DP)

DP can be calculated as: $DP = (N+2)/OD$ where outer diameter (OD)

Figure 105: Transmission Pitch Diameter Calculations (1 of 2)

Senior Design (2/17/2012)

So a simplified equation is: $PD = N/[(N+2)/OD]$

$$PD_1 = \frac{26}{[(26+2)/1.085in]} \Rightarrow 1.0075in \Rightarrow \boxed{PD_1 = 1.01in}$$

$$PD_2 = \frac{8}{[(8+2)/0.389in]} \Rightarrow 0.3112in \Rightarrow PD_2 = 0.311in$$

$$PD_3 = \frac{22}{[(22+2)/0.749in]} \Rightarrow 0.6866in \Rightarrow PD_3 = 0.687in$$

$$PD_4 = \frac{8}{[(8+2)/0.313in]} \Rightarrow 0.2504in \Rightarrow PD_4 = 0.250in$$

$$PD_5 = \frac{28}{[(28+2)/0.705in]} \Rightarrow 0.658in \Rightarrow PD_5 = 0.658in$$

$$PD_6 = \frac{10}{[(10+2)/0.270in]} \Rightarrow 0.225in \Rightarrow PD_6 = 0.225in$$

Now in order to calculate the efficency we shall insert the newly found pitch diameters for the following equation:

← Note: View "Gears-Gear efficency" article for eq.

$$\text{Efficency}(\%) = 100 - P \quad \text{where} \quad P = 50\mu\left[\frac{(H_s^2 + H_t^2)}{(H_s + H_t)}\right]$$

$$F = \cos\alpha(\text{external gears})\,F$$

Develop a Excel spreadsheet for the efficency equation

$$\text{where } H_s = (R_g + 1)\left[\sqrt{\left(\frac{R_o}{R_p}\right)^2 - \cos^2\alpha} - \sin\alpha\right] \text{ and}$$

$$H_t = \left(\frac{R_g + 1}{R_g}\right)\left[\sqrt{\left(\frac{r_o}{r_p}\right)^2 - \cos^2\alpha} - \sin\alpha\right]$$

Figure 106: Transmission Pitch Diameter Calculations (2 of 2)

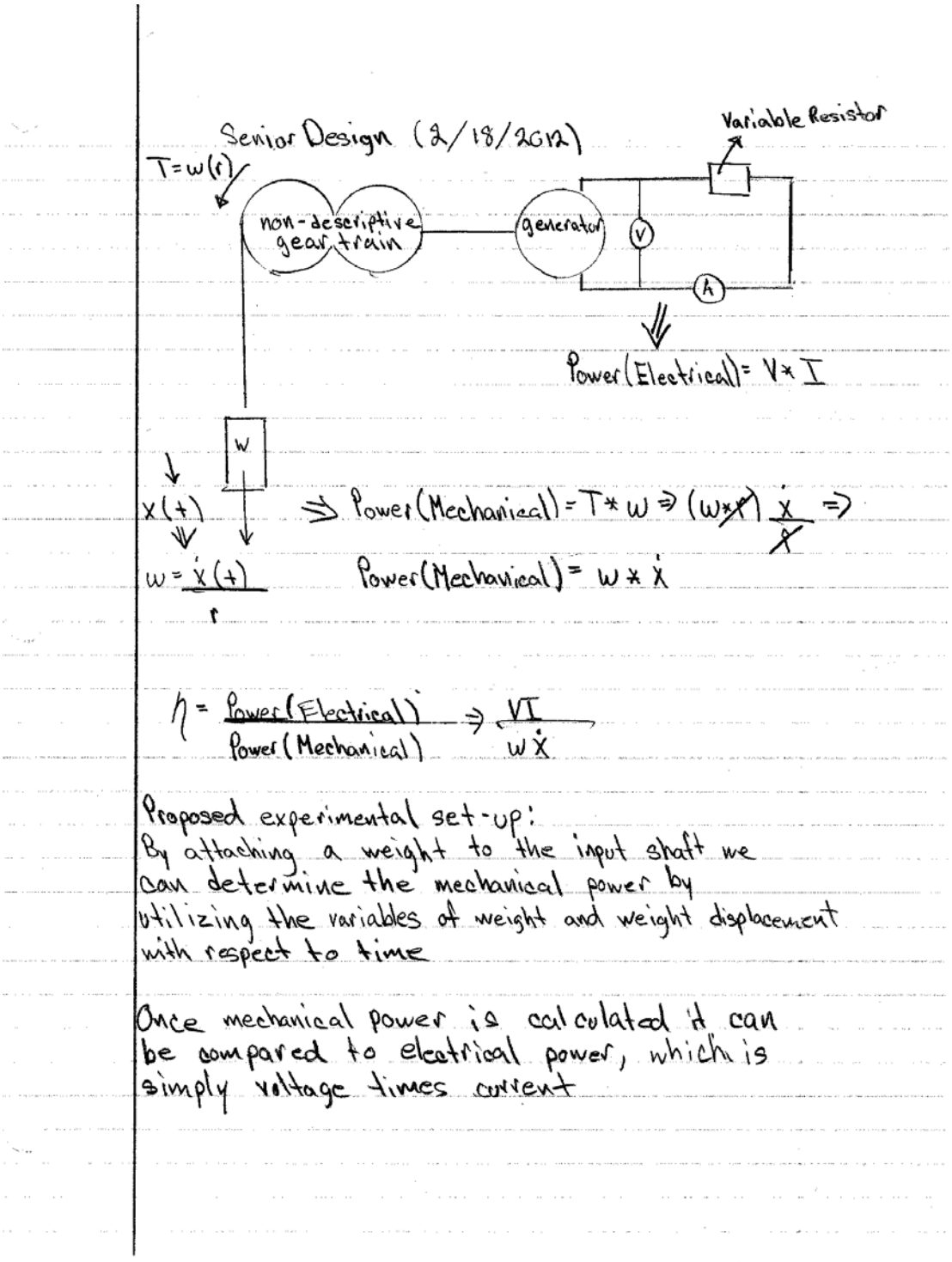

Figure 107: Initial Bench Top Experimental Diagram

Senior Design (2/24/2012)

* High Power Gear Box — 41.7:1, 64.8:1 — Edmunds Scientific

Planetary Gear Box — 16:1 to 400:1
16/20/25/80/100/400

4-Speed Crank Axle — 126:1 to 5402:1
126/441/1543/5402

gear/housing ⇒ polyacetyl resin
friction coefficient (μ) ⇒ .5 ⇒ according to[a] center for polymeric materials report
normal pressure angle ⇒ 20°

* Mueller hinged Knee brace
- Designed for orthosis medial-lateral support
- Contains two side hinge pockets for size alteration (s-xl) ⇒ Hinge material ⇒ 6000 type alloyed w/ magnesium+silicon 6060/
- Neoprene/Polyestrene Blend ⇒ preforated fabric allows for breathability ⇒ eliminates bunching (open back) (13-21 in)
- Prevent hyperextension

Figure 108: Transmission & Mueller Brace Notes

Senior Design (2/28/2012)

EM Generator Output (V_G/A_G)

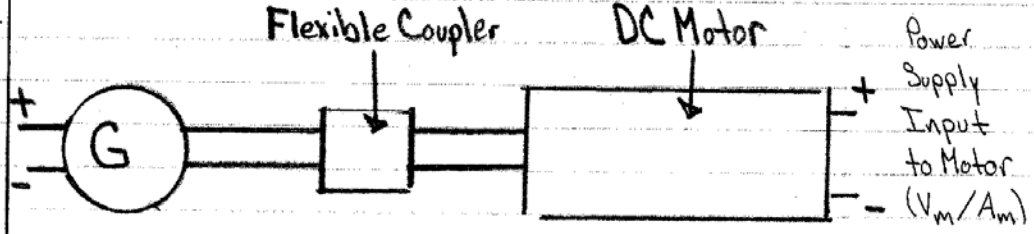

Note: See motor data sheet

Motor Company: Servo Systems Co. Model: RDM103
Voltage Constant: 10.2 V/KRPM ⇒ denoted as VC_m
Torque Constant: 13.7 oz-in/amp ⇒ denoted as TC_m

We can calculate motor torque/velocity utilizing the torque/velocity constant from the motor data sheet

so $\omega_m = \frac{1}{VC_m}(V_m)$ and $T_m = TC_m(A_m)$

Ex ⇒ @ V_m/A_m = 10 volts/1 amp ⇒

$\omega_m = (1000\,RPM/10.2\,V)(10\,V) \Rightarrow \omega_m = 980.3922\,RPM$
$T_m = (13.7\,oz\text{-}in./1\,A)(1\,A) \Rightarrow T_m = 13.7\,oz\text{-}in.$

We can formulate an equation to relate the two shaft velocities and torques

$T_G(\omega_G) = (e)\,T_m(\omega_m)$ assuming a $e = 100\%$
and $\omega_m/\omega_G = 1$ then:

$T_G = T_m$

$V = IR$

Senior Design (3/1/2012)

pg. #1

In order to test the generator efficencies we will determine the efficeney at five speeds:

$$\eta = \frac{P_{out}}{P_{in}} \Rightarrow \frac{P_{generator}}{P_{motor\ (shaft)}} \Rightarrow \frac{\text{Electrical}}{\text{Mechanical}}$$

Using G2

@ 9.997 V and 0.340 A $\Rightarrow$ ω_m = 1221.4 rpm (measured)
9.997 V (1000 RPM / 10.2 V) $\Rightarrow$ ω_m = 980.09 rpm (calculated)

@ 30.988 V and 0.476 A $\Rightarrow$ ω_m = 3917.6 rpm (measured)
30.988 V (1000 rpm / 10.2 V) $\Rightarrow$ ω_m = 3,038.6 rpm (calculated)

@ 19.995 V and 0.397 A $\Rightarrow$ ω_m = 2539.1 rpm (measured)
19.995 V (1000 rpm / 10.2 V) $\Rightarrow$ ω_m = 1960.3 rpm (calculated)

@ 5.000 V and 0.276 A $\Rightarrow$ ω_m = 583.5 rpm (measured)
5.000 V (1000 rpm / 10.2 V) $\Rightarrow$ ω_m = 490.2 rpm (calculated)

@ 14.993 V and 0.356 A $\Rightarrow$ ω_m = 1886.9 rpm (measured)
14.993 V (1000 rpm / 10.2 V) $\Rightarrow$ ω_m = 1469.9 rpm (calculated)

@ 24.992 V and 0.425 A $\Rightarrow$ ω_m = 3186.4 rpm (measured)
24.992 V (1000 rpm / 10.2 V) $\Rightarrow$ ω_m = 2450.2 rpm (calculated)

Since torque constant and voltage constants do not provide reliable data when compared to the measured values we must determine a relationship between the measured and calculated angular velocity vs. voltage curves

Figure 109: Initial Bench Top Testing Data

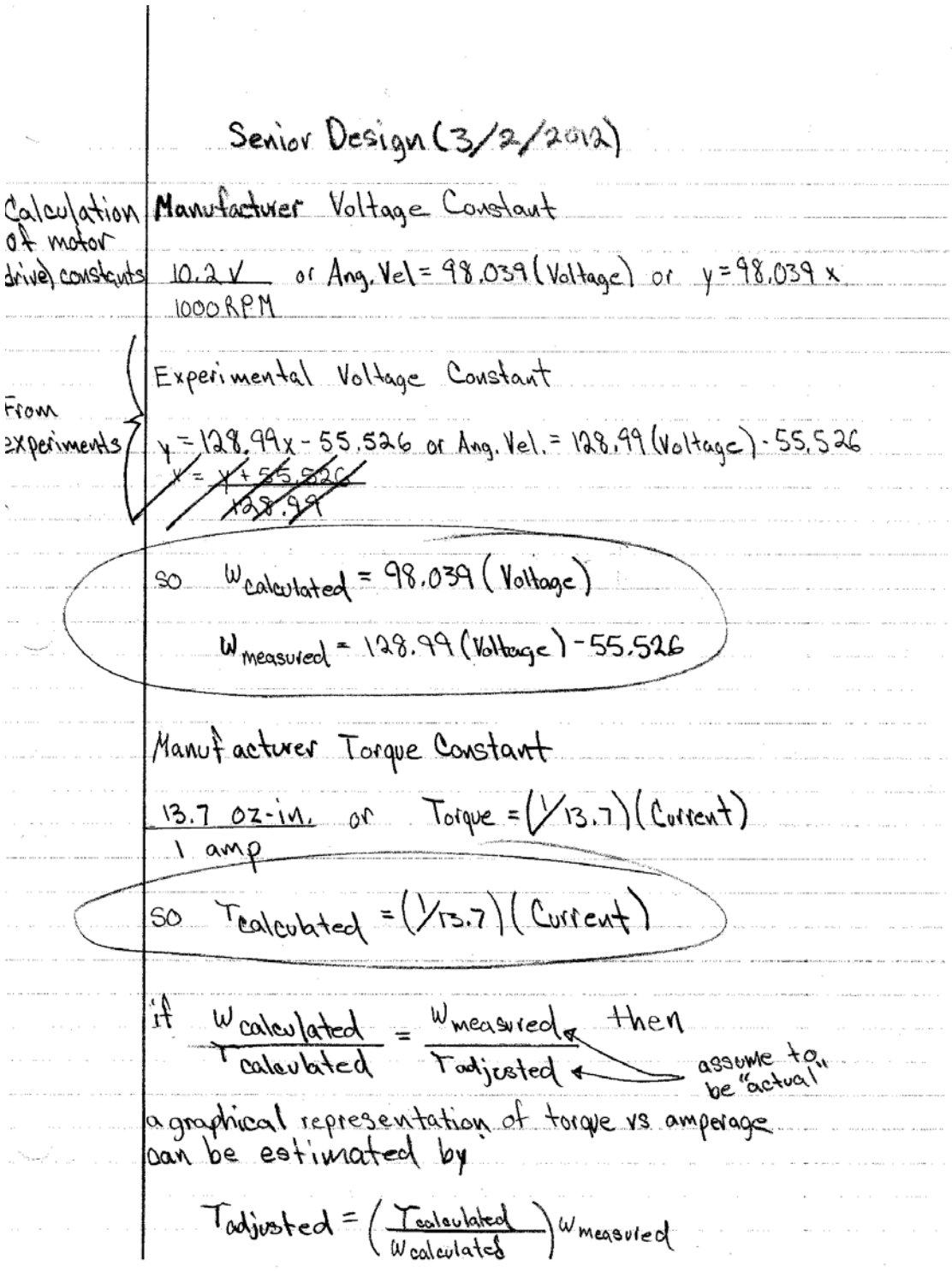

Figure 110: Notes for Adjustment of Bench Top Driver Motor Constants

Senior Design (4/9/2012)

how to name testing files ⇒

apparatus - subject - rate - trial # ⇒ use $\frac{\text{meters}}{\text{hour}}$

for example: treadmill - steve - 5 ~~mph~~ - 3
bike - amador - 50 Kph - 1

*note: $\frac{1 \text{ Kilometer}}{\text{hour}} = \frac{.621371 \text{ miles}}{\text{hour}}$

*note: Data from Riemer + Shapiro: Biomechanical Energy Harvesting... is given at a speed of 1.3 m/s and .9 Hz cycle frequency

$1.3 \frac{\text{meters}}{\text{second}} \times \frac{3600 \text{ sec}}{1 \text{ hr}} \times \frac{1 \text{ mile}}{1{,}609.344 \text{ meters}} \Rightarrow 2.9080 \text{ mph}$

2.908 mph ≈ 3mph

Testing will be conducted as follows

apparatus ⇒ treadmill and bike we be tested
subject ⇒ Steve and Amador will be the subjects
rate ⇒ treadmill @ 3 mph / 5 mph / 7 mph
bike @ 30/50/70 Km/hr *Note: bike will be tested if time permits also incline gradients
trial # ⇒ begin @ 1 and continue till 5 trials have been completed

Figure 111: Subject Testing Guidelines

Senior Design (4/20/2012)

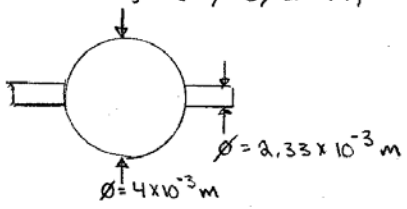

$T = V \times R \Rightarrow V = T/R \Rightarrow 40\ Nm / 2\times10^{-3}\ m \Rightarrow V = 20\times10^{3}\ N$

Since we have a double pin system shear force is halved

$V/2 \Rightarrow 20\times10^{3}\ N/2 \Rightarrow \boxed{V = 10\times10^{3}\ N}$

This force should be distributed through half the surface area length, but to simplify calculation and examine the worst case scenario we will apply concentrated shear force loads at the base of the pin interface to the shaft

Shear stress can be solved for utilizing either of the following equations

average shear stress $\Rightarrow \tau_{avg} = \frac{V}{A}$ or shear stress $\Rightarrow \tau = \frac{VQ}{It}$

Calculations for a solid and hollow pin will be calculated utilizing the average shear stress formula first

$\tau_{Avg}(Solid) = V/A \Rightarrow 10\times10^{3}\ N \Big/ \left(\frac{\pi(2.33\times10^{-3}\ m)^2}{4}\right) \Rightarrow$

$\boxed{\tau_{Avg}(Solid) = 2.395\times10^{9}\ Pa}$

Figure 112: Analytical Calculations of Pin Failure (1 of 3)

Senior Design (4/20/2012)

$\tau_{Avg}(Hollow) = V/A \Rightarrow \frac{10\times10^{3}\ N}{\left[\frac{\pi(2.33\times10^{-3}\ m)^2}{4} - \frac{\pi(1.55\times10^{-3}\ m)^2}{4}\right]}$

pg. 2 of 3

$\boxed{\tau_{Avg}(Hollow) = 4.207\times10^{9}\ Pa}$

Secondly, calculations for the solid and hollow pins utilizing the shear stress formula must now be performed

*Note: Incorrect Calculation for scenario

$\tau(Solid) = \frac{VQ}{It}$ where $Q = \int_{A'} y\,dA' = \bar{y}'A'$

$\tau(Solid) = \frac{(10\times10^{3}\ N)\left\{\left[\frac{\pi(1.165\times10^{-3}\ m)^2}{2}\right]\times\left[\frac{4(1.165\times10^{-3}\ m)}{3\pi}\right]\right\}}{\left[\frac{1}{4}\pi(1.165\times10^{-3}\ m)^4\right](2.33\times10^{-3}\ m)} \Rightarrow$

Disregard the lower calculations for analysis

$\tau(Solid) = \frac{1.054\times10^{-5}\ N\,m}{3.371\times10^{-15}\ m^3\,m^2} \Rightarrow$

$\boxed{\tau(Solid) = 3.127\times10^{9}\ Pa}$

C

$\tau(Hollow) = \frac{(10\times10^{3}\ N)\left\{\left[\frac{\pi(1.165\times10^{-3}\ m)^2}{2} - \frac{\pi(1\times10^{-3}\ m)^2}{2}\right]\times\frac{2(1.165\times10^{-3}\ m)}{\pi}\right\}}{\left[\frac{1}{4}\pi[(1.165\times10^{-3}\ m)^4 - (1\times10^{-3}\ m)^4\right](2.33\times10^{-3}\ m)}$

D

A $\Rightarrow$ B $\frac{(10\times10^{3}\ N)\left\{\left[5.6113\times10^{-7}\ m^2\right]\times 1.165\times10^{-3}\ m\right\}}{1.5409\times10^{-15}\ m^5}$

$\boxed{\tau(Hollow) = 4.242\times10^{9}\ Pa}$

[redacted]

Figure 113: Analytical Calculations of Pin Failure (2 of 3)

Senior Design (4/20/2012)

pg. 3 of 3

Once FEA is done compare the results to the analytically calculated figures

pg. 557 By utilizing the maximum-shear-stress theory a material may be choosen for the shear loading conditions

$$\tau_{max} = \frac{\sigma_y}{2}$$

assuming a structual steel of A36 ($\sigma_y = 250\,MPa$)

$$\tau_{max} = 250\,MPa/2 \Rightarrow 125\,MPa$$

Utilizing the factor of safety equation

$$FS = \frac{F_{fail}}{F_{allow}} \Rightarrow \frac{250 \times 10^6\,Pa}{2,395 \times 10^9\,Pa} \Rightarrow .104$$

Since $0.104 < 1$ this steel is not appropiate for this application

redesign of pinning mechanism is suggested; also, a secondary analysis of the forces should be done since the analysis was considered in a "worst-case scenario", locked transmission with a loading of 40 N·m

[redacted]

Figure 114: Analytical Calculations of Pin Failure (3 of 3)

Senior Design (4/25/2012)

Power generation of prototype system pg1 of 2

We can calculate the power generation of the bioenergy harvester by first identify the human subject data we will use

Utilizing Subject 1 data ⇒ @ 3MPH — Avg. V_{RMS} = 0.187
@ 5MPH — Avg. V_{RMS} = 0.347
@ 7MPH — Avg. V_{RMS} = 0.459

Since we utilized generator 5 and a electrical loading of 500 Ω

The equation for the current vs voltage @ 500Ω is:

$y = 1.9513x + 0.0041$ where x = voltage, y = current

@ 3MPH ⇒ $y = 1.9513(0.187) + 0.0041$ ⇒ y = .369 amps

@ 5MPH ⇒ $y = 1.9513(0.347) + 0.0041$ ⇒ y = .681 amps

@ 7MPH ⇒ $y = 1.9513(.459) + 0.0041$ ⇒ y = .899 amps

The equation for the power vs voltage @ 500Ω is:

$y = 1.9319x^2 + 0.0123x - 0.0006$ where x = voltage, y = power

@ 3MPH ⇒ $1.9319(0.187)^2 + 0.0123(0.187) - 0.0006$ ⇒
y = 0.069 watts

[redacted]

Figure 115: Power/Current Generation of Subject 1 (1 of 2)

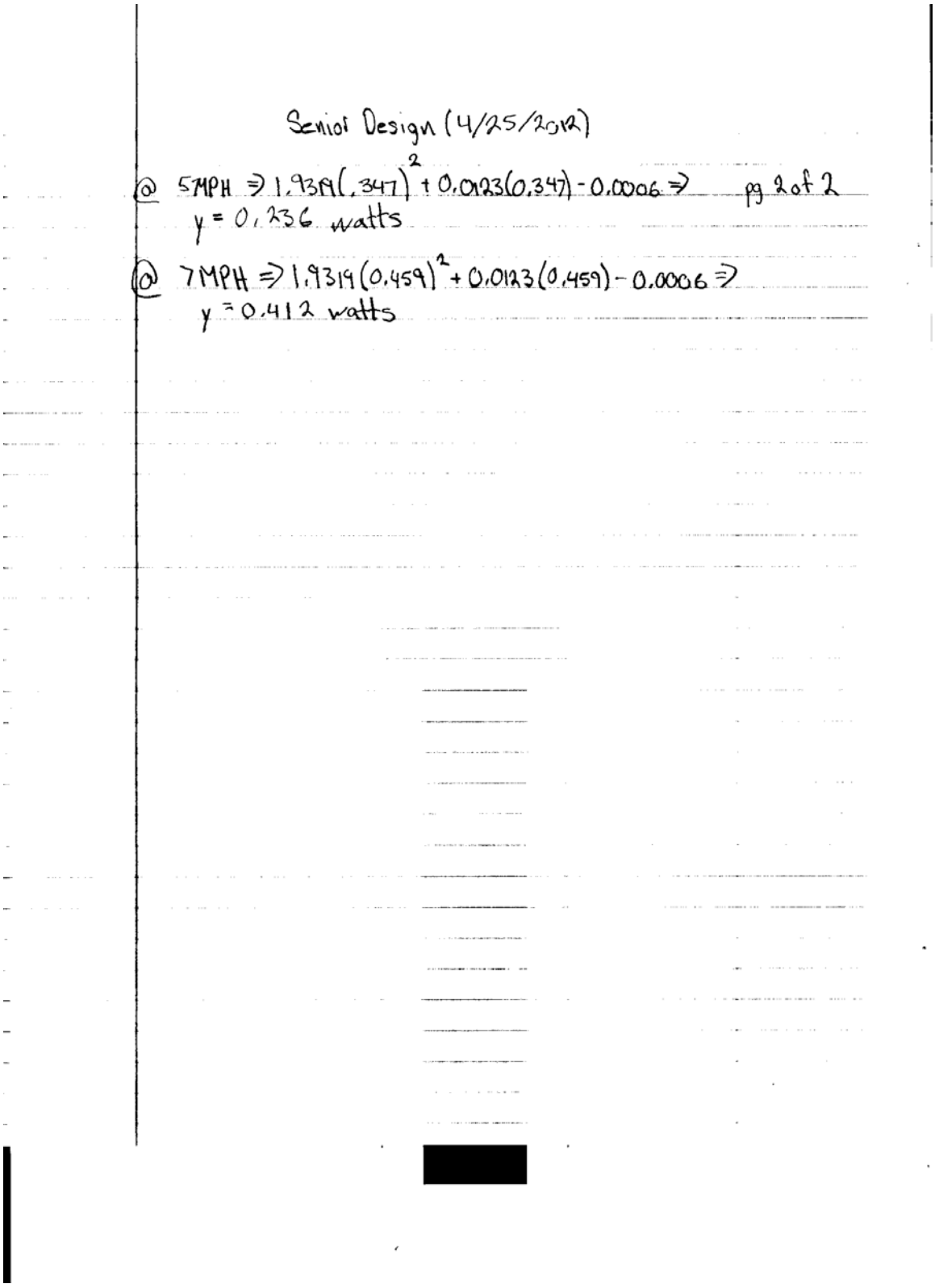

Figure 116: Power/Current Generation of Subject 1 (2 of 2)

A.4 Technical Drawings

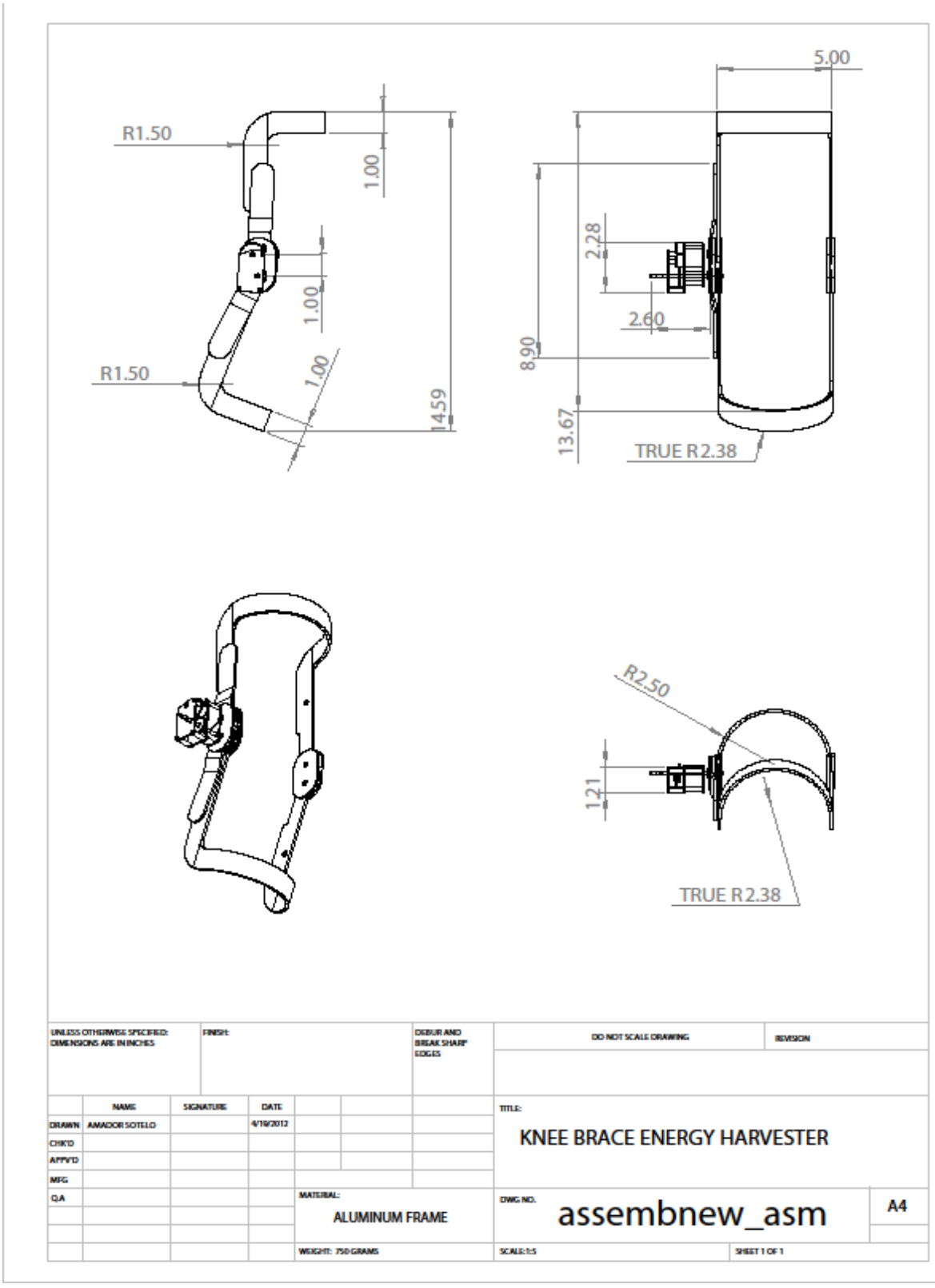

Figure 117: Solidworks Knee Brace 3D Drawing (1-pt, 2-pt, 3-pt) Unit-inches

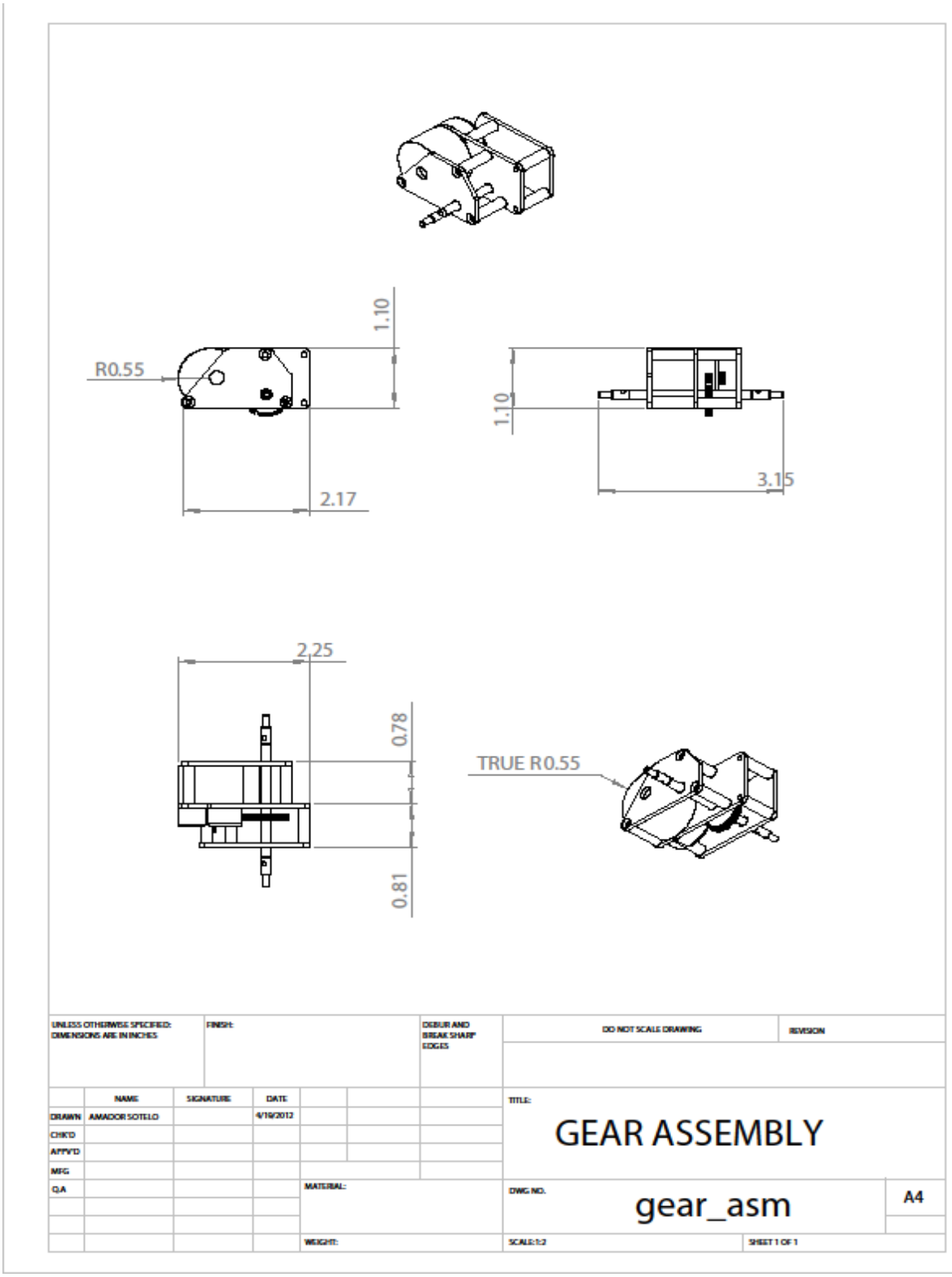

Figure 118: Solidworks Generator/Transmission 3D Drawing (1-pt, 2-pt, 3-pt) Unit-inches

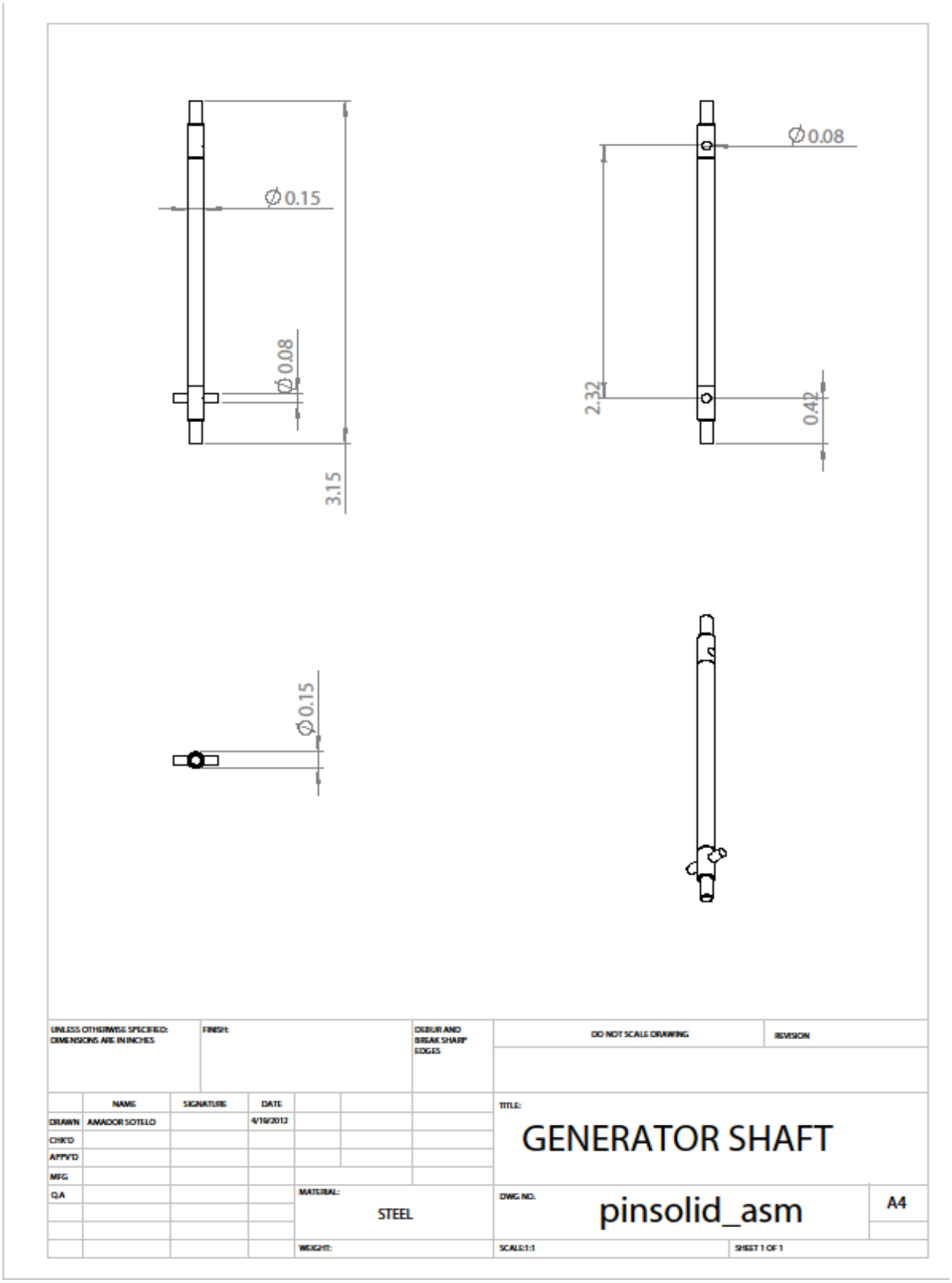

Figure 119: Solidworks Drive Shaft/Pin 3D Drawing (1-pt, 2-pt, 3-pt) Unit-inches

Bibliography

Northrop Grumman. (1994). Retrieved December 6, 2011, from Wikipedia: The Free Encyclopedia: http://en.wikipedia.org/wiki/Northrop_Grumman

Ferro Solutions, VEH360 datasheet. (2008, Jan. 7). Retrieved Oct. 19, 2011, from ferrosi.com: http://www.ferrosi.com/files/VEH360_datasheet.pdf

Mide. (2008, Jan. 7). PEH20W Datasheet. (2008, Jan. 7). Retrieved Oct. 19, 2011, from mide.com: http://www.mide.com/products/volture/peh20w/peh20w.php

Perpetuum Limited, PMG17 datasheet. (2008, Jan. 7). Retrieved Oct. 19, 2011, from perpetuum.co.uk: http://www.perpetuum.co.uk/resource/PMG17-100_dsheet.pdf

Alter, L. (2008). Ugly Sneakers Generate Power While You Walk. *Tree Hugger: A Discovery Company*, 1.

Beardmore, R. (2012, April 2). *Gear Efficency.* Retrieved January 20, 2012, from Roymech Design: http://www.roymech.co.uk/index3.htm

Bionic Power Inc. (n.d.). *Bionic Power*. Retrieved July 26, 2011, from http://bionic-power.com/index.htm

Bledsoe Brace Systems. (2009). *Axiom Functional Knee Brace.* Retrieved April 1, 2012, from Bledsoe Brace: http://www.bledsoebrace.com/custom/axiom.asp

C. Saha, T. O. (2006). Optimization of an electromagnetic energy harvesting device. *IEEE Trans. Magn.*, 3509-3511.

C. Serre, A. P.-R. (2006). Vibrational energy scavenging with si technology electromagnetic inertial microgenerators. *DTIP MEMS MOEMS*.

C.B. Williams, C. S. (2001). Development of an electromagnetic micro-generator. *Circuits, Devices, and Systems, IEE Proceedings*, 337-342.

C.R. Saha, T. O. (2008). Electromagnetic Generator for Harvesting Energy from Human Motion. *Sensors and Actuators A: Physical*, 248-253.

CalRecycle. (2011, July 21). *Electrical Storage: Present, Past, and Future.* Retrieved October 12, 2011, from CalRecycle: http://www.calrecycle.ca.gov/reducewaste/Power/ElectricStor.htm

Chetwynd, M. M. (2003). Investigation of a resonance microgenerator. *J. Micromech. Microeng.*, 209-216.

Continuous Improvement Center. (2008). *Engineering Design Methodology.* Retrieved December 7, 2011, from University of Puerto Rico at Mayaguez: http://www.me.uprm.edu/inme_CIC/IMPROVEMENT%20NEW/ContinuousImprovementCenter/Design%20Methodology.pdf

E. Lefeuvre, A. B. (2006). A comparison between several vibration-powered piezoelectric generators for standalone systems. *Sensors Actuators A, Phys.*, 405-416.

E. Lefeuvre, A. B. (2006). Optimization of Piezoelectric Electrical Generators Powered by Random Vibrations. *DTIP MEMS MOEMS*, 338-343.

Electropedia. (2005). *Alternate Energy Storage Methods*. Retrieved October 12, 2011, from http://www.mpoweruk.com/alternatives.htm

Eppinger, K. T. (1995). *Product Design and Developement.* New York: McGraw-Hill, Inc.

G. Despesse, J. C. (2005). High damping electrostatic system for vibration energy scavenging. *Proc. 2005 Joint Conf. Smart Objects Ambient Intell.VInnov. Context-Aware Services: Usages Technol.*, 283-286.

H. A. Sodano, G. P. (2004). Estimation of Electric Charge Output for Piezoeletric Energy Harvesting. *Strain, 40*, 49-58.

H. Tanaka, G. O. (2005). Electric power generation using piezoelectric resonator for power-free sensor node. *Proc. IEEE Custom Integr. Circuits Conf., 2005*, 97-100.

H.-B. Fang, J.-q. L.-Y.-C. (2006). Fabrication and performance of MEMS-based piezoelectric power generator for vibration energy harvesting. *Microelectron. J.*, 1280-1284.

Hanna, Z. (2011). Young Harvard Women Release Alternative Energy Soccer Ball, Revolutionize. *PR Web*, 1-2.

Heimbuch, J. (2008). Sanyo's Pedometer Charges With Each Step. *Tree Hugger: A Discovery Company*, 1.

Hibbler, R. C. (2008). *Mechanics of Materials.* Upper Saddle River, New Jersey, United States of America: Prentice Hall.

Hoffman, N. G. (2010). *A Miniature Electromechanical Generator Design Utilizing Human Motion.* Monterey: Naval Postgraduate School.

J. M. Donelan, e. a. (2008). Biomechanical Energy Harvesting: Generating Electricity During Walking with Minimal User Effort. *Science*, 807-810.

J. M. H. Lee, S. C. (2003). Development of an AA size energy transducer with micro resonators. *Proc. Int. Symp. Circuits Syst.*, 876-879.

Joint Pain Institute. (2010). *Types of Knee Braces*. Retrieved 4 03, 2012, from The Knee: http://www.theknee.com/knee-brace/knee-braces-support/

K. Hammond, E. L. (2005). An integrated node for energy-scavenging, sensing, and data-transmission: Applications in medical diagnostics. *Proc. 2nd Int. Workshop Wearable Implatable Body Sensor Network*.

Kaajakari, V. (2010, April 21). Microstructured Piezoeletric Shoe Power Generator Outperforms Batteries. *MEMS Investor Journal*, 1.

Knutzen, J. H. (2009). *Biomechanical Basis of Human Movement.* Baltimore, Maryland, United States of America: Lippincott Williams & Wilkins.

Kumar, B. S. (2008, April 7). *Knee Mounted Power Generator Concept-Jog Up Your* . Retrieved October 1, 2011, from EcoFriend: http://www.ecofriend.com/entry/philips-knee-mounted-power-generator-jog-up-your-music/

Lang, B. C. (2006). A variable-capacitance vibration-to-electric energy harvester. *IEEE Trans. Circuits Syst. I, Regular Papers*, 288-295.

Lawrence W. Rome, L. F. (2005, September 9). Generating Electricty While Walking with Loads. *American Association for the Advancement of Science, 309*, 1725-1728.

Lepore, B. J. (2010, April 26). Defense Infrastructure: Department of Defense Renewable Energy Initiatives. *United States Government Accountability Office*. Washington, DC.

LeVeau, B. F. (2011). *Biomechanics of Human Motion: Basics and Beyond for the Health Professions.* Thorofare, New Jersey, United States of America: Slack, Inc.

Liao, T. H. (2005). Sensitivity analysis and energy harvesting for a self-powered piezoelectric sensor. *J. Intell. Mater. Syst. Struct.*, 785-797.

M. El-hami, P. G.-J. (2001). Design and fabrication of a new vibration-based electromechanical power generator. *Sensors Actuators A. Phys,*, 335-342.

M. Ferrari, V. F. (2006). Modeling, fabrication and performance measurements of a piezoelectric energy converter for power harvesting in autonomous microsystems. *IEEE Trans. Instrum. Meas.*, 2096-2101.

M. Miyazaki, H. T. (2003). Electric-energy generation using variable-capacitive resonator for power-free LSI: Efficiency analysis and fundamental experiment. *Proc. Int. Symp. Low Power Electron. Design*, 193-198.

McArdle W.D., K. F. (2001). *Exercise Physiology: Energy, Nutrition, and Human Performance* (5th Edition ed.). New York, New York, United States of America: Williams & Wilkins.

Myer, J. (2012). *Normal Walking Speed: Average Human Walking Pace, Average Speed Walker, Running Speed.* Retrieved 3 24, 2012, from Eat Run Play: http://eatrunplay.com/normal-walking-speed-average-human-walking-pace-average-speed-walker-running-speed/

N. G. Elvin, N. L. (2006). Feasibility of structural monitoring with vibration powered sensors. *Smart Mater. Struct.*, 977-986.

N. N. H. Ching, H. Y. (2001). A laser-micromachined vibrational to electrical power transducer for wireless sensing systems. *Proc. 11th Int. Conf. Solid-State Sensors Actuators*.

N.N.H. Ching, G. C. (2000). PCB integrated micro-generator for wireless systems. *Proc. Int. Symp. Smart Struct.*

N.N.H. Ching, H. W. (2002). A laser-micromachined multi-modal resonationg poer transducer for wireless sensing systems. *Sensors Actuators A, Phys.*, 685-690.

P. D. Mitcheson, e. a. (2008). Energy Harvesting from Human and Machine Motion for Wireless Electronic Devices. *Proceedings of the IEEE*, (pp. 1457-1486).

P. Glynne-Jones, M. J. (2004). An electromagnetic, vibration-powered generator for intelligent sensor systems. *Sensors Actuators A, Phys.*, 344-349.

P. Miao, P. M. (2006). MEMS inertial power generators for biomedical applications. *Microsystems and Technology*, 1079-1083.

P. Niu, P. C. (2004). Evaluation of Motions and Actuation Methods for Biomechanical Energy Harvesting. *35th Annual IEEE Power Electronics Specialists Conference* (pp. 2100-2106). Aachen: IEEE.

Pace Calculator. (n.d.). *Average 5K Pace by Age and Sex.* Retrieved March 24, 2012, from Pace Calculator: http://www.pace-calculator.com/average-5k-pace-by-age-sex.php

Qingguo Li, V. N. (2009, June 23). Development of a Biomechanical Energy Harvester. *Journal of Neuroengineering and Rehabilitation*.

R. Duggirala, R. P. (2006). MEMS radioisotope-powered piezoelectric micro power generator (RPG). *Proc. IEEE 19th Int. Conf. Micro Electro Mech. Syst. 2006*, 94-97.

R. Tashiro, N. K. (2000). Development of an electrostatic generator that harnesses the motion of a living body. *JSME Int. J., ser. C*, 916-922.

R. Tashiro, N. K. (2002). Development of an electrostatic generator that harnesses the ventricular wall motion. *Jpn. Soc. Artif. Organs*, 239-245.

R. Yang, Y. Q. (2009, Febuary 9). Converting Biomechanical Energy into Electricity by a Muscle-Movement Driven Nanogenerator. *Nanoletters, 9*(3), 1201-1205.

Raziel Riemer, A. S. (2011). Biomechanical Energy Harvesting from Human Motion: Theory, State of the Art, Design Guidelines, and Future Directions. *Journal of Neuroengineering and Rehabilitation, 8*(22), 1-13.

Richards, J. (2008). *Biomechanics: In Clinic and Research.* Edinburgh: Elsiver.

Rogers, P. A. (2001, April). *Strong Men Armed.* Retrieved October 19, 2011, from forcerecon: http://www.forcerecon.com/strongmenarmed3.htm

Rome, L. (2006). *Lighting Packs*. Retrieved September 29, 2011, from http://lightningpacks.com/contact.html

S. Beeby, M. T. (2005). Design and performance of a microelectromagnetic vibration powered generator. *13th Int. Conf. Solid-State Sensors, Actuators Microsyst. Dig. Tech. Papers*, 780-783.

S. P. Beeby, M. J. (2006). Macro and micro scale electromagnetic kinetic energy harvesting generators. *DTIP MEMS MOEMS*.

S. Roundy, P. W. (2003). *Energy Scavenging for Wireless Sensor Networks.* Boston, MA: Kluwer Academic.

T. O. Kiper, A. E. (2010). *Batteries on the Battlefield: Developing a Methodology to Estimate the Fully Burdened Cost of Batteries in the Department of Defense.* Montery: Naval Postgraduate School.

T. Tsutsumino, Y. S. (2006). Efficiency evaluation of micro seismic electret power generator. *Proc. 23rd Sensor Symp. Sensors, Micromach. Appl. Syst.*, 521-524.

T. Tsutsumino, Y. S. (2006). Seismic power generator using high-performance polymer electret. *Proc. 19th IEEE Int. Conf. Micro Electro Mech. Syst. (MEMS 2006)*, 98-101.

Thales. (n.d.). *Handheld themal inager- SOPHIE Family.* Retrieved October 19, 2011, from thalesgroup: http://www.thalesgroup.com/Portfolio/Defence/LandJoint_Products_Surveillance_Sophie/

W. J. Li, Z. W. (2000). A micromachined vibration-induced power generator for low power sensors of robotic systems. *Proc. World Automat. Congr. 8th Int. Symp. Robot. Applicat.*

W.J. Li, T. H. (2000). Infrared signal transmission by a laser-micromachined, vibration-induced power generator. *Proc. 43rd IEEE Midwest Symp. Circuits Syst. 2000*, 236-239.

W.-S. Huang, K.-E. T.-C.-S. (2007). A silicon MEMS micro power generator for wearable micro devices. *J. Chin. Inst. Eng.*, 133-140.

Winter, A. D. (2005). *Biomechanics and Motor Control of Human Movement* (3rd Edition ed.). Hoboken, New Jersey: John Wiley and Sons.

Winter, D. A. (2009). *Biomechanics and Motor Control of Human Movement* (4th ed.). Hoboken, New Jersey: John Wiley & Sons, Inc.

Y. Arakawa, Y. S. (2004). Micro seismic electret generator using electret polymer film. *Proc. 4th Int. Workshop Micro and Nanotechnology for Power Generation and Energy Conversion Applicat. Power MEMS*, 187-190.

Y. Jeon, R. S.-H.-G. (2005). MEMS power generator with transverse mode thin film PZT. *Sensors Actuators A*, 16-22.

Y. Naruse, N. M. (2009, August 26). Electrostatic Micro Power Generation from Low-Frequency Vibration Such as Human Motion. *Journal of Micromechanics and Microengineering, 19*, 1-5.